NICKEL DEPOSITION ON HYDRODEMETALLATION CATALYSTS

XINJIN ZHAO

B.S., Taiyuan University of Technology (1982)
M.S., Institute of Coal Chemistry, Academia Sinica (1986)
M.S.C.E.P., Massachusetts Institute of Technology (1990)

Submitted to the Department of Chemical Engineering
in partial fulfillment of the requirements for the degree of

Doctor of Science in Chemical Engineering

at the

MASSACHUSETTS INSTITUTE OF TECHNOLOGY

February 1993

Author_____

Department of Chemical Engineering
November 13, 1993

Certified by_____

James Wei
Professor Emeritus of Chemical Engineering
Thesis Supervisor

Accepted by_____

Robert E. Cohen
Chairman, Departmental Committee on Graduate Students

NICKEL DEPOSITION ON HYDRODEMETALLATION CATALYSTS

by

Xinjin Zhao

Submitted to the Department of Chemical Engineering
on November 13, 1992, in partial fulfillment of the
requirements for the degree of
Doctor of Science in Chemical Engineering

Abstract

The prevailing metals in petroleum are nickel and vanadium which exist in porphyrins and asphaltenes. These organometallic molecules are large and their sizes approach the pore sizes of hydrotreating catalysts. As a result, these compounds deposit on the catalyst surface during hydrotreating processes and irreversibly destroy the catalysts by affecting transport into intraparticle fine pores as well as causing chemical changes when the deposited metals interact with the original active components on the catalysts. A better understanding of the deposition phenomena on the catalysts would establish a basis for developing improved hydrotreating catalysts.

Nickel etio-porphyrin was used as a model compound to study nickel deposition and the interaction of the deposits with the catalytic components on presulfided $CoO - MoO_3/\gamma Al_2O_3$ hydrodemetallation catalysts under industrially-relevant process conditions, though no diffusion effects were present in the study. The structures of the nickel deposits on the aged catalysts were characterized by various microscopic and spectroscopic techniques.

The nickel deposits were identified as nickel sulfide (Ni_7S_6) in crystallite form. At a nickel loading of about 20%, the average size of the crystallites was estimated to be about 10 to 15 nanometers, while crystallites with the sizes up to 100 nanometers were also observed.

X-ray elemental mapping and X-ray microanalysis on a dedicated scanning transmission electron microscope (STEM) and high resolution transmission electron microscope (HRTEM) showed that nickel sulfide deposits were strongly associated with cobalt sulfide (Co_9S_8) on the catalyst. In contrast, only about 20 to 25% of the molybdenum was associated with the nickel deposits as a segregated molybdenum disulfide (MoS_2) surface layer phase, the rest of the molybdenum disulfide forms

separate entities on the catalyst surface.

The association between cobalt and nickel sulfides was shown to be a result of solid solution formation between the two sulfides, while the segregation of molybdenum sulfide is due to its lower surface energy. Segregation of molybdenum disulfide was quantitatively determined by X-ray microanalysis on scanning transmission electron microscope and directly observed on high resolution transmission electron microscope. It was also showed that the degree of segregation decreases for crystallites smaller than about 15 nanometers.

Nickel sulfide deposits enhance the sintering of the catalytic metal sulfides by lowering their Tammann temperatures. Electron microscopic studies showed that the sintering of the catalytic metal sulfides, especially cobalt sulfide, increased with the presence of nickel sulfide deposits. The effect was also discussed on hypothetical phase diagrams. It was showed that there existed a threshold nickel loading above which the catalytic metal sulfides would become mobile. The threshold value was dependent on the specific system and the operating temperature. The enhanced sintering of molybdenum sulfide, rather than *covering-up of active sites by deposits* as being suggested in many literatures, was considered as the major cause for deactivation by metal deposits at diffusion-free conditions.

The morphology of the metal deposits has significant impact on the deactivation of hydrodemetallation catalyst. Therefore, our results could have important implication. Since segregated large crystallites of nickel deposits lead to less deactivation, in comparison with small crystallites or uniform layer deposition, improved hydrodemetallation catalyst could be developed by manipulating the morphology of cobalt on the catalyst surface.

Thesis Supervisor: James Wei

Title: Professor Emeritus of Chemical Engineering
Massachusetts Institute of Technology

Dean
School of Applied Science and Engineering
Princeton University

Acknowledgments

I am indeed indebted to Professor James Wei for mentorship, for lighting the way, for his technical and personal guidance, for an environment I could grow as a scientist.

I am also very grateful to my thesis committee members, Professor Charles N. Satterfield, Dr. Miretta F. Stephanopoulos, Professor Klavs F. Jensen and Dr. Anthony J. Garratt-Reed for sharing their wealth of knowledge and many insights during the course of the investigation. Dr. Garratt-Reed deserves a special mention for his invaluable assistance in performing STEM analysis. I would also like to thank Mr. Michael Frongillo for the superb high resolution TEM work.

The financial support for the research from *Mobil Oil Research and Development Corporation* and *Chevron Research Company*, as well as the Research Assistantship and Fellowships from Department of Chemical Engineering of *Massachusetts Institute of Technology* are gratefully acknowledged. I also thank Dr. James D. Carruthers and Dr. Robert H. Whitman of *American Cyanamid Company* at Stamford, Conneticut for providing catalyst samples.

I wish to acknowledge the valuable discussions and various supports from the past members of the hydrodemetallation laboratory, especially Dr. Barbara Smith, and Dr. Chi-Wen Hung at *Chevron Research Company*, and Dr. Kirk Limbach at *Rohm and Hass Company.* During the first stage of the thesis, fruitful discussions and advice from them were most helpful in defining the scope of the thesis.

The completion of the thesis has cost me four years, but they have not been devoid of excitement. The many friends with whom I shared the time have made of *MIT* a joyful memory, knowing them has been a special prize of four years at *MIT.* Be it a Friday basketball game, an overnight *Practice School* visit to *Tahoe Casino*, or a weekend trip to *Cape Cod* beach, we always managed to have a good time and still get our work done. Grateful appreciation is expressed to the following, though the

list is far from complete: Leo Lue, for all those fun time even since you came to *the Zoo*; Joy Mendoza, for all the joys we had on the basketball court; Gordon Smith, for the fish and lobsters you cooked; Stathis Avgoustiniatos, for all the good and bad time we shared at Practice School; Marc Moran, for teaching me from juggling to driving; and the many others who were responsible, directly or indirectly, wittingly or unconsciously, to my being and well-beings; .....

I benefited greatly from the friendship and advice of Jirong Xiao, Jiang Yue, Zhicheng Hu. Their helps are greatly appreciated.

Many thanks go to Hojoon Park, my first-year roommate, who helped me to adjust from the eastern to the western culture in my crucial first term, and told me the difference between *spaghetti* and *noodle*. I wish you the best.

Thanks are also due to many other friends who contributed my education at MIT. Of those, Yaping Liu for his help in TEM, and Qing Huang for first introducing me into the world of Athena, where the thesis is eventually born[1].

Our secretary, Linda Mousseau catered to my every need in a most generous and cheerful way, for which I am very appreciative.

My deepest appreciation and love go to my wife, Luhong and my far-away parents, who have sacrificed so much for me, and whose unwavering support and love I have depended on my life. Without them, I could never have taken this endeavor. Thank you, Luhong, Thank you, Mom and Dad, I love you all. Always, in all ways.

[1]The thesis is written with LaTeX.

♡ ♡

To Luhong

Who spent so many lonely nights and weekends during the last four years, but wholeheartedly supported my pursuit with love, encouragement and understanding.

To My Parents

who never had a chance to have a formal education, but fully understand the importance and benefits of educating their children to the best of their capabilities.

♡ ♡

Contents

List of Figures

List of Tables

Chapter 1

Introduction and Objectives

Dr. Watson would tell you that these little digressions of mine sometimes prove in the end have some bearing on the matter.

——Sherlock Holmes, *The Adventure of the Three Garridebs*
Sir Arthur Conan Doyle

1.1 Background

Due to both the concern for the environment and the decreasing availability of oil, ever increasing quantities of crude oils and residuals have to be processed. One of the most important features of these crude oil and residuals is their high heteroatom contents. In addition to the improvement of carbon/hydrogen ratios, a major goal of hydrotreating is the removal of heteroatoms, which includes sulfur, nitrogen, oxygen, and trace metals. While the role of catalyst in light hydrotreating is mainly to promote selective removal of sulfur and nitrogen, the catalyst must additionally promote the

removal of metals in processing heavier feeds.

Catalytic hydrotreating is usually performed in the presence of well established catalyst system consisting of $\gamma - Al_2O_3$ supported combination of molybdenum or tungsten and cobalt or nickel, at elevated pressures and temperatures.

In crude oils, nearly half of the metallic elements in the periodic table have been identified as trace elements [130]. The most abundant and troublesome metals in crude oil are nickel and vanadium, present in amounts ranging from a few ppm to over 1000 ppm. These metals usually exists in organometallic molecules, typically metal porphyrins and asphaltenes. Unlike other heteroatoms, such as sulfur, nitrogen or oxygen, which can be removed as gaseous products after hydrotreating, metals stay and accumulate on the hydrotreating catalysts as metal sulfide deposits. The deposits lead to irreversible catalyst deactivation which is a major problem in residuum hydrotreating and can often result in expensive catalyst replacement [85]. Successful ways to regenerate the spent catalysts with metal deposits are yet to be developed [117].

The organometallic molecules are large and approach the same order of magnitude as the pore size of the hydrotreating catalysts. As a result, these compounds deposit close to the mouth of the pore after hydrogenolysis reactions. The deposits destroy the catalyst by affecting transport into intraparticle fine pores as well as causing chemical changes that occur when the deposited metal interacts with the original active sites on the catalyst [9] [19] [69] [113]. Although the diffusion within hydrodemetallation catalysts has been a subject of many experimental and modeling studies[29] [54][55] [60] [64] [75], the interaction of metal deposition with catalytic metals has received less attention [50] [113] [127]. Many technical advances are still based on empirical considerations. A better understanding of the chemical nature of the metal deposits and their interaction with the catalytic metals would establish a fundamental basis for developping improved hydroprocessing catalysts and reactors.

In general, the characteristics of aged and spent catalysts have not been well defined though the metal deposits are increasingly found to take place as crystallites over discrete sites, both in laboratory conditions with clean oil and model compounds [71] [107] and in industrial pilot plant [116], which is in contrary to previous uniform layer assumptions[9] [19] [86]. The implications and control of the metal deposition would have significant consequences on hydrotreating catalyst design.

1.2 Motivation and Objectives

Catalytic hydrotreating of residuum oil is currently conducted at 1.2 million barrels a day in the world, at a replacement cost of more than 200 million dollars per year[126]. This cost is certainly going to increase sharply, as world concern for the environment continues to exert pressure on cleaner fuels. In addition, catalytic hydrotreating is also necessary for making usable coal liquefaction products. The necessity of the costly replacement of hydrodemetallation catalyst in industry has motivated fundamental study to extend the life span of hydrodemetallation catalysts.

The ultimate goals for this studies are:

- **To find efficient ways of using hydrodemetallation catalysts, and to extend the life span of the catalysts;**
- **To improve the design of hydrodemetallation catalysts.**

The objective of this work is to investigate the governing factors that determine the deposition patterns of nickel and the interaction of the nickel deposits with cobalt and molybdenum on hydrodemetallation catalysts under diffusion-free conditions. With this information, we will further try to propose some approaches to hydrodemetallation catalyst design.

More specifically, the objectives of the work are:

- **To identify the location and morphology of nickel sulfide deposits on aged hydrodemetallation catalysts.**
- **To determine the deposition mechanism and the development of the deposition phenomena along the course of hydrodemetallation processes.**
- **To understand the interactions between the nickel sulfide deposits and the catalytic metals, and their implications to catalyst deactivation.**
- **To propose possible approaches to control the morphology of the deposits based on the results.**

In the rest of the chapter, a short review of some subjects closely related with the present work will be discussed. Interested reader can refer to other comprehensive reviews on hydrodemetallation in general[85]. In chapter two, we will present a brief thermodynamic analysis of the system of a catalyst surface with metal sulfide deposits, and attempt to understand the ultimate equilibrium deposition patterns on the hydrodemetallation catalysts. Chapter three describes the hydrodemetallation experiments by using model compound to simulate industrial hydrodemetallation process and to obtain spent and aged catalysts loaded with nickel deposits. In chapters four, five, and six, the results from electron microscopic studies for nickel deposition are presented. Chapter four shows the pattern and morphology of the nickel deposits on hydrodemetallation catalysts. Chapter five discusses the differentiation between two possible mechanisms for the deposition phenomena. Chapter six describes the metal distributions within the crystallites of deposits on the catalyst surfaces. Chapter seven is devoted to the mobility of the catalytic metal sulfides on the catalyst surface. In chapter eight, we attempt to depict a complete picture for the deposition process and the implications to catalyst deactivation. Finally, chapters nine and

ten summarize the main conclusions of the thesis and propose recommendations for future work, respectively.

The main research topics are tabulated in Table 1.1.

1.3 Literature Review

1.3.1 Structure of Sulfided $Co - Mo/\gamma - Al_2O_3$ Catalyst

$CoO - MoO_3/\gamma - Al_2O_3$ is widely applied in industrial catalytic hydroprocessing for all kinds of petroleum feedstocks. Although it has been used for many years, and extensive efforts have been taken to explore the fundamental aspects of the catalyst, its atomic structure and catalytic mechanism are still in dispute. Many different models have been proposed to describe the structure of molybdenum and cobalt, and the mechanism of hydroprocessing reactions on the $CoMo/Al_2O_3$ catalyst[23] [47] [51] [56] [121].

The metal oxide catalyst is usually presulfided to convert the oxides into sulfides. The sulfidation is necessary to prevent metal oxides from being reduced to metals, which are active for hydrogenolysis, thus could lead to rapid coke deactivation to the catalyst[5][99].

Figure 1-1 illustrates the complexity of a $Co - Mo/\gamma Al_2O_3$ catalyst[91] [114], though it may still not be what a real industrial catalyst surface look like. For a typical sulfided $Co - Mo/\gamma Al_2O_3$ catalyst, there are many possible species on the catalyst surface. Typically, the main phase would be poorly or well crystallized MoS_2, decorated with cobalt atoms on the edges of the MoS_2 layers. Co_9S_8 phase is also usually present. Other possible phases include CoS_{1+x}, $CoAl_2O_4$, carbonaceous deposits, *etc.*

Table 1.1: Research Objective

Specific Research Topics	Characterization	Chapters
Hydrodemetallation		Three
Deposition Patterns	STEM, XRD	Four, Six
Deposition Mechanisms	STEM	Five, Six, Two
Molybdenum Surface Segregation	STEM, TEM, XPS	Six, Two
Mobility of Catalytic Metals	STEM, TEM	Seven
Catalyst Deactivation	STEM,TEM	Seven, Eight, One

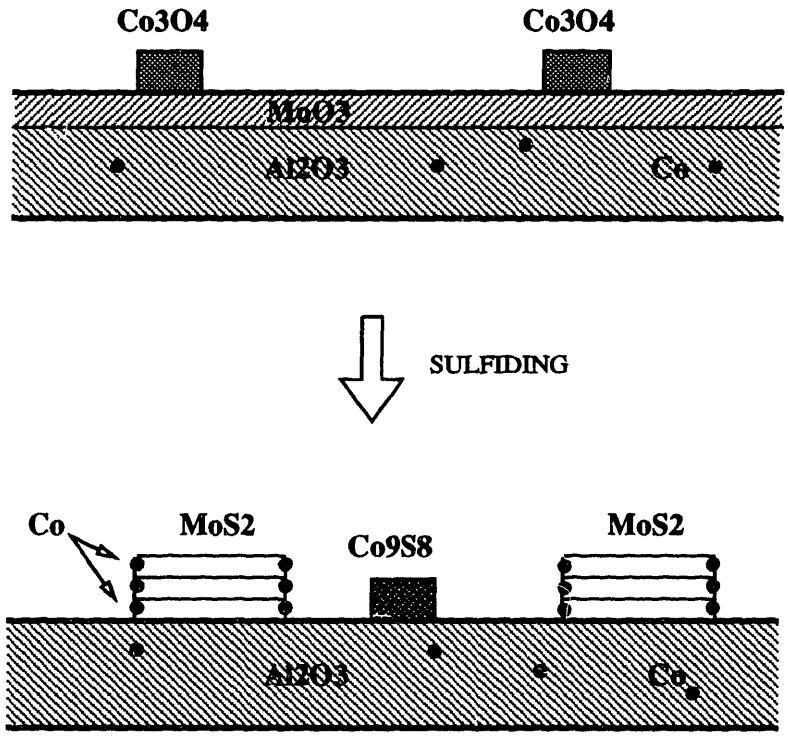

Figure 1-1: General Representation of $CoO - MoO_3/\gamma - Al_2O_3$ Catalyst

The crystallites of molybdenum disulfide are very well dispersed on the alumina surface. High resolution electron microscope could identify the stacking of a very restricted number of layers of molybdenum disulfide. These MoS_2 structures are attached to alumina by either basal or edge plane.

It is generally accepted that the active component for hydrodesulfurization and hydrodenitrogenation is molybdenum sulfide with cobalt as a promoter, though there is no general agreement on the structure and functionality of cobalt [17] [114] [82]. Voorhoeve *et al.* [119] [120] proposed an intercalation model from a solid state point of view. The model proposes that the Co is intercalated into octahedral sites at the edges between the MoS_2 slab (*i.e.*, between the adjacent sulfur layers). The contact synergy model by Delmon *et al.* [22] proposes that cobalt sulfide exists as a separate phase (Co_9S_8) from which spill-over of hydrogen to the MoS_2 phase can occur. Finally, Topsφe and co-workers [114] have proposed the existence of the so-called $Co-Mo-S$ phase as the predominant active species in promoted catalysts. The Co is thought to be located in the same plane as that of the Mo atoms, possibly in interstitial or substitutional posit ions. In addition to the synergistic effect and the $Co-Mo-S$ phase theories, it has been suggested that the presence of cobalt inhibits carbon deposition, thus deceases deactivation rate[49] [131]. Another explanation is that cobalt is needed for keeping the dispersion of molybdenum sulfide on the surface[49].

For hydrodemetallation reactions, it is still unclear what is the active component, or more specifically, the active phases on the catalysts. Under thermal hydroprocessing conditions at temperature above 430°C, noncatalytic demetallation takes place as a result of sulfur-metal coordination and the attack of the nitrogen-metal bonds by activated hydrogen [19]. Takeuchi *et al.* [112] proposed a mechanism for catalytic hydrodemetallation reaction including a model of the active surface site to account for the directionally oriented growth of the V_3S_4 phase. A porphyrin type molecule

releases its vanadyl to the sulfur on the vanadium sulfide surface. The vanadyl is then deoxygenated with H_2S and forms a new sulfide surface to continue the growth process.

It has been showed that the hydrodemetallation occurred via a sequential mechanism involving initial hydrogenation of peripheral double bonds to activate the porphyrin, followed by a hydrogenolysis step which fragments the molecule and remove the metal[1] [122]. This suggests that there are at least two kinds of active sites on the catalyst surface. Ware and Wei [123] used dopants with different acidities to manipulate the acidity of the catalyst surface, as a result, the ratio between hydrogenation and hydrogenolysis reactions changed.

1.3.2 Deposition Patterns

The characterization of metal deposition on hydrotreating catalyst received relatively little attention in the past. It was only in the eighties that researchers began to study the morphology and structure of metal deposits by using electron microscopy and other techniques.

Silbernagel *et al.* [103] [104] used nuclear magnetic resonance (NMR) and electron spin resonance (ESR) to trace the deposition of vanadium onto $CoMo/Al_2O_3$ from heavy oil feeds at 350°C. At low loadings (up to $0.7wt\%$ vanadium), a vanadyl VO^{2+} species dominated ESR spectral components suggested that the VO^{2+} ion was associated with defect sites on the alumina support. At higher vanadium loadings a diamagnetic vanadium species was observed by NMR. The irregularity of the absorption signal suggested that the vanadium was present in a number of physically different sites, so a surface species was suspected. The maximum loading of this diamagnetic species was 5-$10wt\%$. At yet higher loadings vanadium was present as a sulfide, probably V_2S_3. Electron microscopic analysis suggested the sulfide was present as crystallites.

By using electron paramagnetic resonance (EPR) analyses, Ledoux *et al.* [50][51] detected three different vanadyl species on a catalyst aged with vanadium porphyrin at 450°C, one with four nitrogen atoms, a second with four sulfur atoms, and a third with four oxygen atoms. A quantitative distribution between the three was given as 20%, 20% and 60%, respectively. Since the catalyst used was presulfided, no oxygen atoms should be found on the active phase. Therefore, about sixty percent of the vanadium was deposited on the support. They concluded that the vanadium is statistically dispersed on the full surface of the catalyst, both support and active phase. It should be pointed out that the vanadium porphyrin was impregnated on the catalyst, not by demetallatioin reaction, which might have caused the statistical distribution of vanadium on the full substrate.

Loos *et al.* [57][58] compared the X-ray absorption fine structure (XAFS) spectra of pure V_2O_3 and the *pseudo* V_2O_3 phase soaked on $\gamma - Al_2O_3$ support. The two spectra exhibit considerable differences. It was concluded that the vanadium sulfide reacted on or with the support.

Takeuchi *et al.* [112] used transmission electron microscopy and X-ray diffraction to analyze vanadium sulfide deposits formed by the hydrodemetallation of heavy oils. The deposits, which were believed to reside within the pores of the catalyst, were identified as vanadium sulfide crystallites with sizes of about several hundred angstroms to about one thousand angstroms.

Toulhoat *et al.* [116] used a scanning transmission electron microscopy (STEM) fitted with an X-ray analyzer, transmission electron microscopy (TEM), electron microprobe (EMPA), and X-ray diffraction analyzer (XRD) to analyze catalyst aged with a heavy industrial feedstock, pentane deasphalted Boscan crude. The deposits were identified to be vanadium sulfide (V_3S_4) with the presence of nickel. Deposited crystallite diameters observed were 20nm to 40nm near the edge of the catalyst and 5nm to 10nm near the center. However, they found that the number of crystallites

did not change significantly from the edge to the center of the catalyst.

Smith & Wei[107] [108] [109] studied hydrodemetallation with model compounds of nickel and vanadyl porphyrins with clean oil at $280 - 350°C$. The study was conducted with a commercial $CoMo/Al_2O_3$ catalyst, $HDS16A$. The aged catalysts were studied extensively with transmission electron microscopy. Other techniques, including scanning electron microscopy, X-ray diffraction analyzer, X-ray photo-electron spectroscopy (XPS), were also used in the study. Smith found that, for a given hydrotreating catalyst aged at a given set of operating conditions, the number of nickel sulfide crystallites remained relatively constant while the size of these crystallites grew with nickel sulfide loading. The sizes of these crystallites grew from 10nm to 15nm while the metal loading was increased from $37wt\%$ to about $100wt\%$. The corresponding nucleation sites was estimated as $5 \times 10^{-7}\mathring{A}^{-3}$. Smith also studied another catalyst sample with very low loading of molybdenum ($0.24wt\%$) and cobalt ($0.68wt\%$). The numbers of crystallites were estimated at around $5 \times 10^{-9}\mathring{A}^{-3}$, which is about two order of magnitude smaller than that of the $HDS16A$ catalyst. It was suggested that the nucleation numbers of nickel deposits on the aged catalysts were related to the loadings of the catalytic components, *e.g.* molybdenum, cobalt, or phosphorus.

Limbach [53] characterized catalysts aged with vanadium porphyrin. By using analytical electron microscope, he found that the crystallite size of the deposits increased with local loadings on the catalyst particles.

In summary, considerable progress has been realized in the past ten years, but many questions remain to be answered. Metal sulfides generally deposit on catalyst surface as crystallites, though the possibility of a surface layer is not excluded. It is not clear whether deposition is a physical or chemical process, or is dependent on the metal loadings and hydrodemetallation conditions.

1.3.3 Catalyst Deactivation

The deactivation of hydrodemetallation catalyst is a very complex process. Although many factors are contributing to the catalyst deactivation, the accumulation of metal deposits on the catalyst is the most important phenomena causing the deactivation, mainly due to the fact that deactivation caused by metal deposits are not regeneratable. In industrial reactors, a catalyst bed may accumulate nearly double its weight in feedstock contaminants[85]. Obviously, deposits of this magnitude must severely affect the catalyst's ability to function.

Various authors have studied the deactivation of hydrodemetallation reaction by using vanadium poisonous compounds[112], nickel poisonous compounds[128], or both [113], and have observed a very rapid deactivation at low coverage(<1.5% metal) followed by a much monotonous deactivation, and eventually a sharp decrease of activity. Similar results have been reported by others for both pilot experiments and smaller scale experiment[34][70][73]. Figure 1-2 shows one of the earliest results reported by Henke[34]. The results represent a temperature history of a reactor in order to maintain a constant sulfur level in the product. In other words, it represents the history of the catalyst activity.

Most reports attributed the initial deactivation to the build-up of a steady coke loading on the catalysts[74][102]. However, Weitkamp et al [128] and Tamm et al[113] attribute the first stage to *monomolecular layer of nickel species deposited on the active Co-Mo-S sites* and the second stage to the slow buildup of metal deposits layer by layer on the top of an initial monolayer laid down during the rapid deactivation period. They suggested that the catalyst activity is from the deposited species after the first monolayer deposits. Clearly, this does not explain the fact that hydrodemetallation catalyst keeps a high activity far after the monolayer deposition, even though the activity of metal deposits is only about one third or less of that of the promoted catalyst[16][88][112]. There is generally no controversy on the third stage of the de-

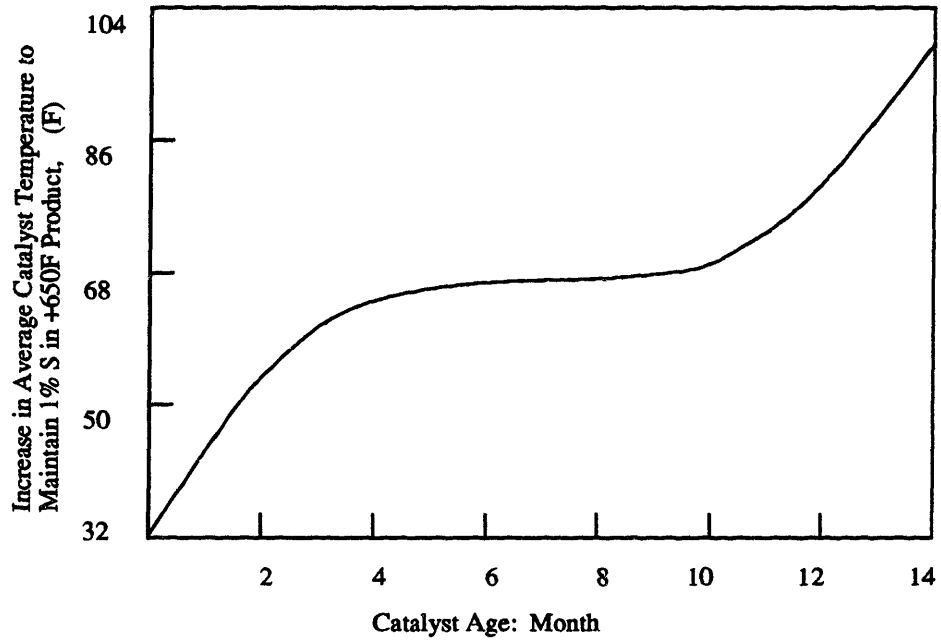

Figure 1-2: Deactivation of Hydrotreating Catalyst in Pilot-Plant Experiments[34]

activation. It is generally agreed that the sharp activity declining was caused by the eventual pore plugging with the build-up of metal deposits.

Ledoux et al[50] proposed that only a very small amount of vanadium was needed to poison the most active sites of Co or Ni promoted molybdenum catalyst by preferentially choose the octahedral cobalt sites and thus destroy the apparent synergy between Co or Ni and Mo.

1.3.4 Migration of Metals on Catalyst Surface

Migration of metals on catalyst surfaces is well studied as a sintering phenomena. Many investigators have studied the migration of nickel on different supports[3] [24] [46] [92]. Generally, temperature and the gaseous environment are two important factors to determine how the metal behaves.

Bogdanor and Rase [9] studied a $NiMo/Al_2O_3$ hydrotreating catalyst aged commercially by a blend of heavy coke and virgin gas oil, without excessive metals. They found that the active components on the catalyst, nickel and molybdenum, were both mobile at reaction, regeneration, and sulfidation stages. It is expected that nickel deposits would behave similarly under similar conditions.

Pazos et al[74] have speculated that the deposited metals might migrate to the free alumina support to explain the maintenance of catalyst activity.

Additional evidence is the findings of Fleisch *et al.* [25]. By using X-ray photoelectron spectroscopy, they found that the ratio of Mo/Al changes with the increase in metal deposits. They speculated that molybdenum may migrate to the top of the contaminated layers and remain exposed to reactants.

Prasada et al[79] studied by X-ray photoelectron spectroscopy the surface enrichment of molybdenum on a multicomponent molybdate catalyst of the composition 50% $Ni_3Co_5Fe_3BiPK_{0.1}Mo_{12}O_{52.5}$ – 50%SiO_2 after being used in ammoxidation of propylene. The molybdenum signal increased by about 10%, while nickel and cobalt

signals decreased by 20% and 10%, respectively.

The effect of temperature on the deposit morphology and deposit structure on hydrotreating catalysts has not been reported in the available literature. However, it is expected that the deposition patterns on catalysts would be affected by hydrodemetallation temperature. Similar to sintering phenomena on catalysts, these deposits are also expected to migrate on the catalyst surface under certain conditions.

Two distinct mechanisms for the growth of metal crystallites on supports have been proposed. A model based on particle migration and coalescence was published by Ruchenstein and Pulvermacher[94], while a model base on the transfer of metal atoms individually from one particle to another (interparticle transport) was proposed by Flynn and Wanke[26][27]. Hughes [36]summerizes that sintering has the following pattern. For very small particles (<20nm) growth occurs predominantly by particle migration. For larger particles, growth occurs by atom migration on the surface.

Chapter 2

Thermodynamic Considerations

When one tries to rise above Nature one is liable to fall below it.

——Sherlock Holmes, *The Adventure of the Creeping Man*

Sir Arthur Conan Doyle

2.1 Introduction

In addressing the metal deposition on hydrodemetallation catalysts, we seek an atomisitic understanding of the nickel distributions on the catalyst surface, and its interaction with the catalytic metals originally on the catalysts. Among the questions to be considered are the following:

What is the thermodynamic equilibrium state of the components on the catalyst surface?

What determines the morphology of the crystallites of deposits?

Are the deposits on the aged catalysts approaching thermodynamic equilibrium

state?

We will attempt to approach these questions from several different perspectives in the coming chapters. In this chapter, we will just present some thermodynamic facts concerning the components on hydrodemetallation catalyst surface.

2.2 Phase Diagrams

As one can imagine, it is naturally difficult to construct a complete diagram for a ternary system in a two dimensional paper. On the hydrodemetallation catalyst, we have nickel deposition, cobalt and molybdenum, in either sulfided or unsulfided forms, excluding the effect of the existence of the substrate, and gaseous phase.

Although the bulk thermodynamics probably inapplicable to catalyst surfaces and to supported catalysts, such data can still be employed in considering what might be the gross state of the catalyst or in determining a proper concentration of hydrogen sulfide in hydrogen to convert a catalyst to a desired state. In the following, we will present a few phase diagrams for the relevant systems. Although one can easily locate phase diagrams for two component systems in well organized literatures[2][61], three component phase diagrams involving solid phases are very scarce. Fortunately, Co-Ni-S system has been studied by some mineralogist[40][45]. One of the diagrams is shown in Figure 2-1. We tried in vain to locate a phase diagram for the system of Ni-Mo-S system.

Figure 2-1 shows that at sulfur level below about 0.6, the corresponding cobalt sulfide and nickel sulfide forms almost complete solid solutions. It should be pointed out that the phase diagram is for 1273K, which is far above the hydrodemetallation temperature.

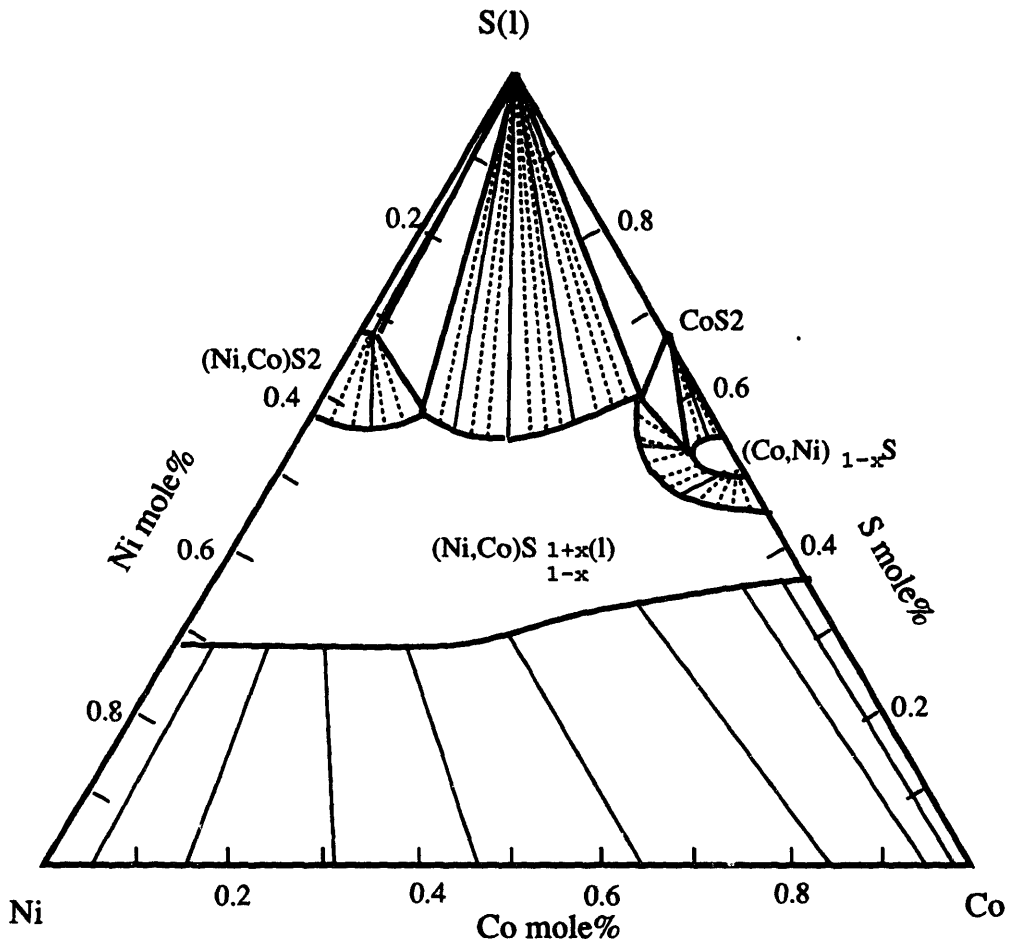

Figure 2-1: Phase Diagram of Ni-Co-S at 1273K[40]

2.2.1 Systems with Hydrogen and Hydrogen Sulfide

For the present hydrodemetallation catalyst system, only the hydrogen reduction equilibria of the sulfides need to be considered inasmuch as these are the final equilibrium states. Accordingly, the hydrogen reduction equilibria for the pertinent sulfides are shown in Figure 2-2, 2-3, 2-4[63].

In the hydrodemetallation temperature range of 600-800K, the metal oxide catalyst and nickel deposits are expected to be readily converted to sulfides, even with a small fraction of one percent of hydrogen sulfide. Molybdenum and cobalt should be in the form of MoS_2 and Co_9S_8 as being reported in literatures.

2.3 Surface Segregation

The surface composition of alloys used in catalysis is in general different from the composition of the bulk, due to the difference in surface tensions between the two components.

The problem of surface enrichment is of particular interest in the case of highly dispersed binary catalysts, composed of microclusters of metals, metal oxides, or metal sulfides in our system on carriers. There are several possibilities for the microstructure of such systems. For a system with two constituents, When the two constituents are immiscible, separate microclusters of A and B on the carrier may be formed (Figure 2-5a). The other limiting case involves constituents of complete miscibility, when microcrystals of single phase solid solution are expected (Figure 2-5b). There are then two possible microstructures with one component segregated to the surface: enrichment of one component in the surface layer with a nearly homogeneous alloy at the center of the microcluster (Figure 2-5c), and separation of the crystal into two concentric phases of different composition, one on the inside and one on the outside(Figure 2-5d)[32].

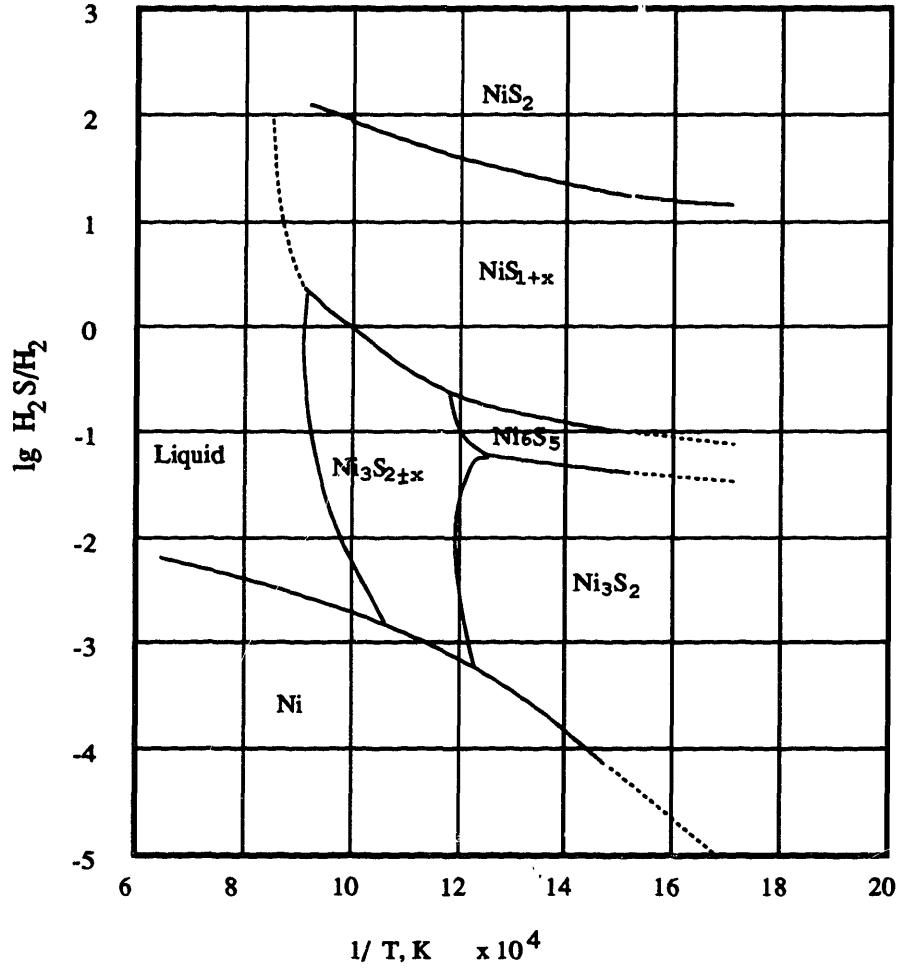

Figure 2-2: Hydrogen Reduction of Nickel Sulfides[63]

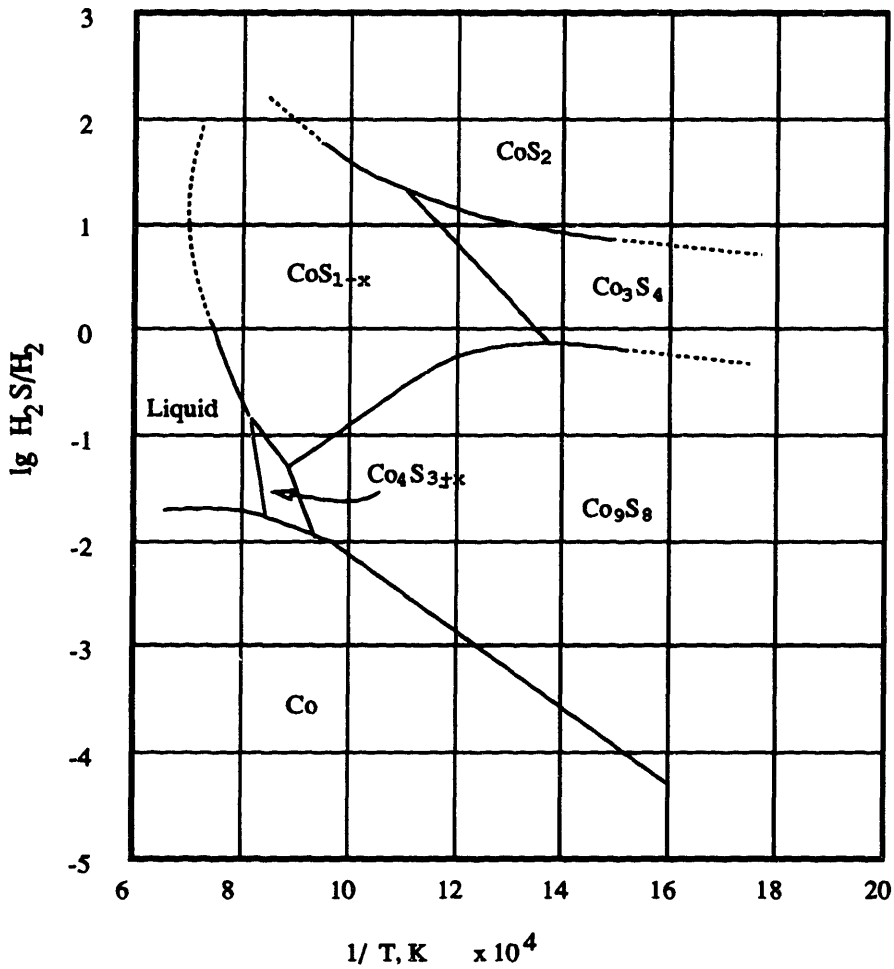

Figure 2-3: Hydrogen Reduction of Cobalt Sulfides[63]

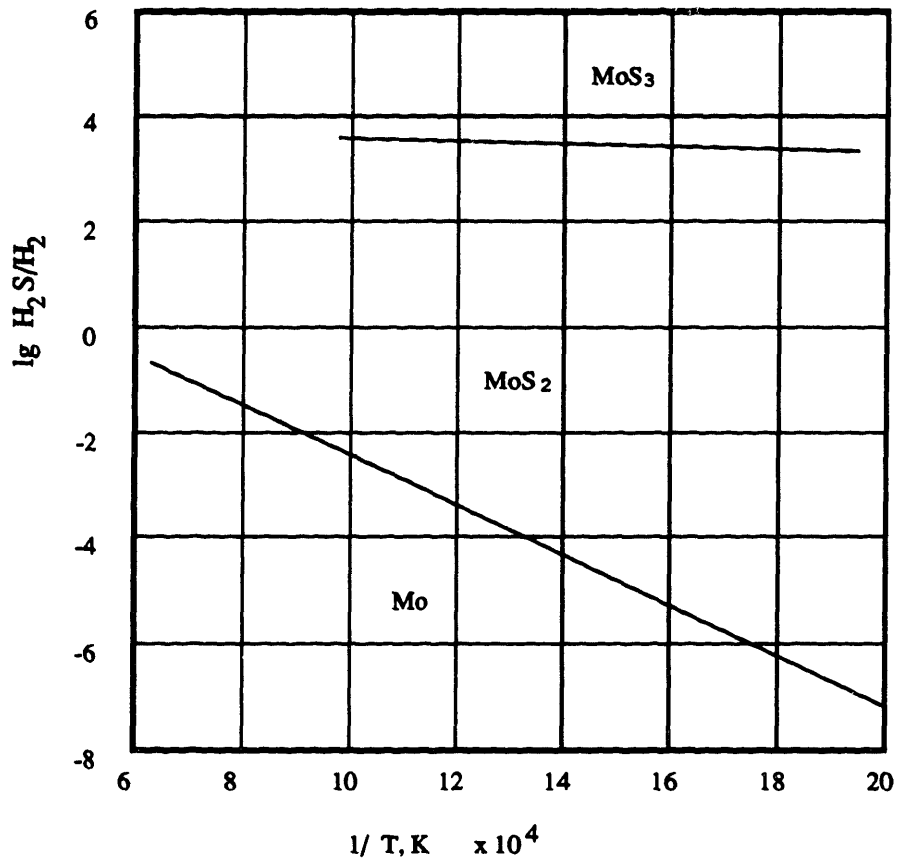

Figure 2-4: Hydrogen Reduction of Molybdenum Sulfides[63]

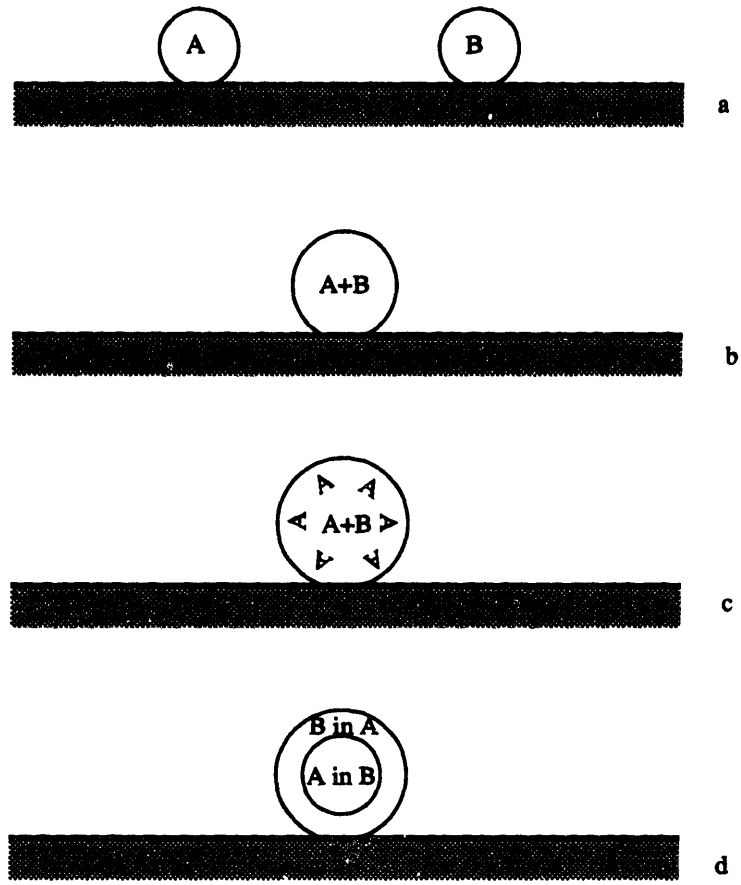

Figure 2-5: Possible Microstructures of a Highly Dispersed Alloy in a Substrate

Over 100 years ago, Gibbs[31] developed a comprehensive thermodynamic formulism for interface. The phenomena of surface segregation can be described in terms of that formulism by the use of the so-called Gibbs Adsorption Equation, which may be written for the case of an A-B binary system as:

$$d\gamma = -S^s dT - \Gamma_A d\mu_A - \Gamma_B d\mu_B \tag{2.1}$$

where γ is the surface energy, S^s is the specific surface excess entropy, Γ_A and Γ_B are the surface excess concentrations, and μ_A and μ_B are the chemical potentials of components A and B in the system, respectively. Applying regular solution model to Equation 2.1, one can obtain the following general result:

$$\frac{X_A^{surface}}{X_B^{surface}} = \frac{X_A^{bulk}}{X_B^{bulk}} exp\{-\frac{\Delta G}{RT}\} \tag{2.2}$$

where $X_A^{surface}$ and $X_B^{surface}$ are the respective fractions of components A and B in the bulk phase, while X_A^{bulk} and X_B^{bulk} are the equilibrium fractions in the surface phase, and ΔG is the molar free energy of segregation.

For solid systems, the free-energy, ΔG, is mainly composed of contributions from two terms: surface energy difference and strain release resulted from segregation, with the surface energy term as the dominant one [97] [101][129].

In a quasichemical approach for ideal solution where free energy ΔG can be expressed in terms of the difference in bond energy between an A atom and a B atom ΔE as:

$$\Delta G = \sum_i \Delta E_i \tag{2.3}$$

where i runs over all broken bonds of the surface atoms.

Therefore, we would expect a compound with a cleavage plane consisting of very

weak bondings should accordingly have low surface energy when the solid is cleaved from that particular plane.

Chapter 3

Hydrodemetallation Experiments

The practical application of what I have said is very close to the problem which I am investigating.

——Sherlock Holmes, *The Adventure of the Creeping Man*
Sir Arthur Conan Doyle

3.1 Chapter summary

Hydrodemetallation experimental procedures and equipment were detailed in this chapter. The properties and specifications of the catalysts, model compounds, and other materials used in the experiments are presented. The planning of the experiments are also discussed. In addition to catalyst sample preparation, the characterization techniques used in this study, including STEM, TEM, XPS, XRD, are briefly described. Characterization by scanning transmission electron microscopy (STEM) and high resolution transmission electron microscopy (HRTEM) showed that the de-

position of nickel sulfide on the catalyst surface enhanced the mobility of the catalytic components on the surface. The increarse of mobility was caused by the lowering melting point of Co_9S_8 and MoS_2. The effect was discussed with conceptual mobility phase diagrams.

3.2 Introduction

A significant part of the metal compounds in petroleum comprises of poorly characterized organometallic molecules. In order to reduce the obscuring occurrence of competing catalytic and thermally induced reactions encountered with petroleum and residual feedstocks and other uncertainties, model compounds are usually used to conduct kinetic and other laboratory studies. As a large part of metallic constituents in crude oil, petroporphyrins have been regarded as a suitable model compounds. Most of the reported hydrodemetallation studies have been performed with synthetic metal porphyrins[1][10][15][39][107][122][124][128]. Compared with industrially aged catalysts, the laboratory aged catalysts are comparatively free of carboceneous deposits. The metal loadings and aged conditions can also be easily controlled in order to obtain a clearer picture of the whole deposition phenomena.

3.3 Equipment

A one-liter batch autoclave reactor (*Autoclave Engineers, Model AFP 1005*) was used for the hydrodemetallation studies. The reactor system has been described previously by Hung [39] and Smith [106]. A schematic of the system is shown in Figure 3-1. The details of the autoclave are shown in Figure 3-2. A dual heating/cooling system in the autoclave allows a rapid isothermality of the reactor after the addition of feed at the initiation of each experiment. Modification to the reactor includes an addition of

a sintered stainless steel basket to hold the catalysts inside the reactor. The nominal pore size of the basket is about 7μm. Since the sizes of the porphyrin molecules are only about 1.0-1.2 nanometers [100], the basket does not block the access of the porphyrin molecules to the catalysts.

3.4 Model Compounds

Metal compounds in a crude oil are usually classified into two groups: porphyrinic and non-porphyrinic metal compounds. The non-porphyrinic part of the metal compounds are not yet to be well characterized, though the chemical information about the porphyrinic compounds are generally available. The latter usually accounts for about 10-50% of the metals found in crude oils [110]. For these reasons, metalporphyrins are regarded as suitable model compounds for studies on hydrodemetallation reaction. In this research, nickel etio-porphyrin, provided by *Midcentury*, (Posen, IL 60469), was used as the model compound for all the hydrodemetallation reaction. The molecular structures of the porphyrin is shown in Figure 3-3. Its solubility in squalane are about 20ppm at room temperature. At 588K, the solubility is unknown but higher than 300ppm [106].

3.5 Solvent

Squalane (2,6,10,15,19,23-hexamethyltetracosane) is used as the liquid carrier for metal porphyrins in the hydrodemetallation experiments. Squalane was supplied by *Sigma Chemical Co.*, (St. Louis, MO). It consists of 97.4% iso-paraffins, a small amount of naphthenes and aromatics. It is free of sulfur, nitrogen, or metal compounds. It is in liquid state at room temperature, and has a relative high boiling point (>673K), so that the vapor pressure is very small at reaction condition. Some

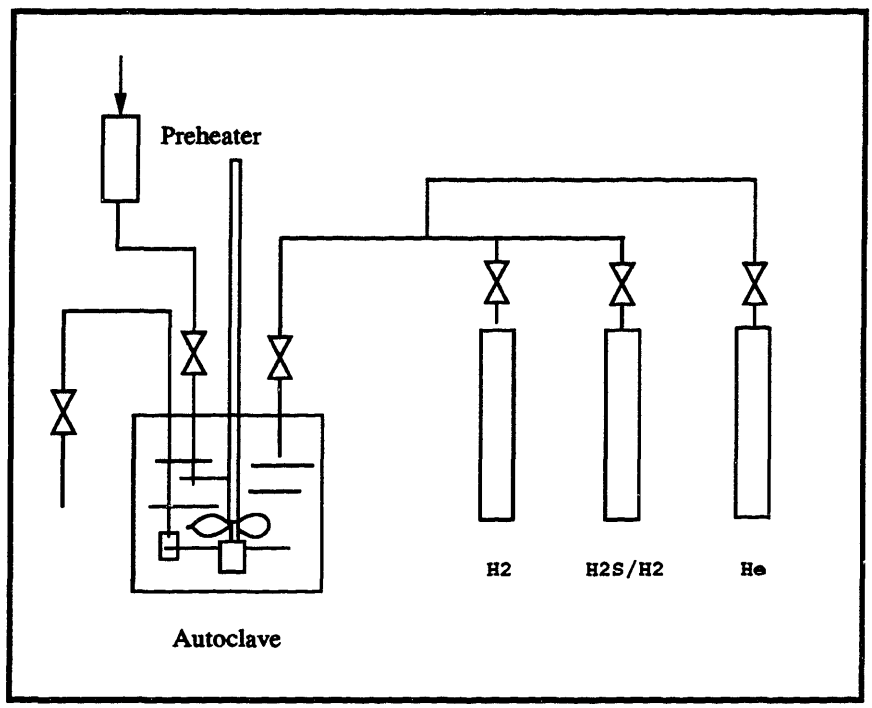

Figure 3-1: Schematic of the Hydrodemetallation Equipment

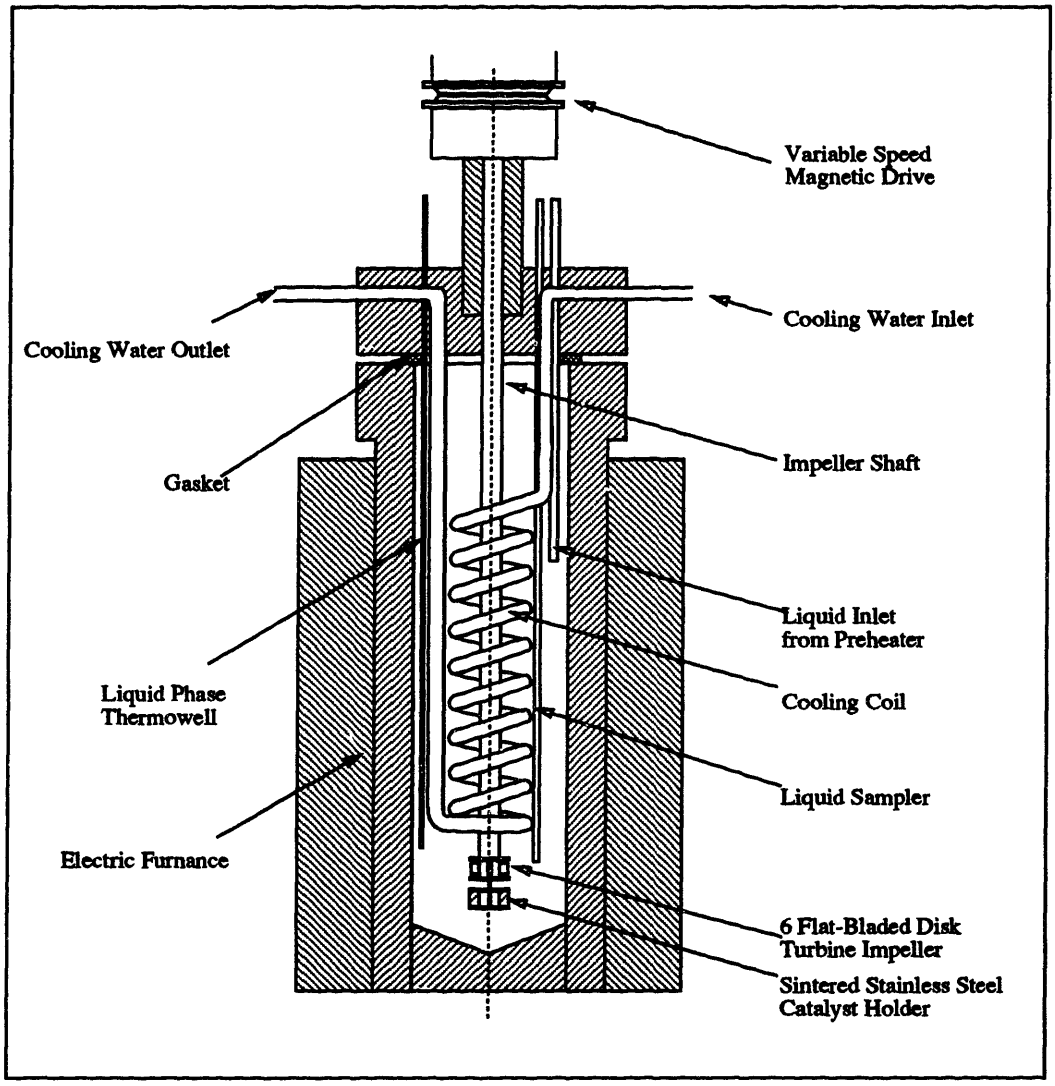

Figure 3-2: Schematic of the 1-litre Autoclave Reactor

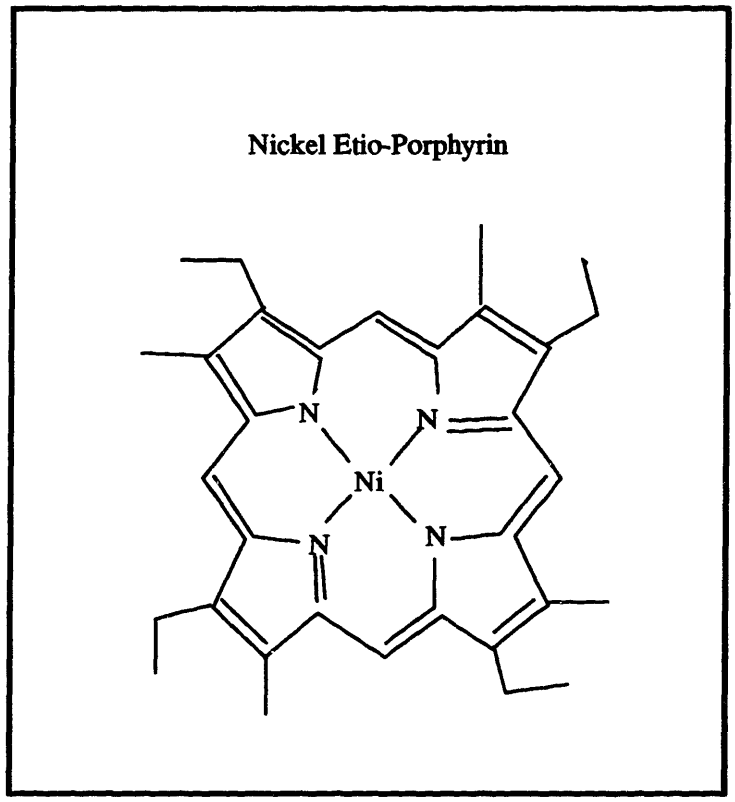

Figure 3-3: Molecular Structure of Nickel Etio-Porphyrin

of the important properties of squalane are listed in Table 3.1.

3.6 Catalysts

Catalysts used for this study are $Co-Mo/\gamma-Al_2O_3$ provided by *American Cyanamid Company.* As supplied, the cobalt molybdate catalysts consists of a mixture of metallic oxides on an alumina support. These catalysts are activated by pretreatment at atmospheric pressure with a mixture of 10 mol% H_2S, 90 mol% H_2. This pretreatment converts the metallic oxides to metallic sulfides (MoS_2, Co_9S_8). The procedure used in this research was adapted from that recommended by *American Cyanamid Company.*

Most of the previous work conducted in the MIT hydrodemetallation research group was conducted on a commercial $CoMo/Al_2O_3$ catalyst *American Cyanamid Aero HDS16A*[1][39][107][122]. In the present work, this catalyst is used as the base case study. Its chemical and physical properties are listed in Table 3.2. Meanwhile, another catalyst was prepared by *American Cyanamid Company* specifically for this work. The chemical compositions of both catalysts are listed in Table 3.2[1]. Both of the catalyst have the same element ratios. The molar ratios of molybdenum to cobalt on both catalysts are about 1.1.

3.7 Hydrodemetallation

The typical operating procedure was to load about 0.1 grams of catalyst of the size of 80μm into the sintered stainless steel basket, and load charge the reactor with about 300grams of squalane. The catalyst was dried at 383K overnight before being loaded.

The catalysts were presulfided *in-situ* by a 10 mol% hydrogen sulfide/hydrogen

[1]Thank Luhong for conducting the BET surface area measurement.

Table 3.1: Properties of Squalane

Supplier	Sigma Chemical Co.
Lot Number	116F-0221
Chemical Formula	2,6,10,15,19,23-hexamethyltetracoane
Molecular Weight	422.8
Elemental	
Sulfur	< 1ppm wt
Nitrogen	1ppm wt
Nickel	0.25ppm wt
Vanadium	< 0.05ppm wt
Hydrogen	< 15.29 wt%
Density at 273K	0.80610
Viscosity at 313K	19.26cS
Viscosity at 373K	4.149cS
P/N/A Distribution (wt%)	
Paraffins	97.40
Mono Naphthenes	0.00
Poly Naphthenes	1.75
Aromatics	0.85
Simulated Distillation by GC Analysis	
IBP	687K
50%	704K
90%	708K
95%	708K
FBP	716K

Table 3.2: Compositions of Catalysts

	Mo *wt%*	Co *wt%*	P *wt%*	Surface Area (m^2/g)
HDS16A	8.13	4.48	3.0	176
SN6931	5.09	2.87	2.21	171

Table 3.3: Properties of Catalyst HDS16A

Supplier	American Cyanamid Co.
Lot Number	MTG-S-0573
Chemical Properties:	
CoO	5.7wt% (dry basis)
MoO_3	12.2wt%
Na_2O	0.03wt%
Fe	0.04wt%
Ni	0.09wt%
Si	0.15wt%
P	3.00wt%
Al_2O_3	base
Physical Properties:	
Average diameter	0.152cm
Average length	0.432cm
Pore volume	$0.43ml/g$
Surface area	$176m^2/g$
Particle density	$1.49g/cm^3$
Median pore diameter	80.4 Å

gas mixture (*Matheson Gas Products*). After pressure testing, the reactor was purged for about 0.5 hours under a flow of helium(99.995% purity, *Matheson Gas Products*). Sulfiding was achieved with a mixture of 10 mol% H_2S/H_2 (*Matheson Gas Products*) flowing at a rate of about 200ml/min, according to the standard temperature program. The temperature was held at 448K for six hours, before being raised to 588K at a rate of 60K/hour, then maintained at the temperature for one hour.

Operating conditions for the hydrodemetallation experiments ranged from 588K to 623K at hydrogen pressure of 4.8mPa. The partial pressure of H_2S was maintained at about 14kPa (0.3vol.%), though it was not precisely controlled. The gas samples were routinely analyzed for hydrogen sulfide concentrations using gas detector tubes (Kitagawa, Japan, H_2S 1-150ppm).

Prior to each hydrodemetallation experiment run, the reactor was pressurized with a mixture of 10 mol% H_2S/H_2 and then hydrogen to pressures which would achieve the desired hydrogen sulfide partial pressure and total hydrogen pressure. Then, a slurry of nickel porphyrin in about 100ml squalane was added to the preheater. The preheater was then purged under the flow of helium before being heated to the same temperature as that of the reactor. Hydrogen was then introduced to the preheater to a pressure a little higher than the reactor pressure. The slurry is then injected to the reactor by open the valve between the reactor and preheater. The procedure was repeated twice with about 100ml squalane to ensure that no undissolved nickel porphyrin was left in the preheater. The flushing was later found essential because of the low solubility of nickel etio-porphyrin in the solvent. Even with the repeated flushing, it was found that some undissolved porphyrin remained in the bottom of the preheater. As a consequence, material balances for nickel were not obtained for most of the runs. The nickel loadings in the subsequent chapters are all referring to the nickel loadings actually obtained through atomic adsorption analyses.

Some of the hydrodemetallation runs were performed in a second reactor system.

The system has a two-liter autoclave reactor. It also allows a constant flow of 10 mol% H_2S/H_2 mixture, thus a better control of the hydrogen sulfide concentration in the system.

Catalyst HDS16A was used to study the development of deposits on the catalyst surface. Hydrodemetallation experiments was also conducted without hydrogen sulfide in the system and with unsulfided catalysts. The purpose was to study the form of different deposits on the catalyst surface.

Table 3.4 is a summary of the hydrodemetallation runs for which the aged catalyst samples were characterized by various techniques. Note that the metal loading are all at about 15-20%. The nickel loading is defined as the amount of nickel on fresh catalyst bases. The relatively lower metal loadings was chosen to avoid the domination of one compound over the others on the catalyst surface. It would be difficult to study the interaction if the nickel loading is either much higher or much lower than the cobalt and molybdenum loadings on the original catalysts.

3.8 Characterization

To prevent the aged catalyst samples from air exposure, both Smith [106] and Limbach [53] transfered the aged samples to a gloves-box filled with argon under the cover of oil before the preparation of characterization samples. The oxidation of the metal sulfide at ambient conditions is a relatively slow process [25] [118]. X-ray photoelectron spectroscopy showed that a minimal sulfur oxidation is observed after exposure to air for a week [25]. Nevertheless, all aged catalyst samples with the stainless steel baskets were transfered to a gloves-box filled with argon, and repeatedly washed with xylene and acetone before being dried in a self-sealing quartz crucible (*Fisher Scientific*). The catalysts are then ready for preparing any samples for characterization.

The major characterization tool was electron microscopy, including high resolu-

Table 3.4: Summary of Hydrodemetallation Runs

run	Catalysts	HDM Conditions			Aging Times (Hrs.)	Ni Loadings (wt.%)
		T (K)	P_{H_2} (MPa)	P_{H_2S} (KPa)		
1	HDS16	623	4.8	14	650	23%
2	HDS16	623	4.8	0	670	22.6%
3	SN6931	588	4.8	14	380	22.1%
4	HDS16	648	4.8	14	200	0%

tion transmission electron microscopy (HRTEM), and scanning transmission electron microscopy (STEM). The high resolution transmission electron microscopy allows us directly observed the structure of the deposits, while the scanning transmission electron microscopy offers a unique approach for measuring individual small crystallites which may be catalytically active as opposed to the averaging method employed in spectroscopic techniques.

During electron microscopic analysis, contamination of the surface of the specimen can be produced by the electrons polymerising hydrocarbons adsorbed on the surface from the residual gases in the vacuum. Contamination can also appear if there are residual oils on the specimen as in catalysts for hydrodemetallation in our system. Therefore, the repeated washing of the samples and careful handling with the specimen during microtome are essential to avoid the contamination during electron microscope analysis.

The sample preparation for electron microscopes was completed by embedding catalyst sample in resin, and ultramicrotoming to get specimen with the thickness of 60 to 80nm slices. The embedding medium was an ultra-low viscosity resin provided by *Ladd Research Industries, Inc.* The composition of the resin is listed in Table 3.5.

The detailed procedure for preparing the specimen is as follows:

1. A very small amount of aged catalyst particles are dispersed in a plastic embedding capsule. Any chucky clusters would be carefully blown away with a dust chaser. The particles should be in a very well dispersed layer on the bottom. The amount of catalyst particle should be as small as possible. Excessive amount of particles would cause difficulty to get complete specimens during microtoming.

2. Slowly pour the well-mixed resin into the capsules, and let the capsules sit overnight in a desicator for better infiltration. The resin was then cured in an

Table 3.5: Ladd Ultra-lowViscosity Embedding Medium

Weight	Materials	Weight Percentage
2.5g	4-vinylcyclohexene dioxide (VCD)	31.85%
5.25g	n-Hexenyl succinic anhydride (HXSA)	66.88%
0g	Diglycidyl ether of polypropylene glycol (DER-736)	0%
0.1g	Dimethylaminoethanol (DMAE)	1.27%

oven by slowly heating up to 333K and maintaining the temperature for 3 to 5 days. Some samples were cured at 333K for 10 hours, followed by 24 hours curing at 353K. Both of the curing procedures were found adequate for getting good block quality for microtoming.

3. The embedded samples were trimmed with a self-prepared glass knife into a trapezoidal shape on an LKB Ultratome III machine, with a face containing the specimen exposed to the knife for slicing. The face should be as small as possible to avoid unnecessary knife damage. Diamond knife was then used to cut the sample to get thin specimens with the thickness of about 60 to 80 nanometers. The microtome was conducted by following the procedure recommended by Jones[42]. The article by Rice & Treacy[90] also contains useful information on ultramicrotomy. Figure 3-4 schematically shows the slicing of samples during microtomy.

4. The specimen film is then supported on a copper grid and then coated with carbon for enhancing electron conductivity. The samples for TEM and STEM are virtually the same, though a thicker carbon coating was needed for STEM to allow the X-ray analysis.

The sample preparation for XPS and XRD are comparatively much simpler. The XPS sample was prepared by pressing the aged catalyst particles into an indium foil. The XRD sample is mounted in cement.

Total metal contents on the catalysts were analyzed at *Galbraith Laboratory, Inc.* by atomic absorption spectrophotometry (AAS).

Next, we will briefly discuss each of the techniques used in the studies, and show their uniqueness in characterizing catalyst samples.

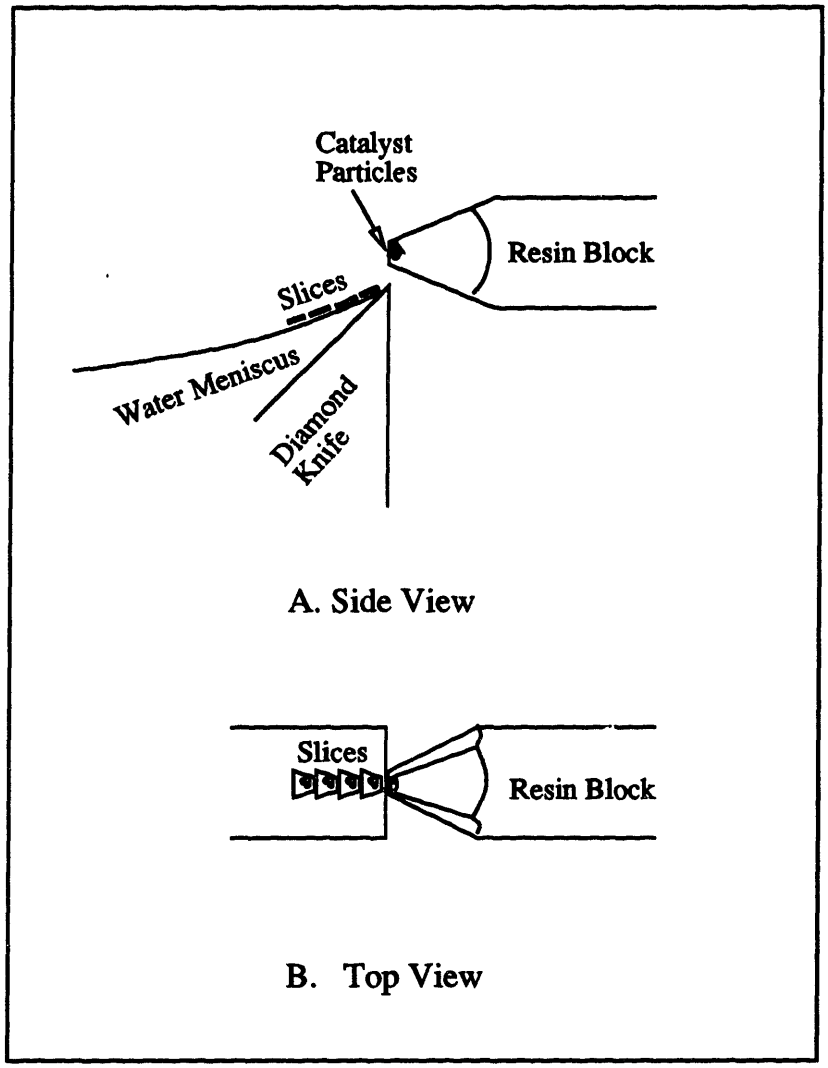

Figure 3-4: Schematic Diagrams of Ultramicrotomy

3.8.1 High Resolution Transmission Electron Microscope (HRTEM)

High Resolution Transmission Electron Microscopy is the only technique that make possible the direct description of the microstructure of solids in real space.

In a transmission electron microscope, a thin specimen is irradiated with an electron beam of uniform current density. Electrons are emitted in the electron gun by thermionic emission or by field emission. A two stage condenser-lens system permits variation of the illumination aperture and the area of the specimen illuminated. The electron-intensity distribution behind the specimen is imaged with a three or four stage lens system, onto a fluorescent screen. The image can be recorded by direct exposure of a photographic emulsion inside the vacuum.

Figure 3-5 illustrates the interaction of electron with a specimen. The electrons interact strongly with atoms by elastic and inelastic scattering. The specimen must therefore be very thin, typically of the order of a few tens up to a few hundred nanometers, depending on the density and elemental composition of the object and the resolution required.

TEM can provide high resolution because elastic scattering is an interaction process that is highly localized to the region occupied by the screened Coulomb potential of an atomic nucleus[89].

3.8.2 Scanning Transmission Electron Microscope (STEM)

As the name scanning transmission implies, an electron probe, formed by an objective lens incident on a thin specimen is scanned across it, and either the directly transmitted (bright field) or scattered (dark field) electrons are collected by an annular detector, whose output modulates a display scanned in synchronism with the signal in the scanning coils in the instrument. An energy analyzer is used to give elemen-

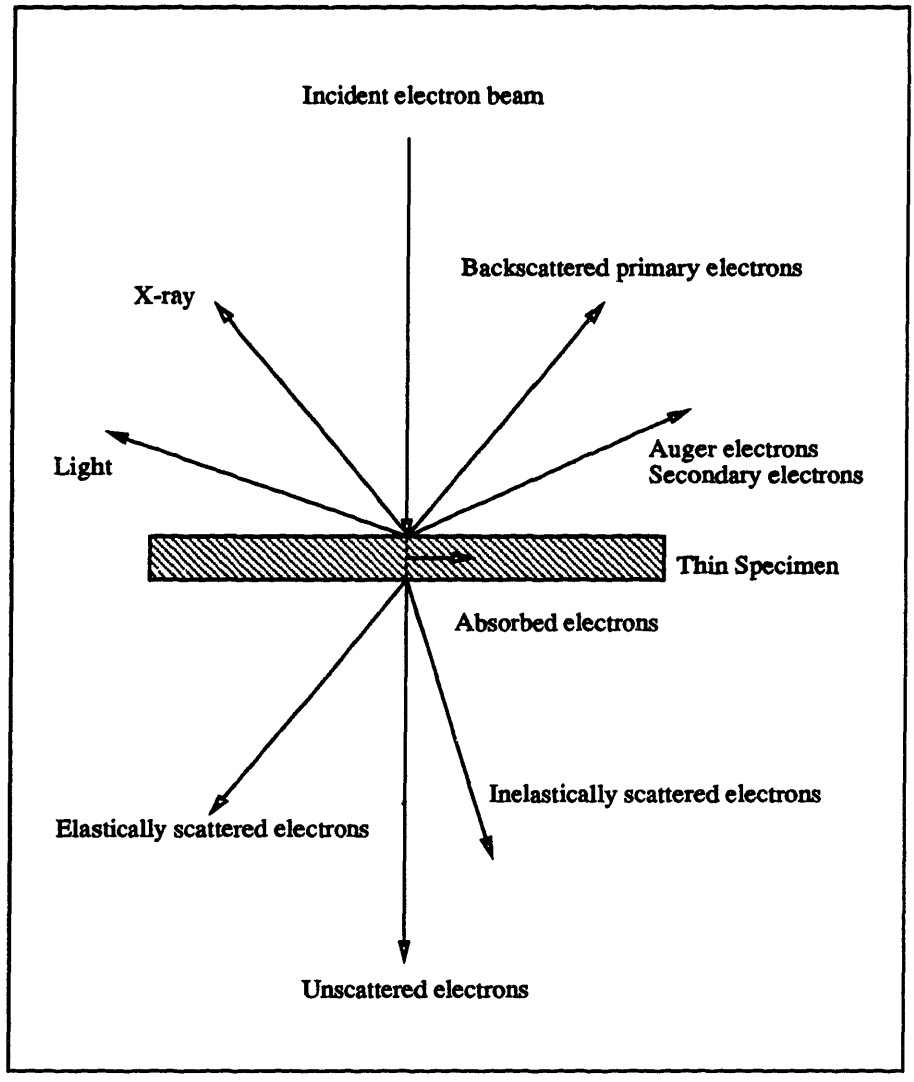

Figure 3-5: Signals Created by the Interaction of High Energy Electrons with the Specimen

tal analysis from specific energy losses. For a dedicated STEM, the scanning spots can be down to 1nm in diameter, obtained by demagnifying a field emitter source of electrons.

STEM is most attractive for a number of reasons. Firstly, it can be used to select very small (1-2nm) individual crystals, and give their diffraction patterns and X-ray emmision spectra, or *characteristic X-ray lines.* There is a simple relationship between X-ray frequency ν (or energy) and atomic number Z given by

$$\nu = 0.248(Z-1)^2 \times 10^{16} \tag{3.1}$$

Hence measurement of the energy of one of the X-ray emissions from an element allows that element to be identified.

Since the image of a thin specimen is always in view on the fluorescent screen, the area chosen for analysis can be located very accurately. An even greater advantage of thin specimens is that the resolution of the transmission image, which is about 10 -20 times greater that that of a scanning electron microscope image of a bulk specimen, allows the analysis to be correlated with fine details of ultrastructure[95][98].

The spatial resolution for analysis in a STEM system may well be limited by the stability of the specimen. Very small particles may move by more than the beam size during the time required to accumulate counts for analysis, and so for this application it is most important that the stage of the instrument be as free from drift as possible[30].

3.8.3 X-ray Photoelectron Spectroscopy (XPS)

X-ray photoelectron spectroscopy uses monochromatic X-rays such as Mg K_α (1254.6eV) or Al K_α (1486.6eV) as an energy source to irradiate the sample. Core electrons in the target with binding energy less than that of the incident photon can be ejected

and the energy spectrum of these photoelectrons are analyzed in a multiplier. Since the mean free paths of these low energy electrons are relatively small, typically below 5nm, XPS signals are very surface sensitive.

Since the energies of inner electrons are characteristic of the atom concerned, the identification of the atomic species present at the surface region of a solid may be carried out in a straightforward manner by X-ray photoelectron spectroscopy. One can identify the existence of specific elements by comparing the excitation lines with standard spectra.

One important application of the XPS is its ability for depth profiling, which can be accomplished by controlled erosion of the surface by ion sputtering. With alternating sputtering and XPS analysis, it can provide a concentration profile within the outmost layer of a material.

3.8.4 X-ray Diffraction Analyzer (XRD)

X-ray diffraction was conducted for the aged catalyst samples to identify the crystal structure of the nickel deposits on the catalyst surfaces.

3.8.5 Surface Area Measurement(BET)

The surface area of the catalysts were measured by nitrogen desorption with the standard one-point B.E.T. method.

Chapter 4

Nickel Deposition on $Co-Mo$ Catalyst

The world is full of obvious things which nobody by any chance ever observes.

——Sherlock Holmes, *The Hound of Baskervilles*
Sir Arthur Conan Doyle

4.1 Chapter Summary

Nickel deposition from nickel-etio porphyrin on sulfided and unsulfided $CoMo/\gamma Al_2O_3$ hydrodemetallation catalysts were investigated. The bare and aged catalysts were characterized by high resolution electron microscope, scanning transmission electron microscopy and X-ray diffraction analyzer. Nickel deposits are found in crystallite

[1]This chapter is a revision of reference[127] J. Wei & X. Zhao, Chem. Eng. Sci. 47, 2721, 1992.

form. The average sizes of the crystallites are about 10 to 15 nanometers at the nickel loading of about 20%. Both element mapping and XEDS microanalysis from scanning transmission electron microscope showed that the elemental distribution of deposited nickel were correlated with elemental distributions of cobalt, but not with elemental distributions of molybdenum.

4.2 Introduction

Although electron microscopic investigation of hydrotreating catalysts has been a subject of many researches[20] [21], studies on aged catalysts are still very scarce[108] [112] [116] .

Metal deposition patterns on hydrodemetallation catalyst has been a subject of wide speculations. Uniform layer deposition was the most widely assumption until Toulhoat *et al.*[116] and Smith & Wei[108] directly showed by using microscopic techniques that nickel deposits are in segregated large crystallite forms. Smith & Wei suggested that the number density of nickel deposit crystallites might be related with the loadings of catalytic metals on the catalyst surface. However, they did not speculate with which component that nickel might be associated.

4.3 Electron Microscopy Results

In the microscopic studies reported in this and subsequent chapters, care was taken to ensure that the area and particles studied and analyzed are representative of the catalyst samples. Samples are usually examined at low magnification for any inhomogeneities.

The characterization was conducted on two electron microscopes. One was a dedicated scanning transmission electron microscopy (VG HB5, *Vacuum Generator*)

equipped with Link energy dispersive X-ray analyzer. X-ray mapping and chemical microanalysis were obtained at 100keV, with a nominal probe size of about 2nm. The other was a high resolution transmission electron microscope (Akashi Topcon EM002B, *Akashi Beam Technology Corporation*) with a point to point resolution of 0.18nm(200keV).

4.3.1 Bare Catalyst

Figure 4-1 is a micrograph taken on STEM of a HDS16A catalyst sample. The catalyst sample was sulfided but was not subjected to hydrodemetallation. We could see from the picture the existence of the alumina platelets of the catalyst substrate. The sizes of these alumina platelets are estimated to be about 100 nanometers in length and 5 nanometers in width. No structures of the molybdenum or cobalt sulfides could be observed due to the resolution of the instrument. An X-ray elemental mapping of the catalyst did not reveal much details either (Figure 4-2). However, The mapping results did tell us that both cobalt and molybdenum are very well dispersed on the substrate.

Figure 4-3 is a micrograph from high resolution transmission electron microscope for the same catalyst sample. Consistent with literature reports[18][20][80][96], we could see many randomly oriented molybdenum disulfide slabs. The lengthes of the slabs usually exceeds 10 nanometers. The slabs have usually four to five layers, but it would be difficult to observe the slab of one or two layers. No cobalt sulfide was observed on the surface. According to literature[20][21], the difficulty of observing Co_9S_8 may be associate with the low intensity of the main reflections of Co_9S_8 crystals. Comparatively, the existence of a strong (002) reflection for MoS_2 made it relatively easier to be observed and to be distinguished from other crystals. Thus, the absence of electron microscopic evidence does not rule out the existence of tiny Co_9S_8 crystals.

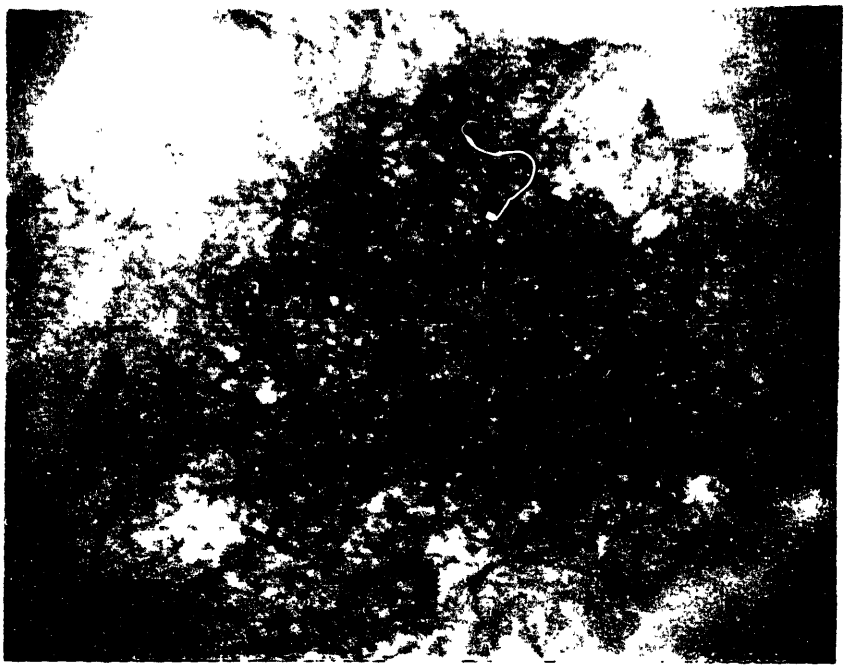

Scale: 100nm

Catalyst: HDS16A
Aging Time: 0hrs.

Temperature:
H_2 Pressure:

Figure 4-1: Electron Micrograph of Bare HDS16A Catalyst

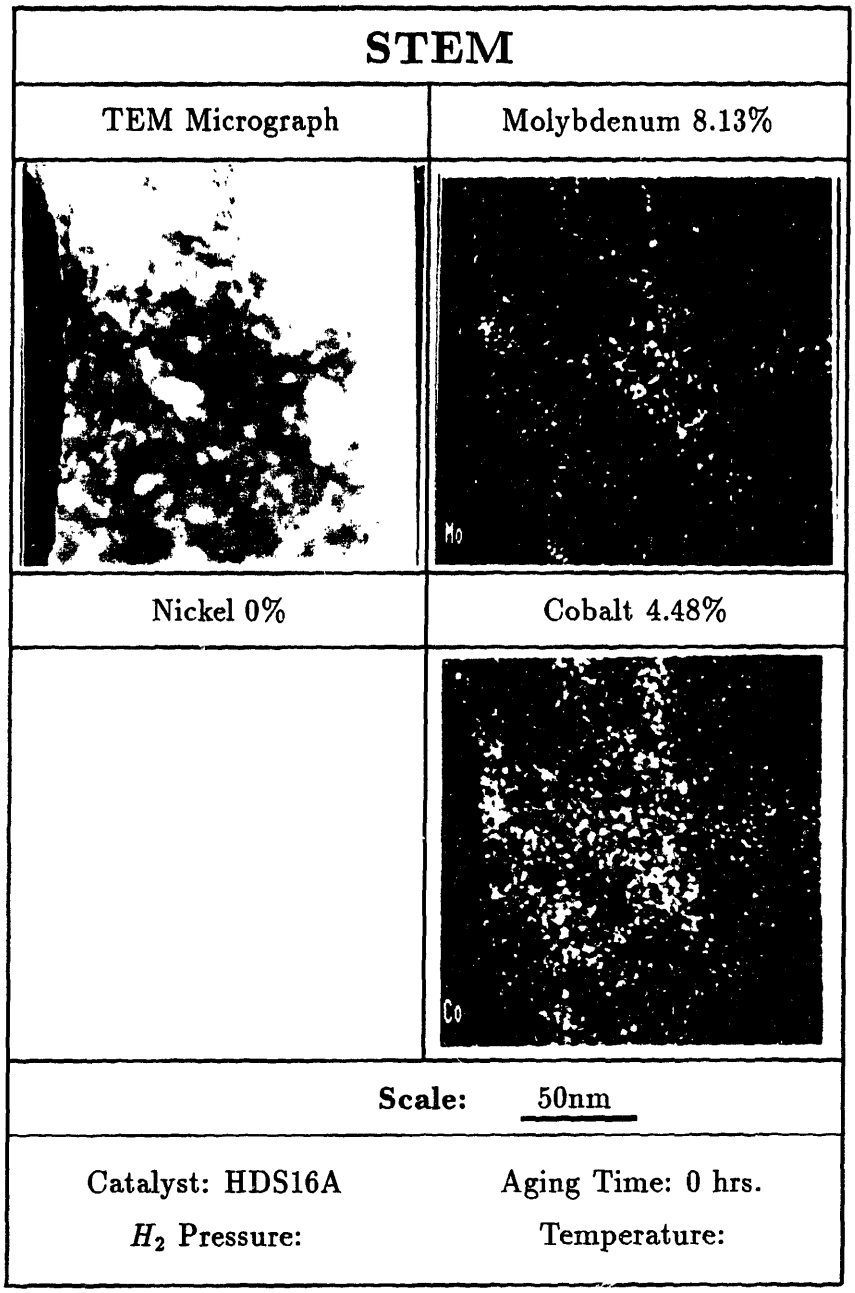

Figure 4-2: Elemental Mapping of Bare HDS16A Catalyst

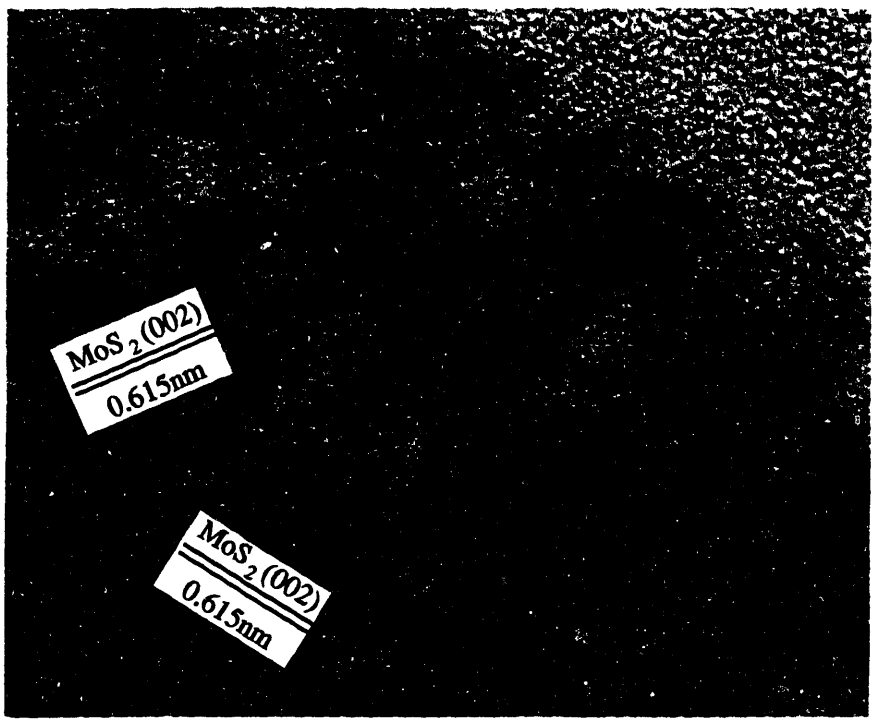

Scale: 5nm

Catalyst: HDS16A Temperature:

Aging Time: 0 hrs. H_2 Pressure:

Figure 4-3: High Resolution Image of Sulfided Bare HDS16A Catalyst

4.3.2 Sulfided Catalysts

Figure 4-4 is the micrographic image of a sulfided catalyst sample (SN6931) aged at 588K. One dominant feature is the presence of many dark spots, which XEDS confirm to be nickel sulfide crystallites.

Figure 4-5 is a set of element mapping images of the central area of the sample in Figure 4-4, which gives us not only the sizes and numbers of the deposition crystallites, but also direct information of the locations of each element and their interrelations. Although many crystallites are as large as 30 to 40 nm, there are also many crystallites of about 0.5nm. The average sizes of the crystallites were very roughly estimated to be about 10 to 15 nanometers. One important finding is the association between cobalt and nickel on the mapping. Particularly, we can see a distinct nickel crystallite at lower left side of the map, and there is a corresponding cobalt site, but no detectable molybdenum was seen at that site. In addition, we can also see that the cobalt crystallite on the catalyst seems in discrete forms, but the nickel deposition crystallite come together and form large entities. It suggests that at high metal loading, the neighboring deposition crystallites could coa lesce.

Figure 4-6 is a set elemental mapping results for an aged HDS16A catalyst with about 23% nickel loadings. The association between nickel and cobalt is apparent. The nickel and cobalt maps well correspond to the black spots on the TEM micrograph. The large crystallite in the left side of the picture will be further characterized for elemental distribution in Chapter six.

STEM has a fine probe beam size of about 2nm, while the sizes of many deposition particles are about 10nm or even larger. Therefore, it was possible to place the beam on some distinct crystallites to analyze the compositions of individual crystallites. Unfortunately, we can not determine the absolute composition for each particular analysis, since we do not know the amount of alumina and other elements in this particular area. Nevertheless, we can still get the relative compositions of each

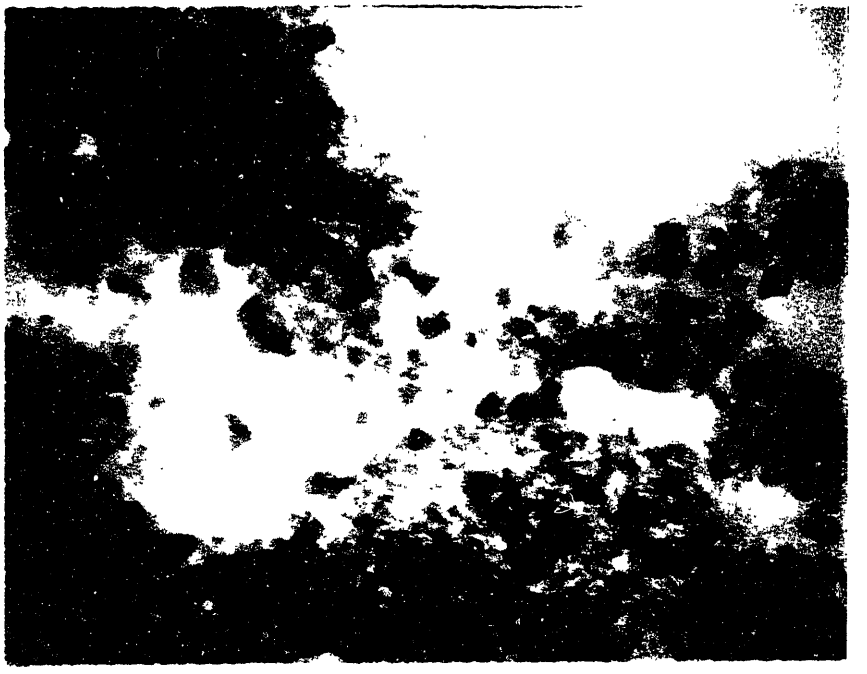

Scale: 50nm

Catalyst: SN6931 Temperature: 623K

Aging Time: 380hrs. H_2 Pressure: 4.8 MPa

Figure 4-4: Electron Micrograph of Aged Sulfided SN6931 Catalyst

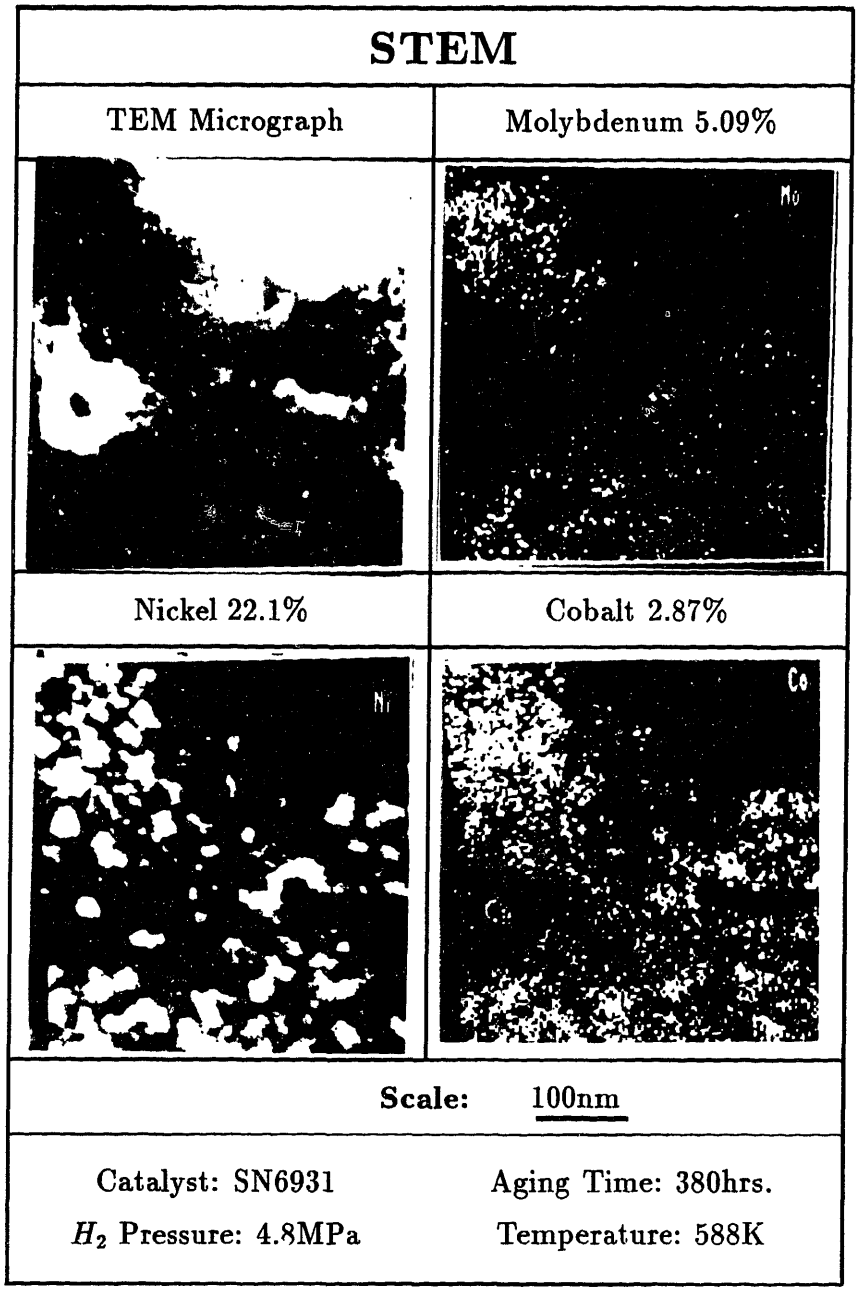

Figure 4-5: Elemental Mapping of Aged SN6931 Catalyst with Sulfur

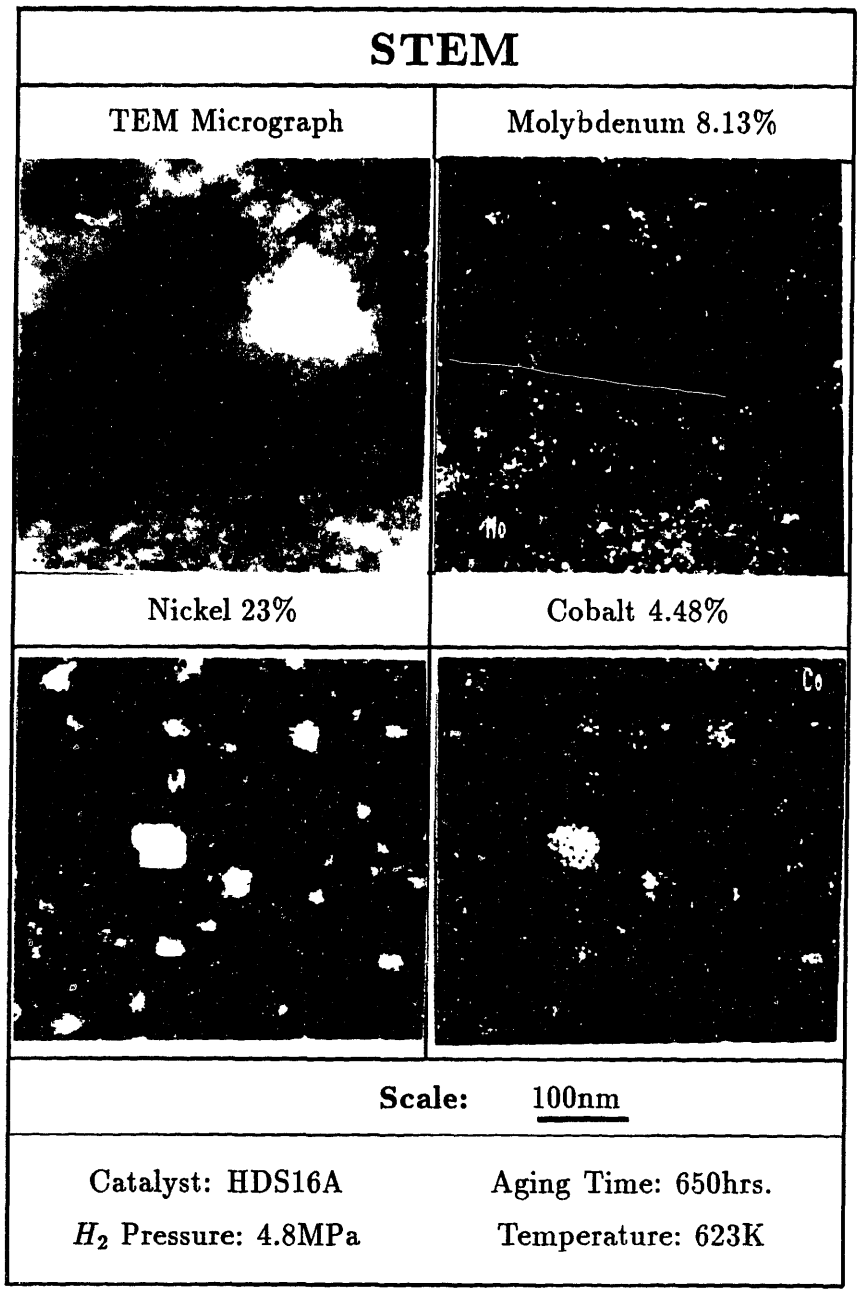

Figure 4-6: Elemental Mapping of Aged HDS16A Catalyst with Sulfur

crystallites. Although most of the analyses were conducted by focusing the beam on distinct crystallites, some analyses were conducted by purposely positioning the beam on some featureless background. Figure 4-7 and 4-8 are plots of the normalized compositions of the deposited nickel and the two catalytic metals, cobalt and molybdenum in triangular and cartesian plots. The line in the triangular plot represents the molybdenum/cobalt ratio on the original catalyst. It is clear that those sites with lower Co/Mo ratio have a lower concentration of nickel deposition, while those sites with higher Co/Mo ratio show a much higher nickel concentration, indicating that most of the nickel is associated with cobalt, but not with molybdenum. The error bar represents a typical intrinsic error of the EDS technique calculated from the counts when conducting analysis. The procedure worked out by Furdanowicz[28] was used for the calculation of multicomponent analysis. The trends are significant. Emphasis was placed on identifying qualitative trends rather than quantitative results which would be difficult to support because of the variations within the small samples.

It should be noted that each sample on the X-ray microanalysis plot corresponds to one particular sites on the catalyst surfaces. The absolute composition of each particular element is unknown since the amount of other elements are not available. Therefore, the absolute amount of the elements are not comparable for the different analyzing sites. Nevertheless, we can still see a clear tendency of the association between Co and Ni. As we have pointed out, The aim is to develop physical insight and to recognize trends, rather than to explain every observation.

4.3.3 Unsulfided Catalysts

Figure 4-9 shows a set of elemental maps of unsulfided HDS16A aged at 623K. The image of nickel deposition shows a striking correspondence to that of the cobalt. Some of the interesting locations are marked on the mapping pictures. While there is no apparent correspondent molybdenum at location 3, the images of nickel and cobalt

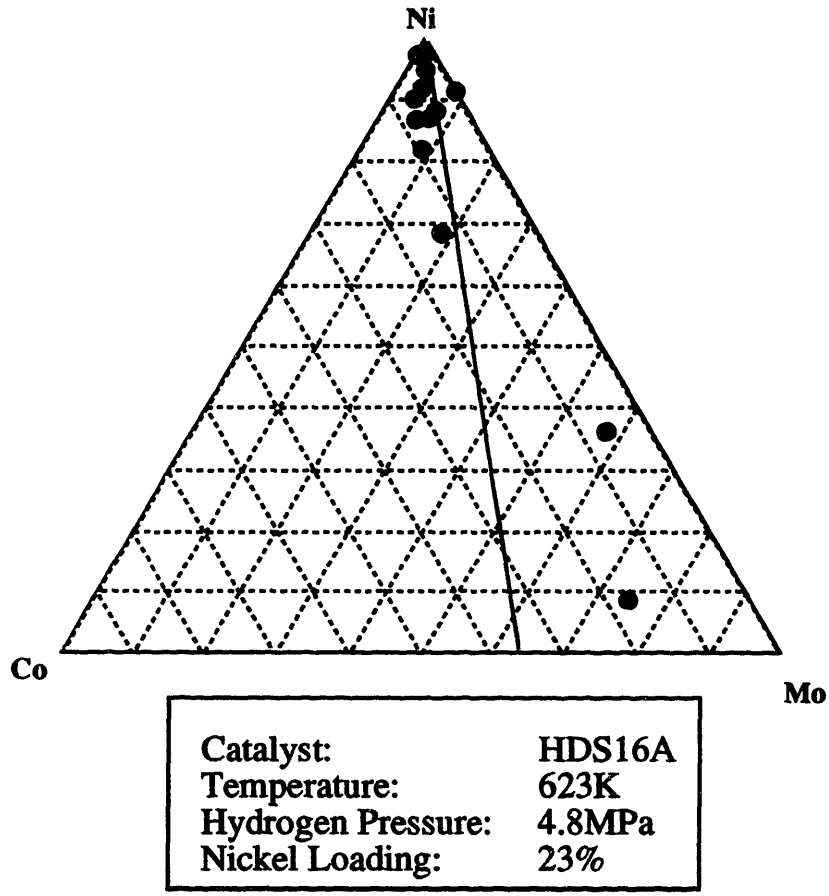

Figure 4-7: EDS Microanalysis of Aged HDS16A Catalyst

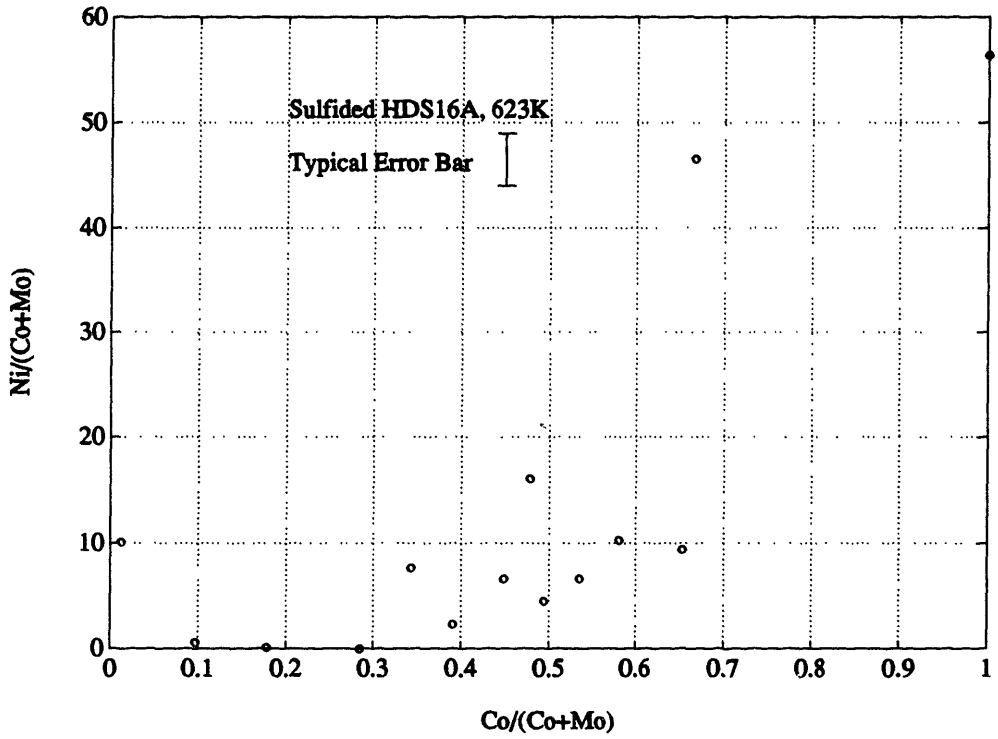

Figure 4-8: EDS Microanalysis of Aged HDS16A Catalyst

are apparently similar. The image of molybdenum is more or less randomly dispersed on the whole surface. In addition, it was observed that the distribution of iron on the catalyst was very well corresponded to that of cobalt. The iron was probably from the sintered stainless steel basket holding the catalyst during the hydrodemetallation reaction.

Similarly, microanalysis was also conducted on the unsulfided aged catalyst. The result is shown in Figure 4-10 and Figure 4-11. Apparently, the trend is quite similar with the one observed on sulfide catalyst.

4.4 X-ray Diffraction Results

The X-ray diffraction was conducted on a Rigaku diffractameter. Figure 4-12 shows the X-ray diffraction spectra for an aged HDS16A catalyst sample, which has about 23% of nickel loading. The spectra clearly indicate the existence of bulk phase Ni_7S_6, although we were expecting Ni_3S_2, as being obtained from the work of Smith & Wei[108]. The difference is probably a result of the inaccurate control of the partial pressure of hydrogen sulfide for the hydrodemetallation experiments.

It is peculiar that there is no Ni_7S_6 in the reduction phase diagram we presented in chapter two. One literature[48] did indicate that the diffraction pattern of Ni_7S_6 was very similar to the earlier reported diffraction pattern of Ni_6S_5 by Lundqvist[59]. Considering the data used for the phase diagram shown in Figure 2-2 was reported in 1954 [93], the Ni_6S_5 phase in the phase diagram could be simply a misidentification.

4.5 Discussions

There were a lot of speculations about the possible deposition patterns of nickel deposits on the catalyst surface, *e.g.* layer deposition, random deposition, crystallites.

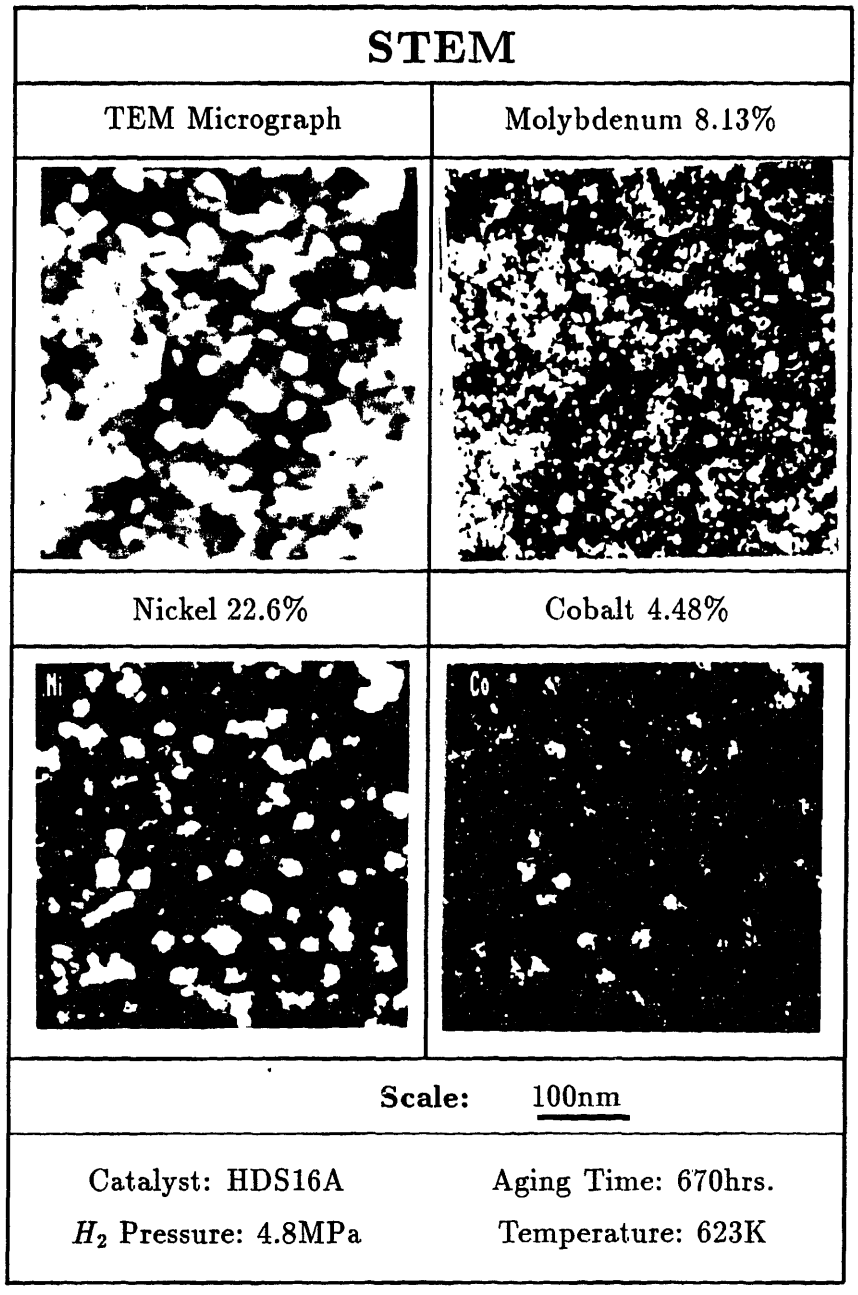

Figure 4-9: Elemental Mapping of Aged HDS16A Catalyst without Sulfur

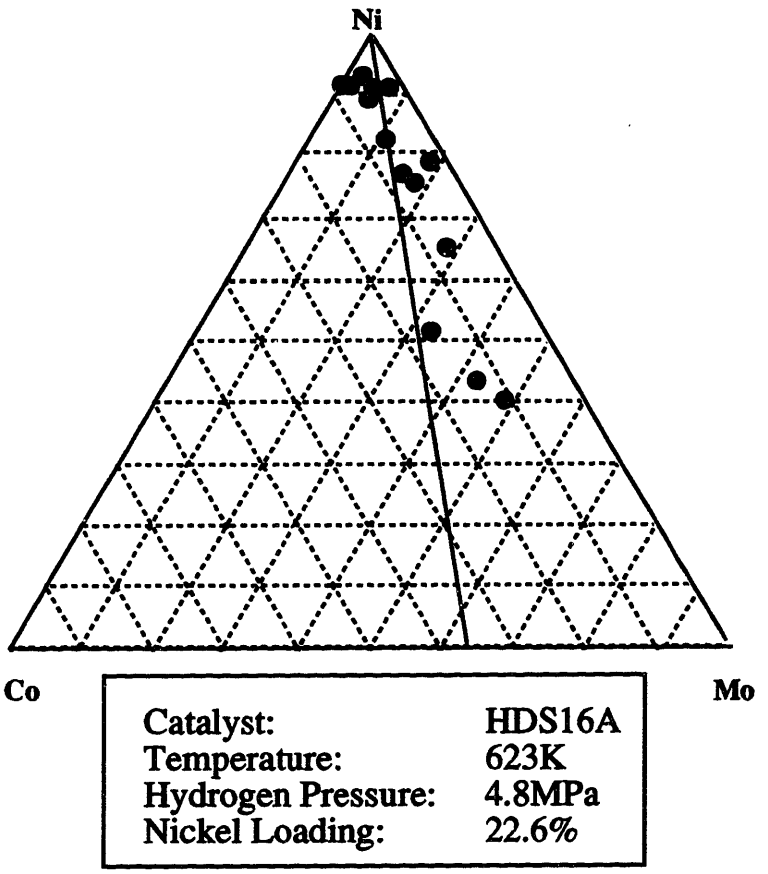

Figure 4-10: EDS Microanalysis of Aged HDS16A Catalyst without Sulfur

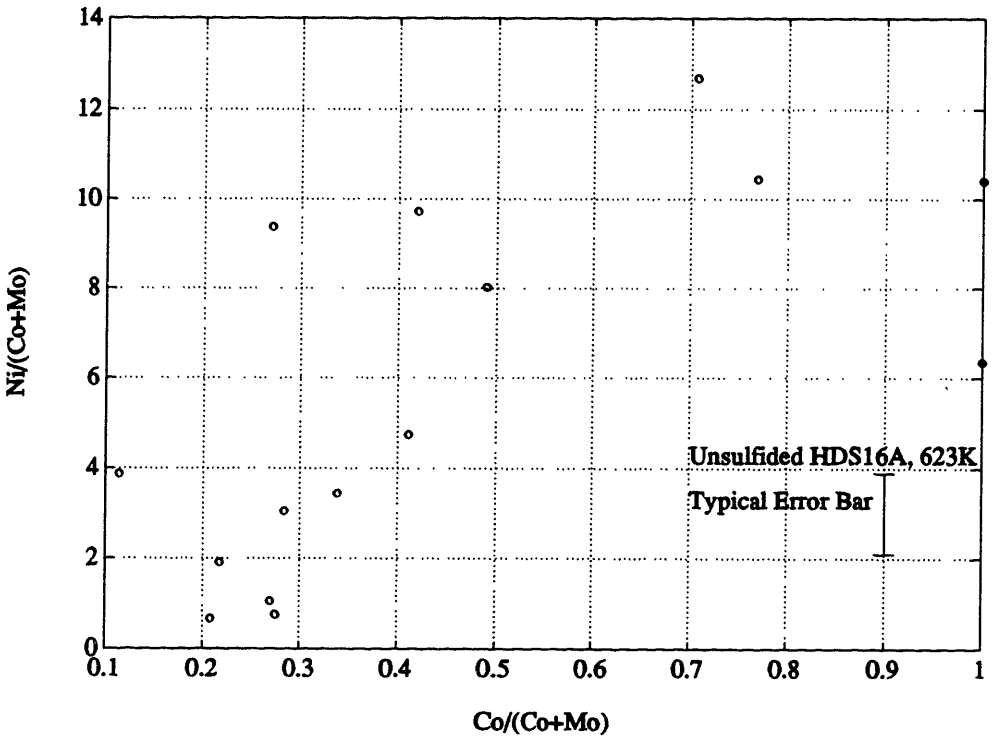

Figure 4-11: EDS Microanalysis of Aged HDS16A Catalyst without Sulfur

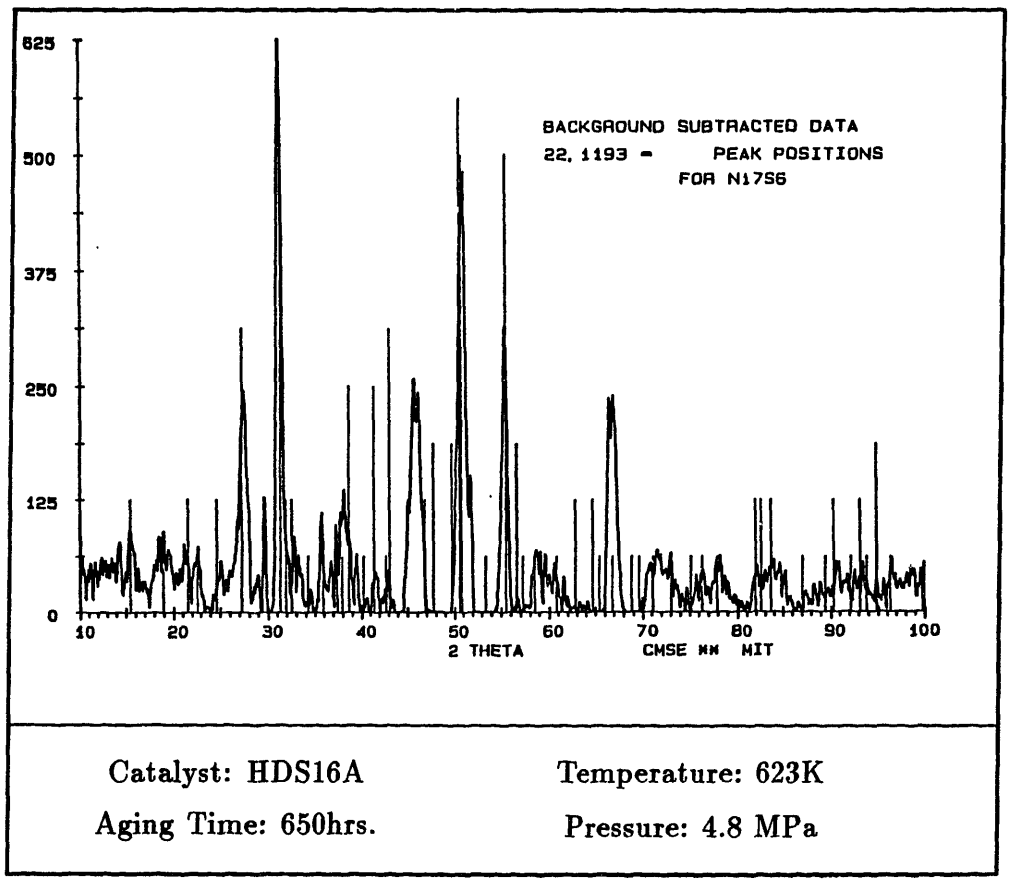

Figure 4-12: X-ray Diffraction Spectra of Aged HDS16A Catalyst

Smith & Wei[108] suggested that the nucleation sites for nickel deposits on the catalyst surface might be related with the loadings of catalytic components *Co, Mo, P*, on the catalysts. Among all the possible deposition sites, cobalt is the less expected sites for nickel deposits, due to the fact that molybdenum sulfide is the active sites. We will address the mechanism for the deposition and the reason that nickel is associated with cobalt on the catalyst surface in the coming chapter. Here we want to emphasize that the observation itself is a very significant result in a sense that we, for the first time, know that nickel deposits are not randomly distributed are the catalyst surface. Instead, it forms identities with cobalt sulfide on the catalyst surface. The understanding of the structure of the deposits maybe well be the first step for the development of improved hydrodemetallation catalysts.

4.6 Conclusions

Catalytic hydrodemetallation of model compound nickel etio-porphyrin was conducted with presulfided $Co - Mo/\gamma Al_2O_3$ catalysts. The catalysts before and after hydrodemetallation were characterized by using scanning transmission electron microscope, high resolution transmission electron microscope, and X-ray diffraction analyzer. On a separate experiment, an unsulfided catalyst aged under similar condition is also characterized by scanning transmission electron microscope.

1. On the sulfided catalyst before being subjected to hydrodemetallation, we could observe the layer structure of molybdenum sulfide. The crystals usually consists of about four to five layers of S-Mo-S, with the average lengths on the order of a few nanometers. No crystals of cobalt sulfide were observed.

2. Nickel deposits on hydrodemetallation catalyst in crystallite form. The sizes of these crystallites vary in a wide range. At the metal loading of about 20%, the

largest ones observed are around 40nm, while the smallest ones detected are around 0.5nm. The average sizes were roughly estimated to be about 10 to 15 nanometers.

3. Elemental mapping and XEDS microanalysis show that nickel deposits are preferentially associated with cobalt for both sulfided and unsulfided systems. This is a very significant result for the following reasons. First of all, the results for the first time directly shows that the deposition is neither a uniform layer distribution as being modeled[43][55][86], nor randomly distributed on the catalyst surface, as has been suggested[125]. Secondly, since molybdenum sulfide is considered the active sites for all the hydrotreating reactions, including hydrodemetallation, while cobalt sulfide is only a promoter on the catalyst. The fact we showed that nickel deposits are associated with cobalt instead of molybdenum could have significant implications on the deactivation of hydrodemetallation catalysts. This subject will be pursued further in the coming chapters.

Chapter 5

Deposition Mechanism

We imagined what might have happened, acted upon the supposition, and find ourselves justified.

——Sherlock Holmes, *Silver Blaze*
Sir Arthur Conan Doyle

5.1 Chapter Summary

Two possible mechanisms for the associations of nickel and cobalt are proposed: activity of cobalt site, or migration after deposition. To differentiate the two deposition mechanisms, $CoMo/\gamma Al_2O_3$ catalyst with 10% impregnated nickel was treated under hydrotreating conditions without nickel-porphyrins. It was observed that the nickel on the catalyst surface migrates towards cobalt sites, though the initial deposition was uniformly distributed on the surface without any preference to either cobalt or molybdenum. Previous activity studies on cobalt-only or molybdenum-only catalysts

support the theory that molybdenum sulfide, not cobalt sulfide, is acting as the main active component.

5.2 Introduction

The association of nickel with cobalt on the elemental mapping could have two different implications. Either the activity of cobalt sites or the migration of nickel deposits could have been caused the association. The thermodynamic analysis in chapter two favors the argument of migration of deposits and formation of solid solution. However it did not exclude the possibility of the activity of cobalt. We found a previous work by Hung [38]. Hung conducted kinetic studies on $Co/\gamma Al_2O_3$ catalyst, $Mo/\gamma Al_2O_3$ catalyst and $CoMo/\gamma Al_2O_3$ catalysts for hydrodemetallation reaction, respectively. It was shown that the Mo-catalyst is much more active than Co-catalyst, although both of them are active for the hydrodemetallation reaction, as shown in Figure 5.2. Therefore, it is unlikely that cobalt solely is acting as the active entity for hydrodemetallation on $CoMo/\gamma Al_2O_3$ catalysts. A plausible explanation for the association of nickel with cobalt is that the nickel sulfide preferentially migrates to cobalt sites after being deposited on the catalyst surface. Considering that the Tammann temperature for nickel sulfide is only about 530K, which is much lower than the hydrodemetallation temperature of about 588-623K, nickel sulfide should be very mobile. The mobility of nickel sulfide on hydrotreating catalyst was reported in literature [9].

It should be pointed out that Hung's work [38] was conducted in unsulfided systems.

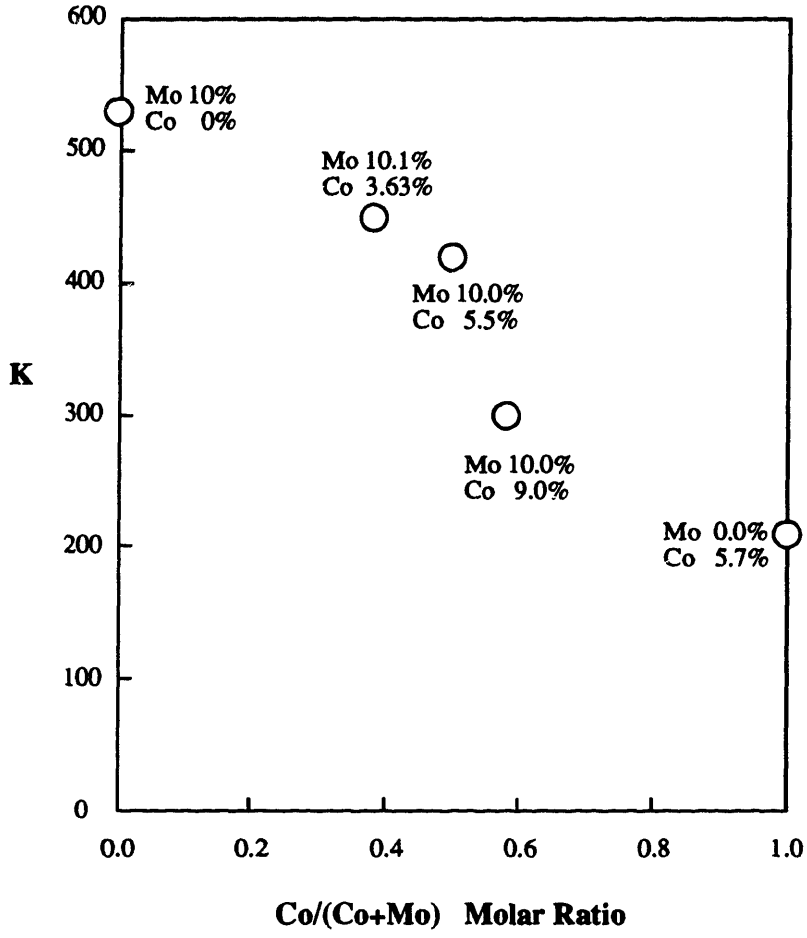

Figure 5-1: Activity of Catalysts with different Cobalt Contents[9]

5.3 Migration Experiment

To further confirm the migration of nickel deposits on the catalyst surface, the following experiment was designed. Instead of hydrodemetallation reaction, nickel was impregnated on the CoMo catalyst. The catalyst with nickel was put back to the reactor under the same condition with hydrodemetallation reaction condition, but with no nickel porphyrin added. The aim was to observe the development of the nickel on the surface.

The impregnation procedure was the same as the way to making nickel catalyst, the procedures is as follows[38]:

1. The HDS16A $CoO-MoO_3/\gamma Al_2O_3$ catalyst was crushed into 170-200 mesh size (d=0.081mm), and then placed in a tubular furnace at 713K to for 24 hours to remove water.

2. Nickel solution was prepared from nickel nitrate, *Fisher Scientific Co., Fair Lawns, N.J.;* $Ni(NO_3)_2 * 6H_2O$*; F.W. = 290.81;* NiO *=25.69%.* To prepare a solution which would give a 10% nickel loading on the catalyst, 4.42grams of nickel nitrate was dissolved in 5ml distilled water.

3. Two grams of the dried catalyst was placed in 20ml beaker. Nickel nitrate solution in amount equal to the pore volume of the catalyst sample (0.88ml) was added slowly. The mixture was then stirred for 20 minutes to ensure proper mixing. It was then placed in an oven at 383K for 5 hours to evaporate water.

4. The sample was then placed in a quartz tube and calcined in a preheated tubular furnace at 823K for 8 hours under a slow flow of air (1-2mm/sec).

5. The sample was then cooled and stored for further experiment and characterization.

5.4 Characterization Results

Again, the characterization was conducted on the same dedicated scanning transmission electron microscopy *VG HB5* with *Link* energy dispersive X-ray analyzer we have discussed in Chapter 4. The X-ray mapping and microanalysis were obtained at 100kev, with a nominal probe size of about 2nm.

5.4.1 Catalyst with Impregnated Nickel

The element mapping showed that the impregnated nickel and the catalytic metals, or Mo and Co, are all very well dispersed on the surface. A typical crystallite measures about 1.5 to 2nm, though that is the limit of the STEM instrument.

Since no apparent crystallites could be observed within the limit of instrument. XEDS analysis was basically conducted on some random locations on the catalyst. The analysis result is shown in Figure 5-3. Apparently, nickel has no preference to either cobalt or molybdenum as expected.

5.4.2 Catalyst with Impregnated Nickel after Being Treated

The catalyst with nickel was then put into a reactor under the same condition with the hydrodemetallation experiment. The aim was to observe the development of the deposition on the catalyst surface.

After about 200 hours under the temperature of 648K and hydrogen pressure of 4.8 MPa with 0.3% of hydrogen sulfide, the catalyst sample with impregnated nickel was characterized again by the STEM. Although some crystallites were observed on the surface, elemental mapping was not sufficient to provide the evidence for migration. On the other hand, the XEDS analysis result evidently indicates that nickel and coablt are associated with each other as shown in Figure 5-5. The normalized local loading of nickel deposits increases with the normalized local loadings of cobalt, which

indicates the association between nickel and cobalt on the catalyst.

Compared with Figure 4-7 and Figure 4-10, the association of cobalt with nickel is not as strong. It is due to either the shorter time, or the difficult of migration once the nickel deposits on the surface.

It should also be pointed out that the average nickel composition in Figure 5-5 is slightly lower than the average composition on Figure 5-3. There are two possible explanations. There was some nickel loss during the processes, which caused the decreasing of nickel contents on the catalyst surface. Alternatively, it may simply a matter of sample selection. Figure 5-3 was obtained from analyzing 5 different catalyst particles, we do see there are some discrepancies between the particles. Figure 5-5 includes data from 6 catalyst particles.

5.5 Discussion

The following two questions can be raised with the experimental results on migration study:

- Why are the nickel deposits mobile?
- Why do the nickel deposits migrate towards cobalt?

These two questions will be discussed in the following. The first question is discussed in two aspects: Tammann temperature and surface diffusivity. The question on the association between nickel and cobalt are discussed in terms of atomic compatibilities between the metal sulfides.

5.5.1 Tammann Temperature

The higher the cohesive energy, the slower the migration is expected. Therefore, it is expected that the migration of metal or metal sulfides on a support surface should

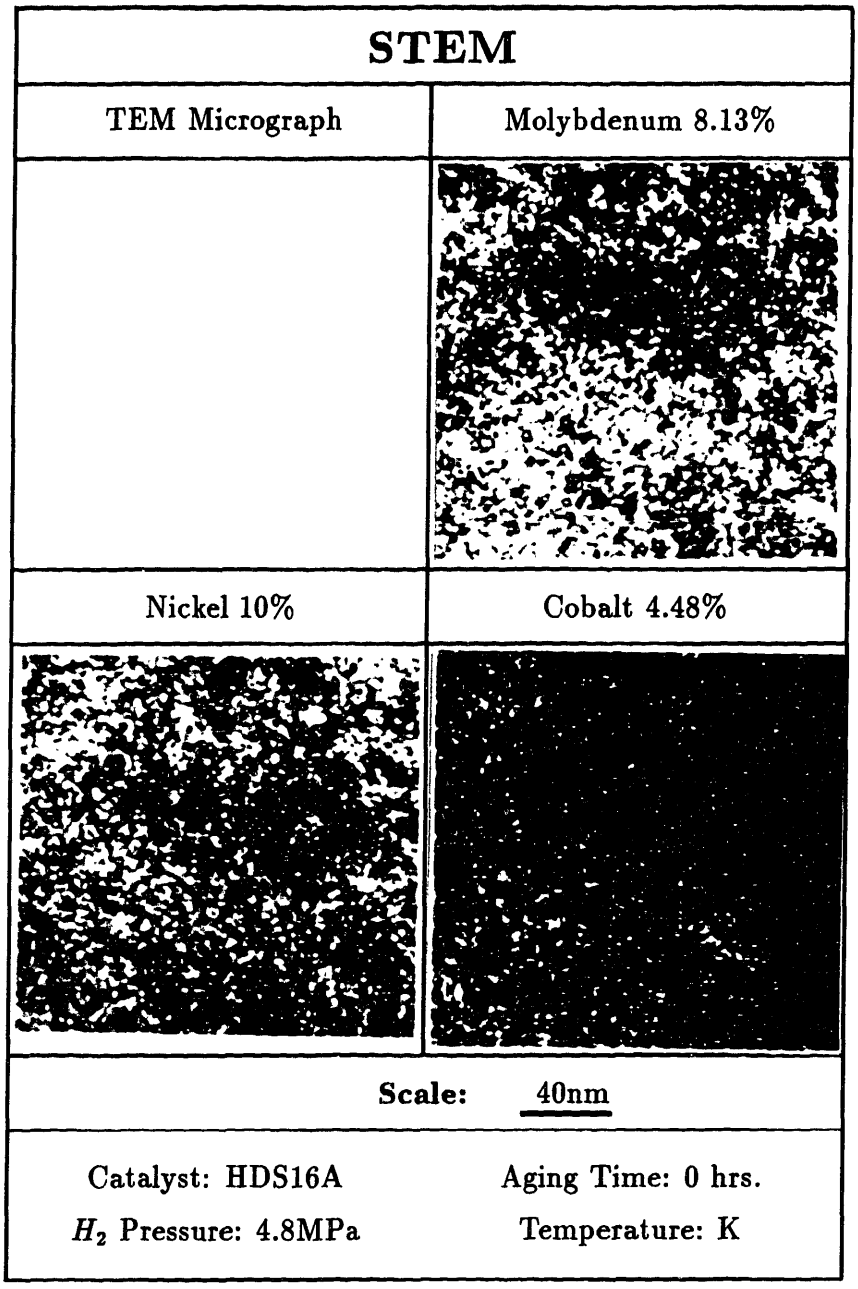

Figure 5-2: Elemental Mapping of HDS16 with Impregnated Nickel

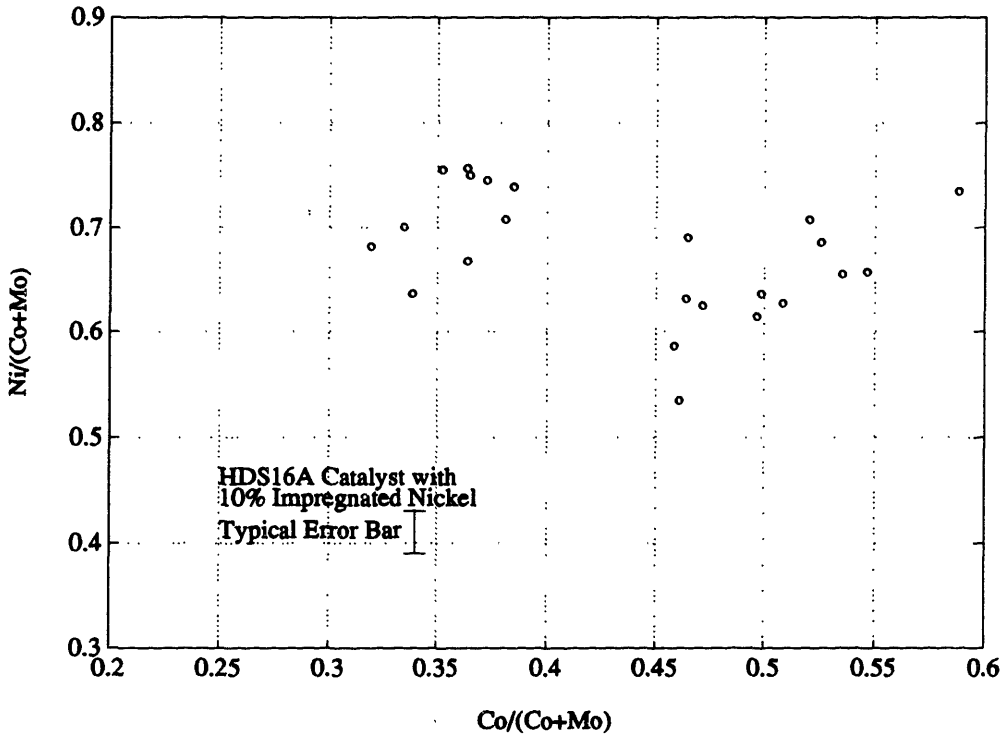

Figure 5-3: Microanalysis of HDS16A with Impregnated Nickel

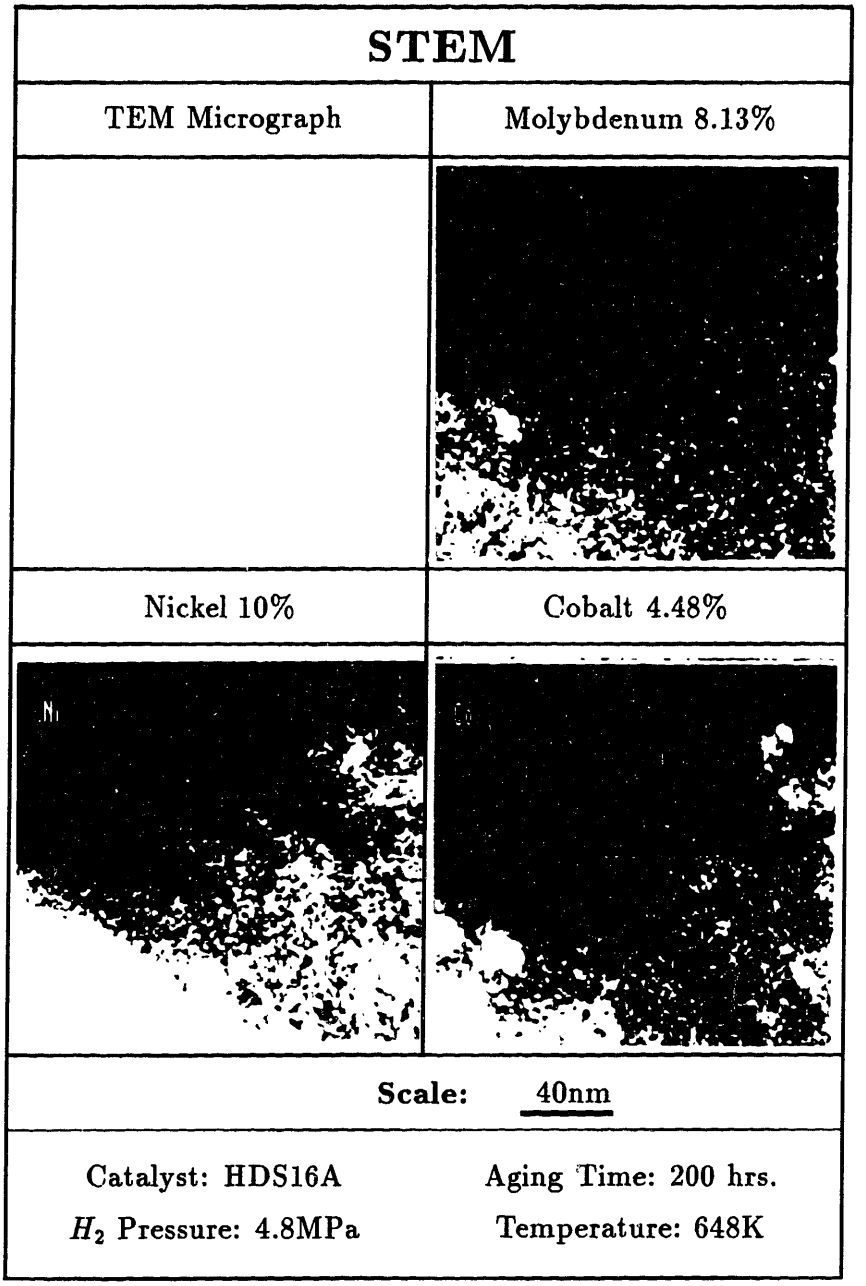

Figure 5-4: Elemental Mapping of HDS16 with Impregnated Nickel after Treating

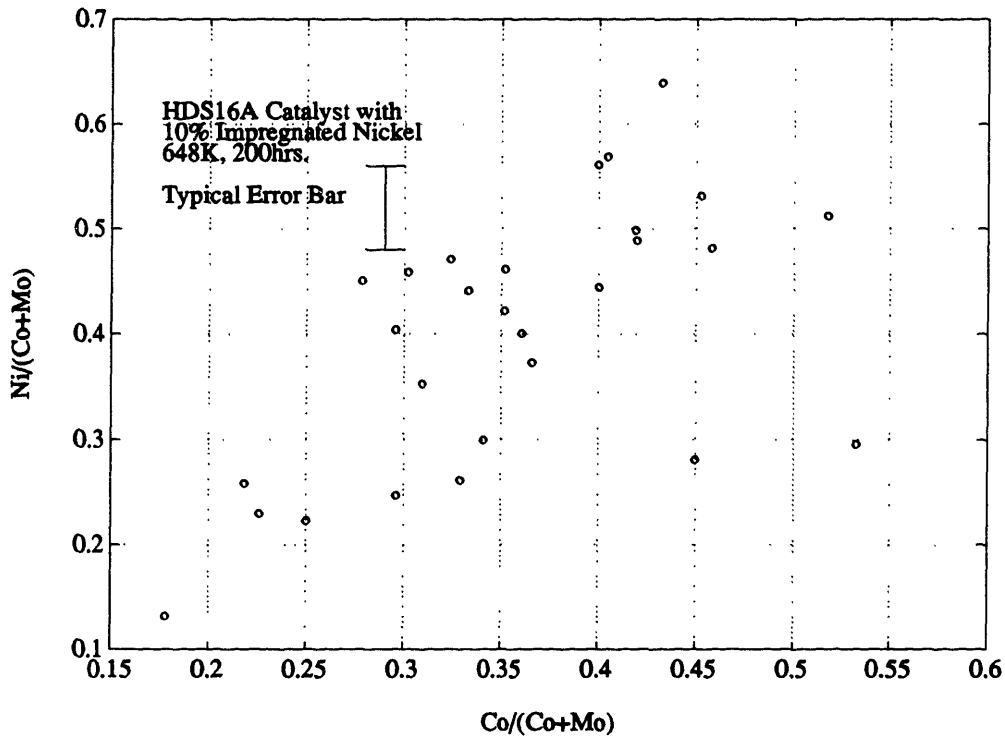

Figure 5-5: Microanalysis of HDS16A with Impregnated Nickel after Treating

have a relationship with cohesive energy (and thus also with the melting point).

The mobility of the atoms on the surface of a crystallite can significantly affect the migration process. Tammann temperature, T_{Tam}, which is defined as half of the melting temperature Tm of the bulk solid in degrees K, provides a measure of the extent of mobility of the atoms. Similarly, Hüttig temperature, one third of the melting point, is considered the temperature at which surface atoms become mobile. It is suggested that the Tammann temperature is associated with a two dimensional melting of the surface of the solid, *i.e.*, to the transition from a solid to a liquid-like behavior of the surface[111]. Table 5.1 shows the melting points and Tammann temperatures of the relevant metal sulfides. The operating temperature range of 588-623K is well over the Tammann temperature of nickel sulfide. As a consequences, we expect that the nickel deposits are relatively mobile on the catalyst surface and ready to migrate towards thermodynamically more stable form. The mobil ity of molybdenum sulfide and cobalt sulfide will be studied in chapter seven.

5.5.2 Surface Diffusivity

Assuming the sintering occurs because of the migration of the islands, effective diffusion coefficients of the order of 10^{-15} to 10^{-17} cm^2/sec were obtained[84][111].

Let's take a rough estimation of the diffusivity for the present work. The migration distance on the catalyst surface is around 50nm, and the hydrodemetallation experiment ran typically about 500 hours. The effective diffusion coefficient can be estimated to be $(r^2)/t$, or 10^{-17}, which falls in the range of the literature data.

5.5.3 Affinity between Nickel and Cobalt Sulfides

The association between nickel and cobalt sulfides suggested that the formation of solid solution between the two sulfides. Next, we will discuss whether the conditions

Table 5.1: Characteristic Temperatures of Metal Sulfides

	Ni_7S_6	Co_9S_8	MoS_2
$T_{Melting}$ (^oC)	790	1100	1750
$T_{Tammann}$ (^oC)	258	414	738
T_{Huttig} (^oC)	81	185	401
Order of Mobility: $Ni_7S_6 > Co_9S_8 > MoS_2$			

for the formation of solid solutions exist between the two metal sulfids.

The conditions for formation of solid solutions are dependent upon the atomic compatibility between the two components. The principal relationship between phase diagrams and crystal chemistry is this: *miscibility occurs when atoms have similar size, valence and structure, and compounds form when they do not*[44][68].

- Ionic sizes ;
- Valence;
- Molecular structure.

Field Strength

For metal oxides or metal sulfides, the major factors determining the extent of solid solutions are the relative ionic sizes and valences. Although different ionic sizes can definitely preclude extensive solid solution formation, valence difference can frequently be made up in other ways[44]. Using field strength as a parameter, Berkes & Roy [6] correlated several characteristics of binary phase diagrams of about 160 oxide systems. Field strength was defined as cation valence divided by the square of cation-anion distance (Z/d^2). The number of compounds in the binary system increases as a function of $\Delta(Z/d^2)$, the difference in the field strength of the end-member cations. As expected, the extent of solid solution is a maximum when $\Delta(Z/d^2) = 0$, and decreases rapidly as $\Delta(Z/d^2)$ increases. When $\Delta(Z/d^2)$ is less then 10%, extensive or complete solid solution take place. When $\Delta(Z/d^2)$ is large than 0.4, there are virtually no solid solution.

In the present system, there exist three metal sulfides on the aged catalyst surface: Ni_7S_6, Co_9S_8 and MoS_2.

The field strength can be easily calculated from the listed data. The results are listed in Table 5.2. The difference of field strength between Ni_7S_6 and Co_9S_8 is

Table 5.2: Field Strength of Metal Sulfides

	Cation Ionic Radii (nm)	Anion Ionic Radii (nm)	Cation Valence	Field Strength	Difference(%)
Ni_7S_6	0.069	0.170	+2	0.350	
Co_9S_8	0.072	0.170	+2	0.342	2.3%
MoS_2	0.079	0.170	+4	0.645	84.3%
References:[20][37][62][81][87]					

only about 2.3%, which is much less than 10%, extensive formation of solid solution between the two is expected. On the other hand, the difference between MoS_2 and the other two sulfides are significantly larger, therefore, little solid solution can be expected. Although no phase diagram between MoS_2 and Ni_7S_6 is available, the phase diagram of Co-Ni-S showed in Figure 2-1 does show the extensive solid solution formation.

Molecular Structure

Another factor determining the extend of solid solution formation between two solids are their structures. Compared with the cubic structure of cobalt sulfide, molybdenum sulfide has a layered hexagonal structure, while nickel sulfide has an orthorhombic structure with structure parameters quite close to those of the cobalt sulfide, as can be seen in Table 5.3.

Both the field strength and the molecular structure analyses indicate that extensive solid solution between Ni_7S_6 and Co_9S_8 are expected. This is consistent with the phase diagram we showed in Chapter 2. On the other hand, solid solution formation between Ni_7S_6 and MoS_2 is not favored in any way.

5.6 Conclusions

Experiments were designed to differentiate two possible deposition mechanisms: activity or migration. Based on characterization of catalyst with impregnated nickel, in conjunction with data in the literature on activity study, the following two questions were answered in this chapter concerning the development of the nickel deposits on the catalyst surface. First of all, the nickel deposits are mobile on the catalyst surface due to the fact that the hydrodemetallation temperature is higher that the Tammann temperature of nickel sulfide. Secondly, the association between nickel and cobalt is

Table 5.3: Structures and Properties of Metal Sulfides

	M.W.	Space Group	a b c	alpha	Note
MoS_2	161.14	Fm3m Hexagonal	0.31602 1.2294		
Co_9S_8	786.88	P63/mmc Cubic	0.99273		
Ni_7S_6	603.19	Cmcm Orthorhombic	0.918 1.1263 0.9457		close to cubic

resulted from the formation of solid solution between the two sulfides.

Although we do not have experimental basis to claim that nickel initially deposits on molybdenum sites, it is a reasonable postulation since the activity of molybdenum sulfide for hydrodemetallation. Further experiments are necessary to conclusively determine the initial distribution of nickel on the catalyst surface.

Chapter 6

Metal Distribution within Deposition Crystallites

It may, of course, be trivial —— individual eccentricity; or it may be very much deeper than appear on the surface.

——Sherlock Holmes, *The Adventure of the Red Circle*

Sir Arthur Conan Doyle

6.1 Chapter Summary

Structure of nickel deposits on the catalyst surface and the interaction between the deposits and the catalytic metals were characterized by scanning transmission electron microscopy (STEM) and high resolution transmission electron microscopy (HRTEM) analyses. The deposits were in crystallite form of nickel sulfide on the catalyst surface. Within the crystallites, it is found that cobalt sulfide is uniformly distributed

throughout the crystallites. In contrast, only about 20% to 25% of the molybdenum sulfide is associated with the nickel sulfide deposits as a segregated surface layer. The rest of the moybdenum sulfide forms seperate entities on the substrate. For crystallites smaller then about 15 nanometers, the degree of segregation decreases. The implications on the deactivation of hydrodemetallation catalysts are discussed.

6.2 Introduction

In the previous two chapters, resorting to X-ray elemental mapping, we showed that nickel deposits are strongly associated with cobalt on the catalyst surface, but not with molybdenum. Since molybdenum sulfide on sulfided $CoMo/\gamma - Al_2O_3$ is generally considered to be the active component for hydrotreating reactions[16][23], it is important to know how the nickel deposits interact with molybdenum on the surface. The objective of this work is to further characterize the structure of the deposits and the interaction between the deposits with catalytic metals, especially the distribution of molybdenum on the aged catalyst surface, and further the elemental distributions within the nickel deposit crystallites.

6.3 Characterizations

6.3.1 Characterization by STEM

As we have shown in previous chapters, nickel sulfide deposits are in crystallite forms on the catalyst surfaces. The sizes of the crystallites were estimated to be about 10-15 nanometers, though crystallites with sizes up to 50 nanometers could be observed. By positioning the STEM electron probe on some crystallites and conducting EDS analysis, we concluded that nickel is strongly associated with cobalt on the catalyst. However, the structure of molybdenum and its relation with the nickel deposits were

not discussed.

Element distributions within the crystallites are studied in this chapter. The aim is to detect element distributions within the crystallite, more specifically, the existence of a surface enrichment of one component. The idea is schematically shown in Figure 6-1. If the elements are uniformly distributed within the crystallites, we should get the same element ratios when we analyze the center or the edge of the crystallites. On the other hand, if there is an element enriched on the surface of the crystallites, we would get different element ratios at different analyzing positions. Unfortunately, the feature of problems and the limitation of the instrument determine that we could only get qualitative results.

The first sample we analyzed was an aged catalyst HDS16A sample, which is loaded with 23%wt nickel. To facilitate the analysis, we get on to magnification of $\times$1,000,000, and obtained the best resolution we could. At this condition, we moved the sample and located some large crystallites. Figure 6-2 is a TEM micrograph of the area where the crystallite with square shape at the center would be analyzed. The crystallite measures about 50 nanometers. First, we focused the electron probe on the very edge of crystallite and conducting XEDS analysis, which continued for 100 seconds. During the analysis, we would check the sample drifting every 20 seconds to make sure the probe was still on the original positions. After the analysis is complete, we move the probe onto another position.

The analysis results are plotted in Figure 6-3 for the 15 positions analyzed on the particular crystallite. The circles indicate the positions analyzed, and the numbers inside are the relative amounts of cobalt or molybdenum to local nickel contents. Clearly, there is a significant difference between the distributions of cobalt and molybdenum. Although cobalt is virtually uniform throughout the whole crystallite, molybdenum is strongly enriched on certain surfaces of the crystallite. The result is also plotted in Figure 6-4 as the element ratio to the relative distance from the center

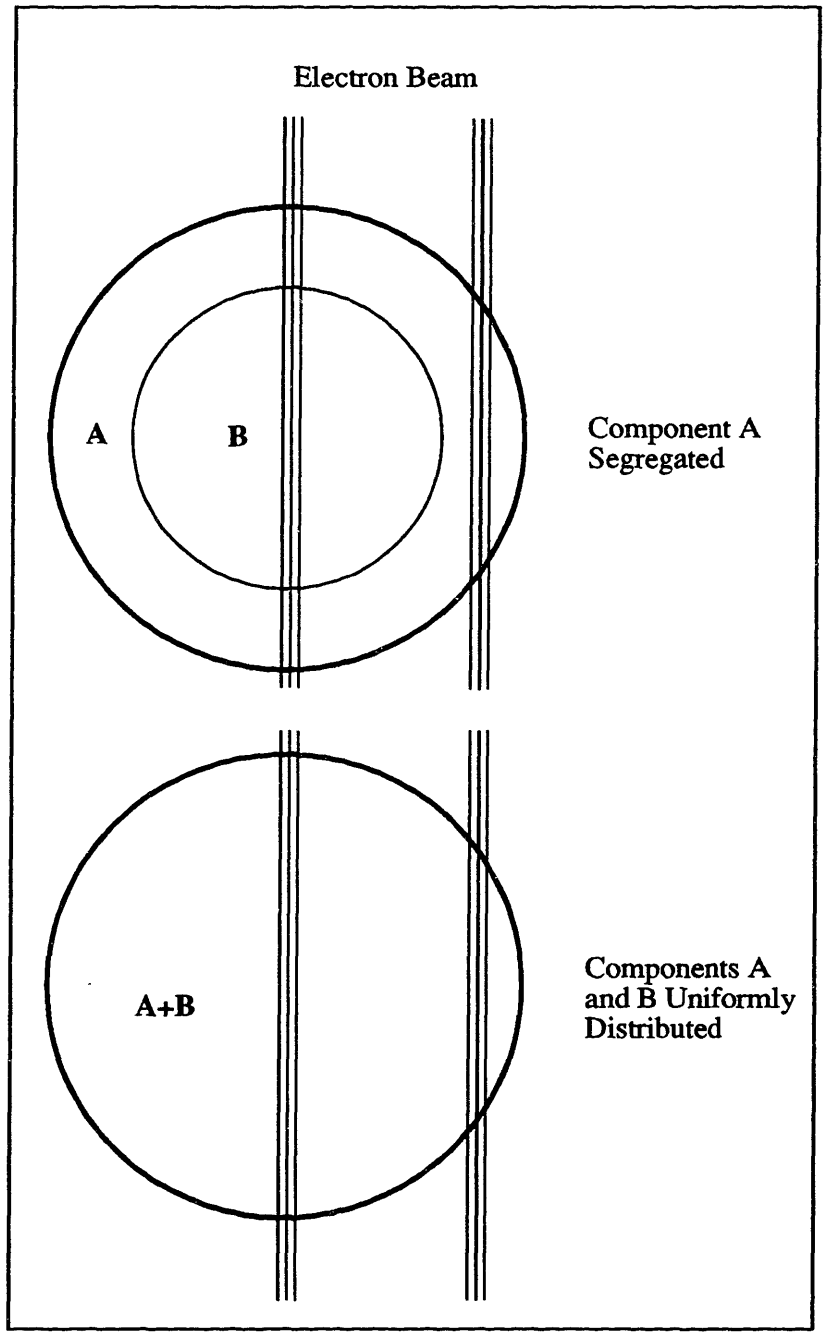

Figure 6-1: Illustration of the Electron Probe on a Crystallite

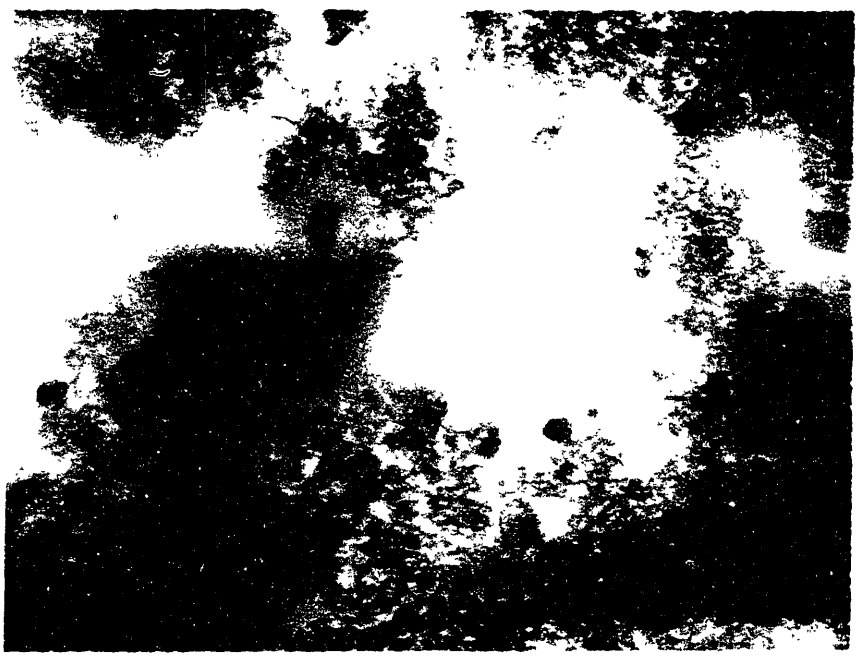

Scale: 50nm

Catalyst: HDS16A	Temperature: 623K
Aging Time: 650hrs.	H_2 Pressure: 4.8 MPa

Figure 6-2: Electron Micrograph of a Crystallite Analyzed

of the crystallite. The error bars represent standard deviations for multiple analyses at the same relative radial positions. The overall ratio of cobalt to nickel within the crystallite was analyzed as 0.17. Considering the small area analyzed, it is very close to the bulk ratio of 0.22. On the other hand, the molybdenum to nickel ratio is much lower than the bulk ratio of about 0.4. These results indicate that much of cobalt on the catalyst is associated with nickel, while only part of the molybdenum is associated with the nickel deposits as a segregated surface layer of molybdenum sulfide. The rest of the molybdenum sulfide forms seperate entities on the substrate. We also noted that molybdenum enrichment only occurred at certain particular surfaces, rather than every surface of the nickel deposits.

Another aged catalyst SN6931 is also characterized with the similar procedure. As shown in Table 3.2, this is a catalyst with lower cobalt and molybdenum loadings. The nickel loading was about 22.1%wt. Figure 6-5 and Figure 6-6 show the micrograph and the analysis results for one crystallite with the size of about 50 nanometer. We can see the results are very similar. Cobalt us distributed throughout the crystallite, while molybdenum has a much higher concentration on the surface. The result is also plotted in Figure 6-7. Again, the ratio of cobalt to nickel is close to the bulk ratio of 0.13, while the molybdenum to nickel ratio much lower than the bulk ratio of 0.2.

To make sure the analyzed crystallites are representative of the nickel deposits, and the results represent at least a qualitative trend, we analyzed more crystallites in the catalyst HDS16A with different sizes ranging from about 6nm to 60 nm. The sketches of some of the crystallites are shown in Figure 6-8. The results are plotted in Figure 6-9 and Figure 6-10. Once again, the ratios of cobalt to nickel are close to the bulk ratio of 0.2, while the molybdenum to nickel ratio of about 0.1 only accounts for about 25% of the bulk molybdenum to nickel ratio.

Another interesting observation was made for the crystallites with different sizes. Similar to two component system, we define the following ratio as the surface enrich-

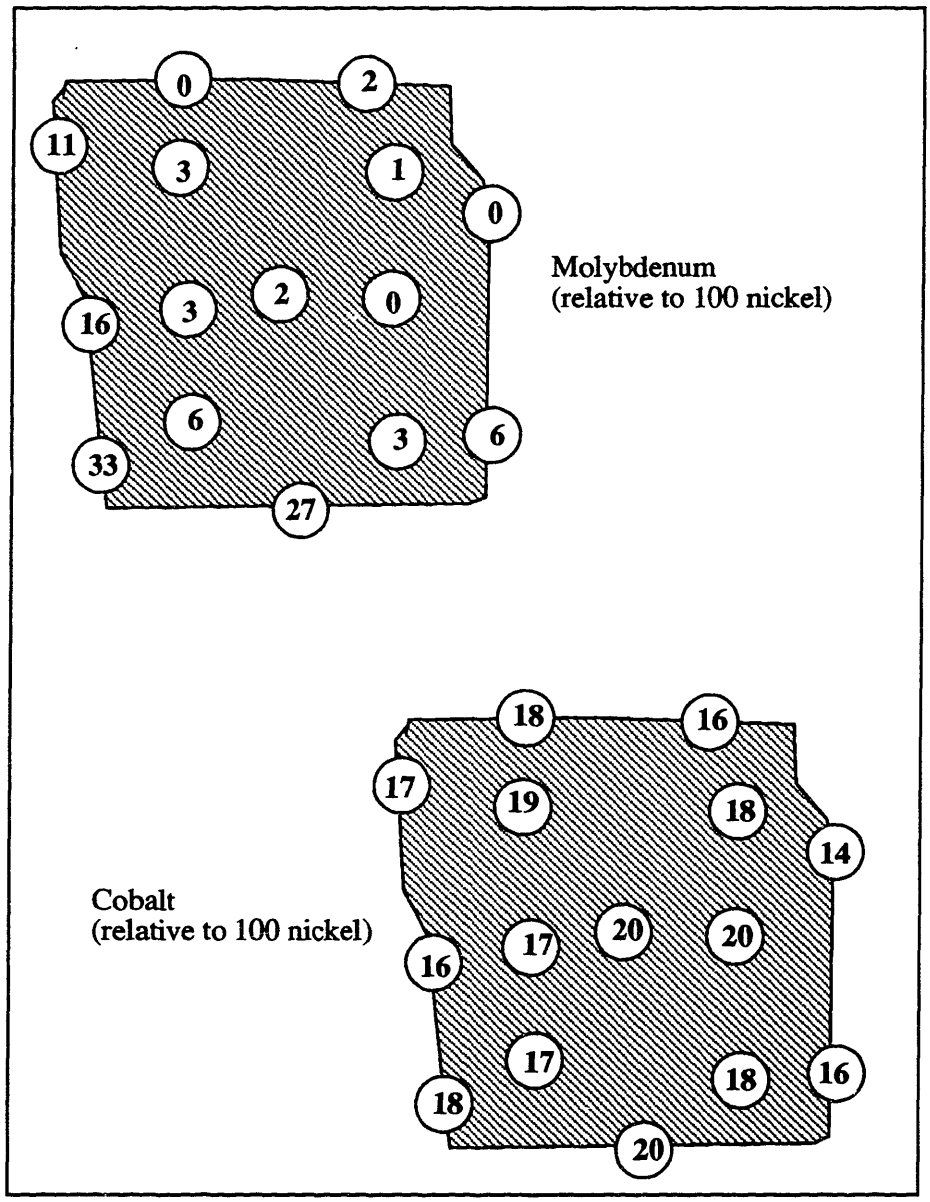

Figure 6-3: Element Ratios within the Crystallite Analyzed

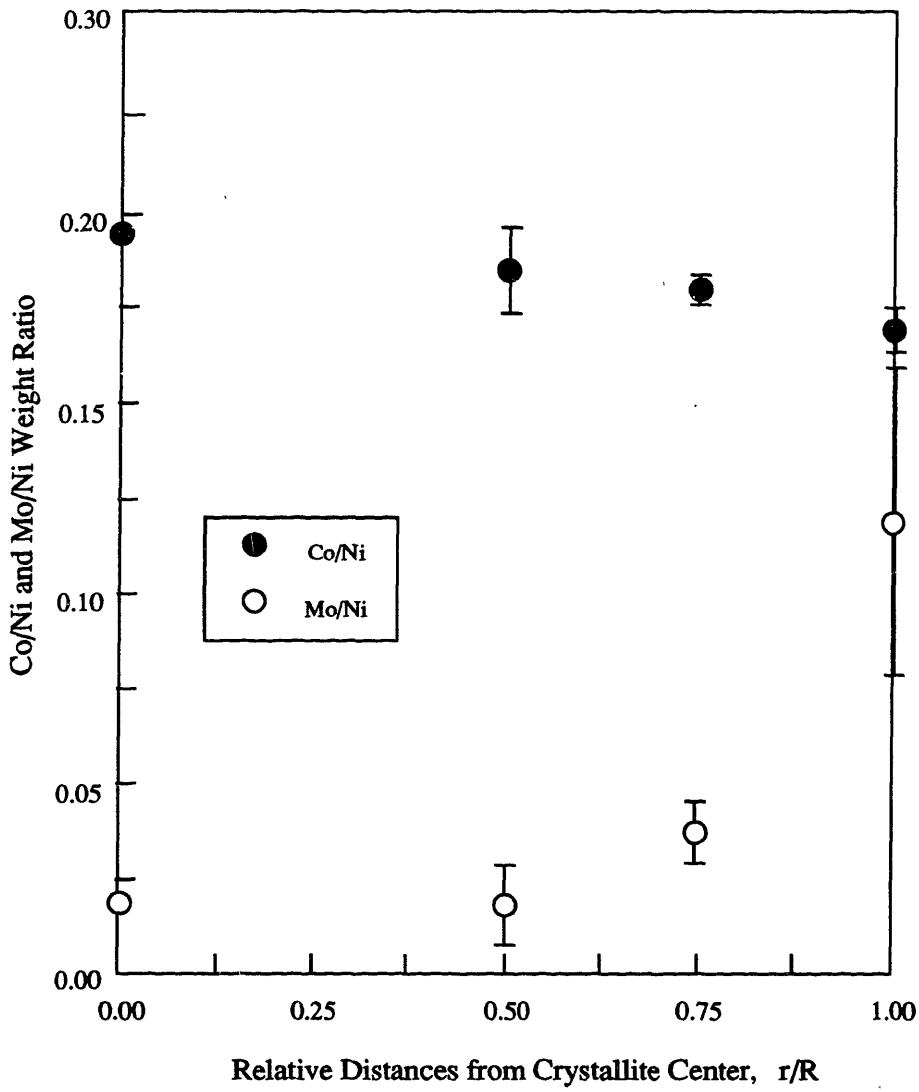

Figure 6-4: Element Distribution within the Crystallite Analyzed

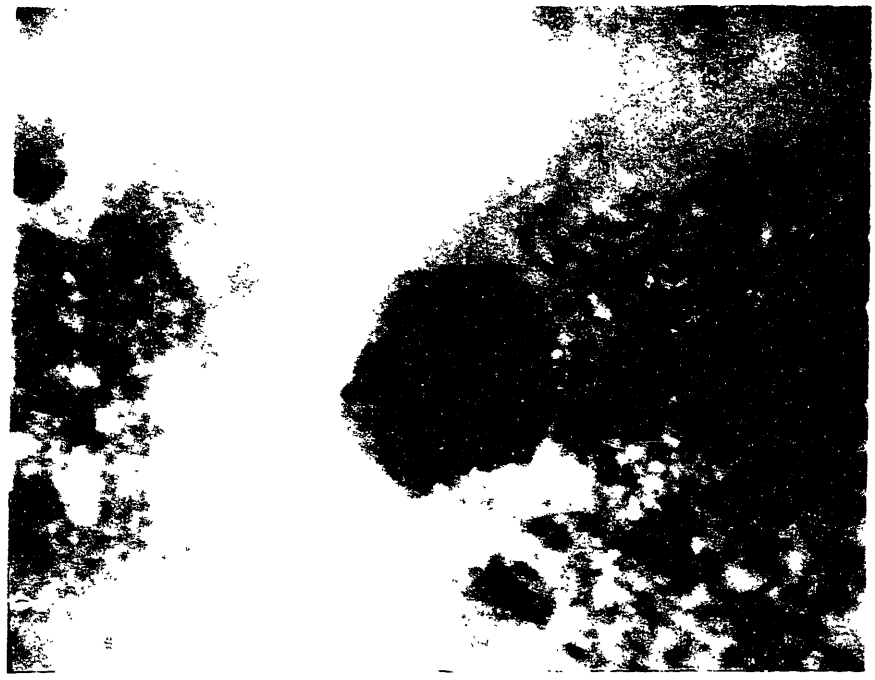

Scale: 10nm

Catalyst: SN6931	Temperature: 588K
Aging Time: 380hrs.	H_2 Pressure: 4.8 MPa

Figure 6-5: Electron Micrograph of a Crystallite Analyzed

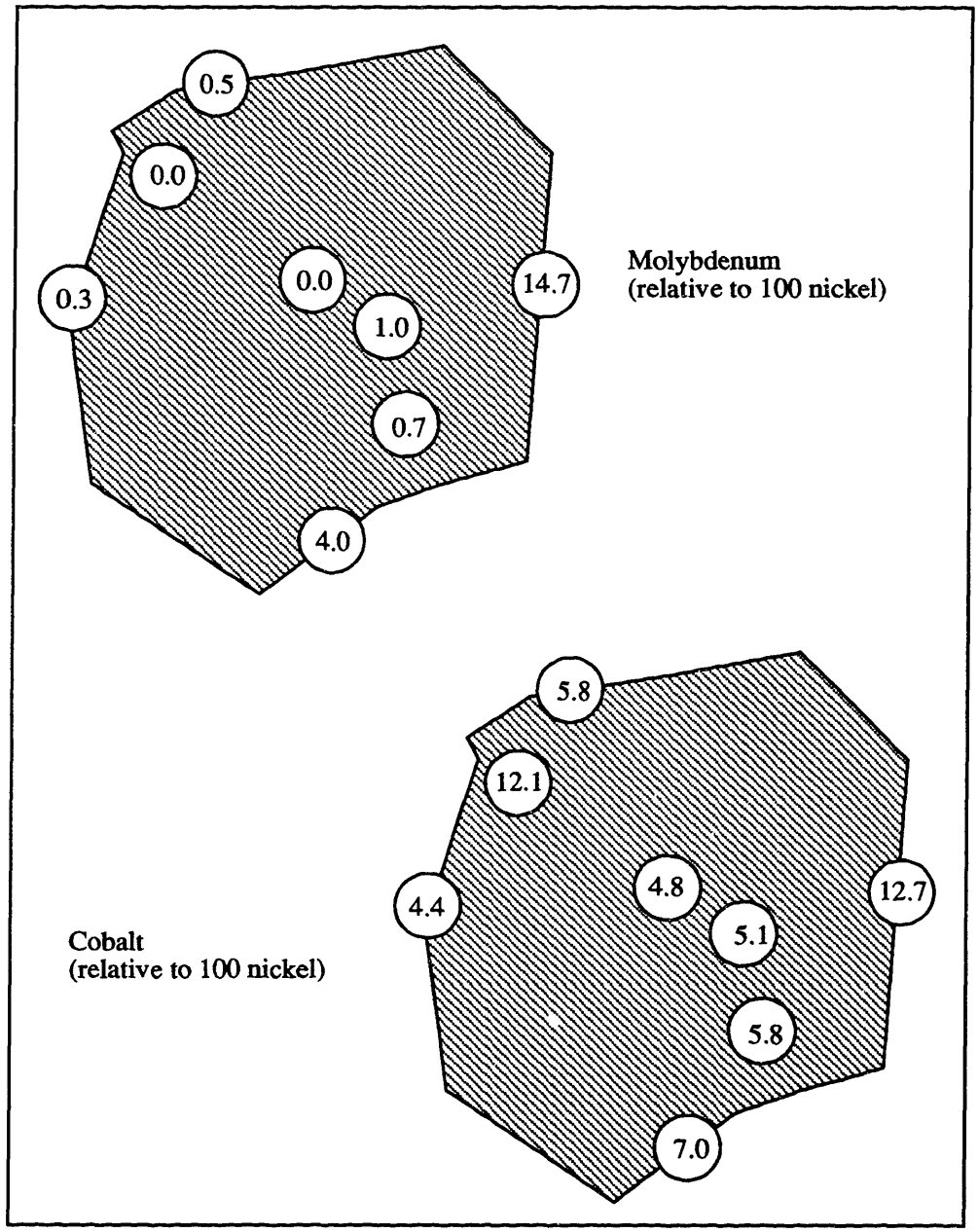

Figure 6-6: Element Ratios within the Crystallite Analyzed

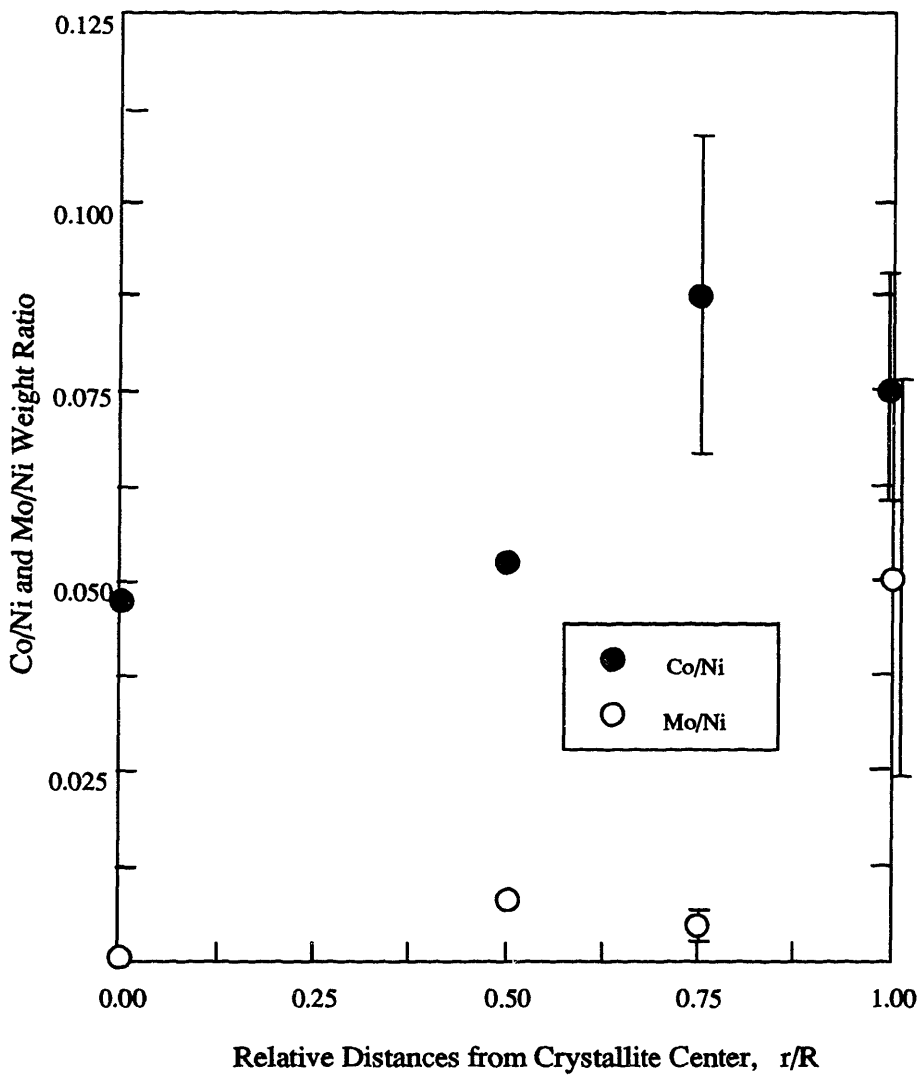

Figure 6-7: Element Distribution within the Crystallite Analyzed

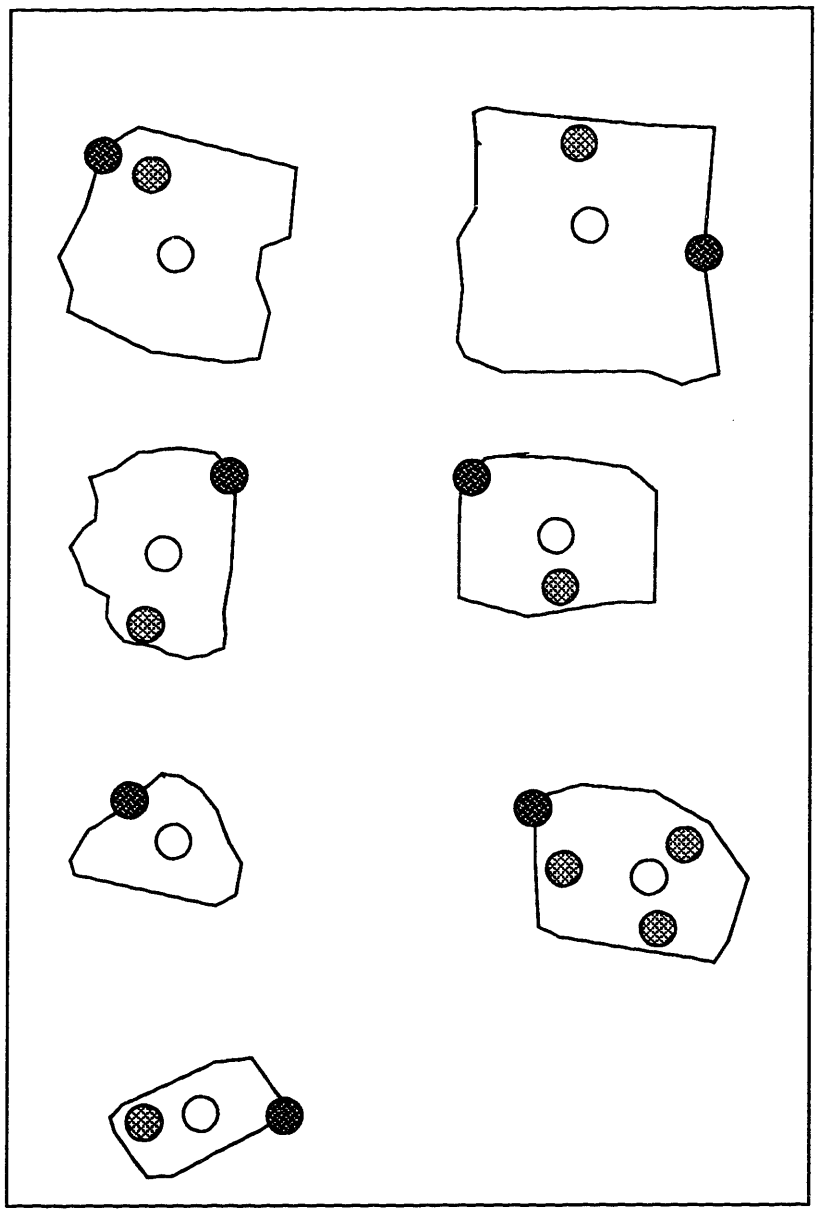

Figure 6-8: Sketches of Seven Crystallites Analyzed

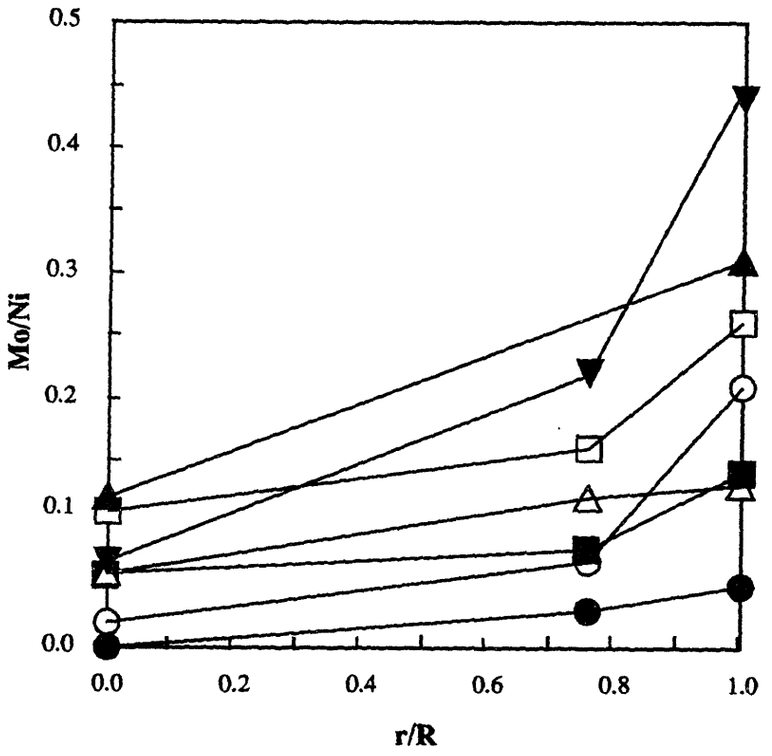

Figure 6-9: Molybdenum/Nickel Radial Distribution within Crystallites

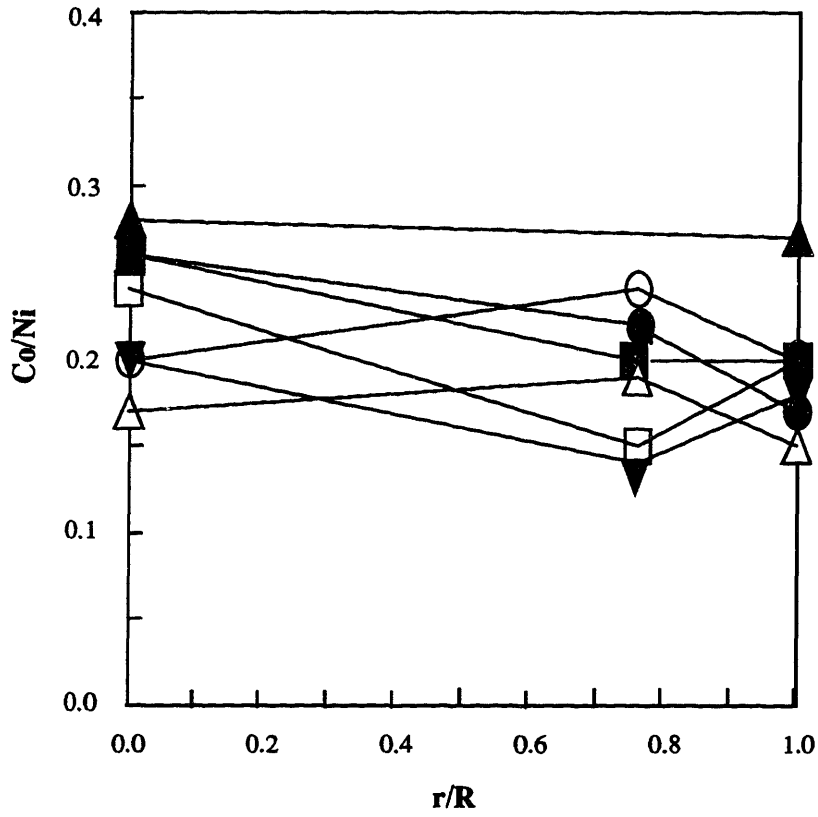

Figure 6-10: Cobalt/Nickel Radial Distribution within Crystallites

ment factor as in a binary system:

$$\chi = (\frac{X_A^{surface}}{X_B^{surface}})/(\frac{X_A^{center}}{X_B^{center}})$$

where A represents the catalytic metals cobalt or molybdenum, and B the nickel deposits.

When we plot the surface enrichment factor against the sizes of the crystallites in Figure 6-11, it is clear that cobalt is uniformly distributed with the crystallites regardless of the sizes of the crystallites, indicated by the fact that the enrichment factor is distributed evenly around one. Molybdenum, however, has a much higher concentration on the surface, though the enrichment factor decreases for crystallites smaller than about 15 nanometers. It is consistent with the theoretical calculations by Helms[33]. By applying a simple mass balance relationship to segregation equation, Helms presented a plot of segregation *vs* the dispersion of particles, which is defined as the ratio of the number of atoms on the surface to the number of the total atoms. It was noted that the effect of particle size could be very significant, depending on the magnitude of the heat of segregation $\{-\Delta G/RT\}$. Intuitively, as the particle size approaches zero, the surface composition must approach the bulk value. For crystallites smaller than about 5 nanometers, we were limited by the resolution of the scanning transmission electron microscope. In addition, the drifting of the samples also causes difficulties for the analysis of even smaller particles.

6.3.2 Characterization by HRTEM

Although the structure of sulfided $CoO - MoO_3/\gamma - Al_2O_3$ catalyst has been studied extensively by high resolution electron microscopy[18][20] [21][80], HRTEM studies for aged catalyst are still scarce[108] [116].

In the last section, we analyzed aged catalyst samples by scanning transmission

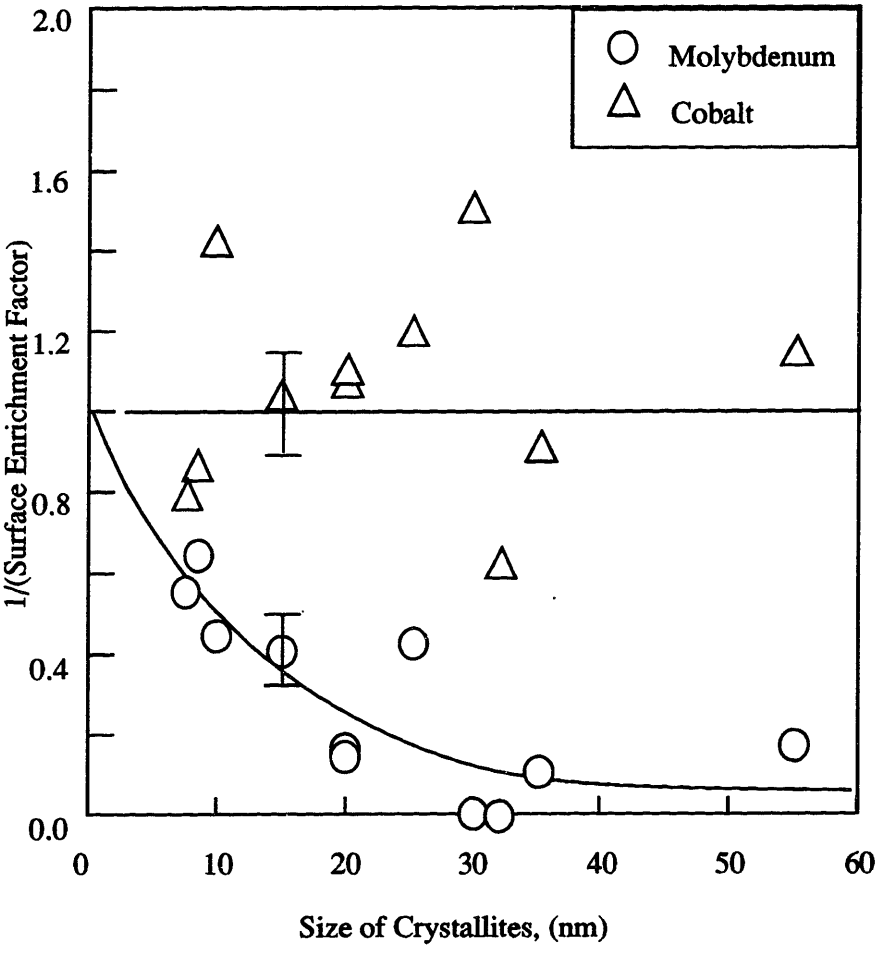

Figure 6-11: Effect of Crystallite Sizes on Segregation

electron microscope, and concluded that there was a segregated surface layer of molybdenum disulfide on the surface of the nickel sulfide deposits. In the following section, we will present results from high resolution transmission electron microscope to directly show the structure of the deposits, and the surface phase of molybdenum sulfide.

Figure 6-12 and 6-13 show two areas of a typical TEM micrograph of the aged HDS16A catalyst sample. Typically, we could see many crystallites on the catalyst surfaces, which STEM analysis and XRD confirmed to be Ni_7S_6. Many different lattice fringe images can be observed on the micrographs. The 111 reflection (d=0.575nm) of Ni_7S_6 can be observed within many crystallites(Figure 6-12). The lattice fringes observed in the figure have spacings of about 0.62nm that one can easily relate to the 0.615nm spacings of the 002 basal planes of MoS_2. The structure made of highly disordered S-Mo-S layers of poorly crystallized MoS_2. Due to lattice relaxation, some of the fringe spacing are larger than 0.615nm.

Consistent with the results from XEDS analyses, molybdenum sulfide was observed on the surfaces of many of the nickel sulfide crystallites. While most of the nickel sulfides have one or two layers of molybdenum sulfide on the surfaces, crystallites with as many as five or six layers of molybdenum sulfide was also observed, as shown in Figure 6-13. The fringe spacing of 0.33nm corresponds to the 131 reflection (d=0.328nm) of Ni_7S_6. For slabs of more than two layers, it is easy to assign them to the basal planes of MoS_2. It is, however, difficult to determine its nature, when there exists only one layer, as in many of the crystallites. According to the shape of the lines, and information from STEM, we believe the thick line around many of the Ni_7S_6 crystallites are a single layer of MoS_2 slab.

Figure 6-14 shows a molybdenum sulfide crystallite. The lattice fringe spacing of 0.28 nm corresponds to the 100 reflection (d=0.274nm). The Moiré fringe is probably caused by overlapping of two crystals. The hexagonal shape of the crystal is very well

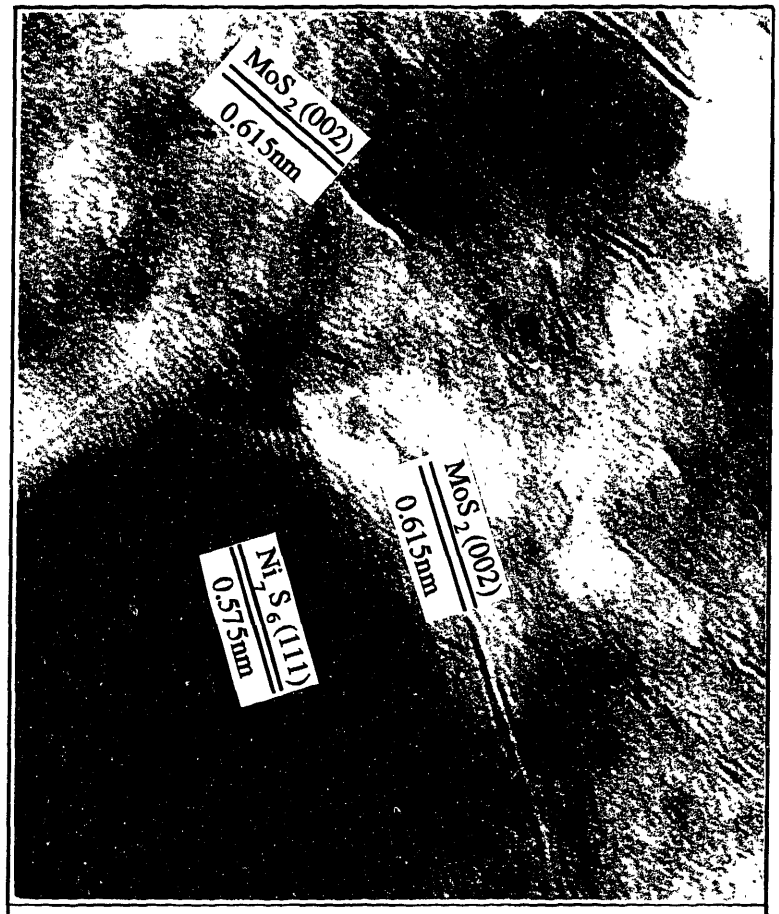

Figure 6-12: Lattice Fringe Image of Aged HDS16 Catalyst

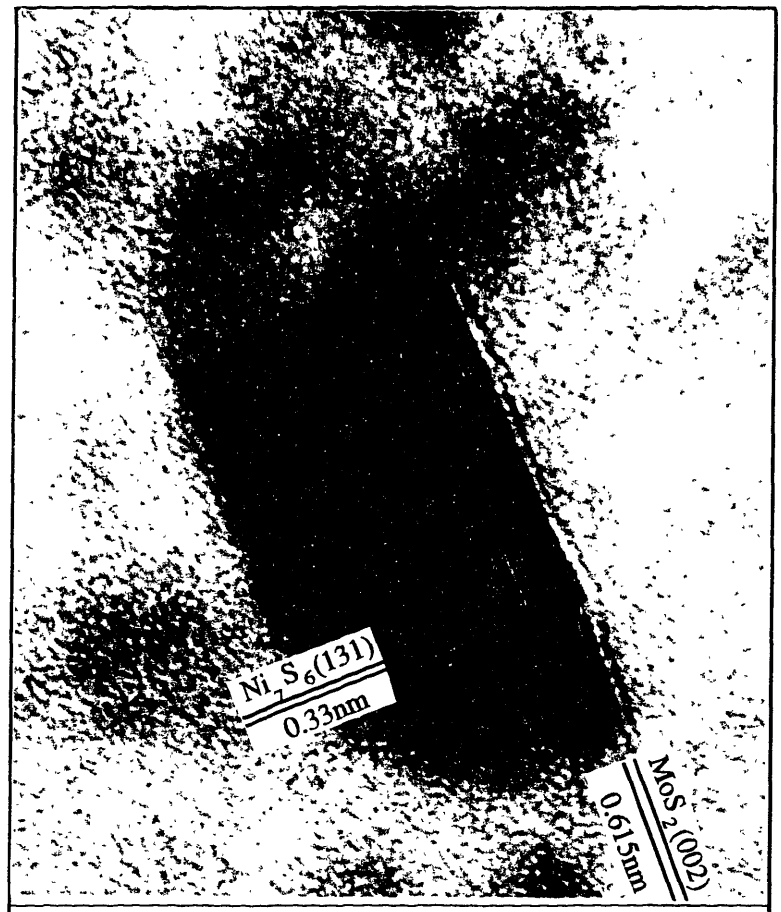

Figure 6-13: Lattice Fringe Image of Aged HDS16 Catalyst

defined. The size of the crystal is about 30 nanometers. Although it is a rarity, the size of the crystal is very significant.

No lattice fringes are definately assigned to Co_9S_8, partly due to the fact that the main reflections 111 (d=0.573nm) and 002 (d=0.496nm) of Co_9S_8 are difficult to be differentiated with those reflections of Ni_7S_6 (d_{111}=0.575nm, d_{002}=0.470nm). The difficulty of locating lattice fringes of Co_9S_8 could also be explained by the formation of solid solution between Co_9S_8 and Ni_7S_6. Many fringe images with spacing at 0.15 to 0.2 can be observed on the pictures, though it is difficult to assign them to a particular compound.

6.3.3 Characterization by XPS

X-ray photoelectron spectroscopy was used characterized the aged catalyst surface. Although most of the XPS literature work has been addressing the chemical state of elements on the catalysts[12], we attempted to get a depth profile of elements with the crystallites. The original aim was to quantify the average thickness of the molybdenum sulfide surface phase on the nickel deposits crystallites by sputtering the catalyst surfaces. However, the actual catalyst surface is far more too complete than the XPS is designed for. First of all, the catalyst is a flat surface. Secondly, the the thickness of the molybdenum sulfide is probably beyond the resolution of the instrument. In addition, the binding energy shifts and peak broading caused by charging effects also make chemical state assignments uncertain. In retrospect, we now understand that most of the molybdenum is still on the substrate, rather than the surface of nickel sulfide. Consequently, it is probably impossible to get an average depth profile as we had expected.

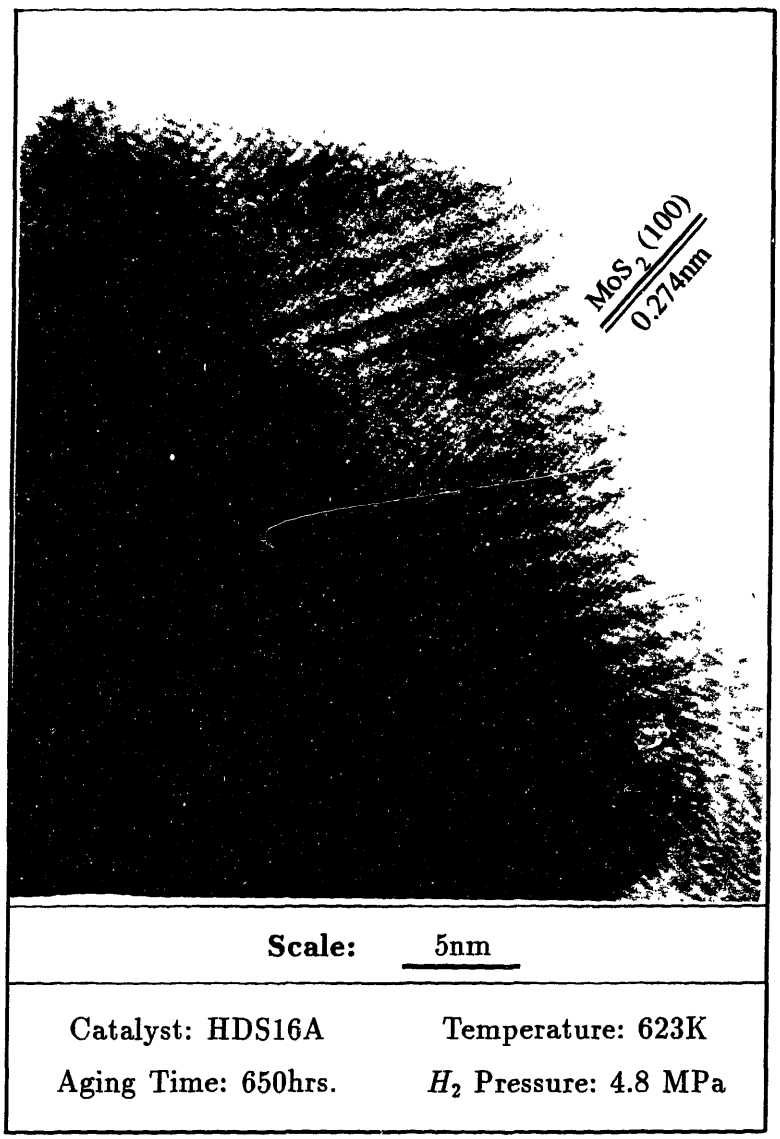

Figure 6-14: Electron Micrograph of a Molybdenum Sulfide Crystallite

6.4 Discussions

Surface segregation in metallic alloys[14] [41] and metal oxides [72] has been studied extensively in material science. There are several possibilities for the microstructure of such systems. One phase or one component could be enriched on the surface of the crystallites. At the present time, a comprehensive theory does not exist, but the following general conclusions have been proposed[8] [32] [97]:

- In one phase alloys the surface tends to be enriched by the component with the lower surface energy;
- When an alloy contains two phases in equilibrium, the alloy with the lower sublimation energy tends to form the outer surface;
- The degree of enrichment decreases with the increasing temperature.

Co-Ni alloy has been studied by using XPS, SIMS and other techniques, and the two metals form a continuous series of solid solutions close to ideal ones[65]. CoO-NiO system has also been studied[11] [66]. They are very well soluble in each other. In the present system, Co_9S_8 has a cubic structure. Although Ni_7S_6 has an orthorhombic structure, it is very close to cubic. The lattice constants of the two are also very close to each other. The difference between the respective constants are about 10%. It is expected that these two sulfides can form solid solutions.

MoS_2 is one of the transition metal dichalcogenides, which belong to a large class of the so-called two-dimensional solids (Figure 6-15). Of course, we are actually dealing with three dimensional solids with strong anisotropy in their physical properties. They are called two dimensional because they are formed in layered structures. Atoms within a layer are bound by strong covalent or ionic forces while individual layers are held together by relatively much weaker forces. The latter are frequently referred

to as 'van der Waals' type of interactions. Among all the transition metal dichalcogenides, MoS_2 has the highest degree of anisotropy on the basis of force constants determined from phonon studies[52]. Due to the special layered structure of MoS_2, it can be very readily cleaved along the basal plane.

From a quasichemical point of view, surface energy of solid is determined by the total bonding energy involved when the surface is formed. Therefore, we know that MoS_2 would have a much lower surface energy when being cleaved along the basal plane.

The other two sulfides involved in the present system have cubic or othorhombic structures. These are no special cleavage planes for such structures. Thus, when the three solids are present in a system, molybdenum sulfide would be expected to be segregated onto the surface to achieve the minimum of energy of the total system.

In addition to the surface energy differences between the two metal sulfides, another energy contribution involved in the segregation of molybdenum sulfide is the interaction energy at the interface. Naturally, the interaction would be different for different planes. This is shown by the fact that molybdenum sulfide only segregated on some surfaces of nickel sulfide crystals, rather than every surface.

Summarizing the electron microscopic observation and the discussion, we can roughly portray the aged catalyst surface with the following physical picture. The metal sulfides on the catalyst surface form three different entities. Most of the nickel sulfide deposits are associated with cobalt sulfides, forming uniform crystallites. For most of the nickel-cobalt sulfide crystallites, a surface layer of molybdenum was observed. This part of molybdenum accounts for about 25% of the total molybdenum on the catalyst surface. The rest of the molybdenum is not directly associated with the nickel deposits, although this part of the molybdenum sulfide is still well dispersed, crystallites with sizes up to 30 nanometers were observed.

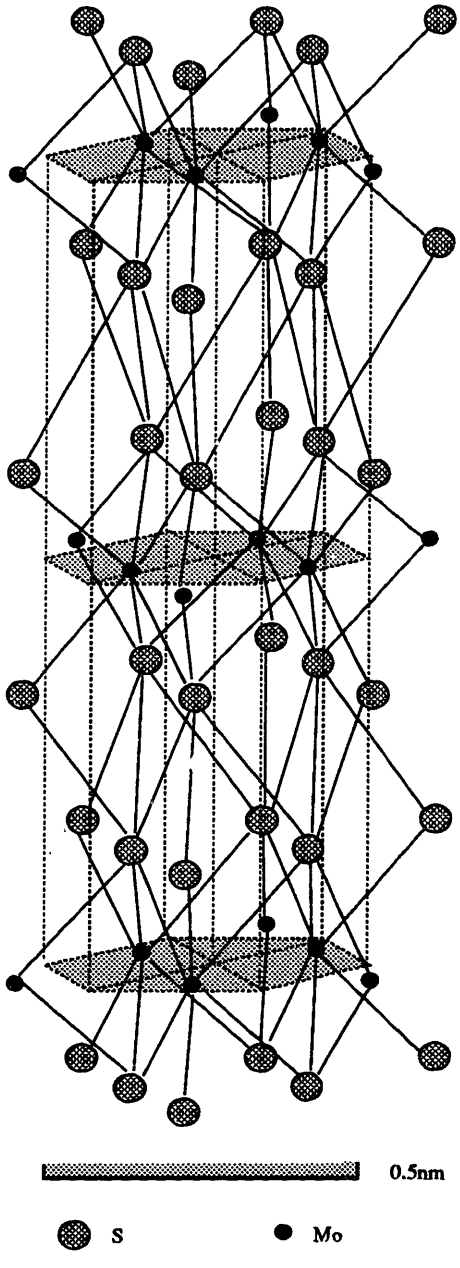

Figure 6-15: Molecular Structure of MoS_2[105]

In addition to the surface energy differences between the two metal sulfides, another energy contribution involved in the segregation of molybdenum sulfide is the interaction energy at the interface. Naturally, the interaction would be different for different planes. This is shown by the fact that molybdenum sulfide only segregated on some surfaces of nickel sulfide crystals, rather than every surface.

By using X-ray photoelectron spectroscopy, Fleisch *et al.*[25] found that the ratio of Mo/Al changes with the increase in metal deposits. They speculated that molybdenum might have migrated to the top of the contaminated layers and remain exposed to reactants. The present work directly showed that molybdenum sulfide is segregated on the surface of the nickel sulfide deposits. We believe that the segregation of molybdenum sulfide is the main reason that the catalyst keeps virtually the same hydrodemetallation activity with metal loading as high as 60wt%[107].

Another point we should mention here is concerning the resolution of the instrument used. From the elemental mapping results shown in chapter four, we did not see a surface layer of molybdenum sulfide corresponding to the surfaces of nickel sulfide crystallites. It is simply beyond the limits of the instrument resolution.

6.5 Conclusions

Electron microscopic characterization were performed to elucidate the metal distribution within the crystallites of nickel sulfide deposits observed on the surfaces of aged hydrodemetallation catalysts. Especially, the distribution of molybdenum on the catalyst surface is investigated. The following conclusions can be drawn from the work:

1. Within the crystallites of nickel deposits on the aged hydrodemetallation catalysts, cobalt sulfide and nickel sulfide are uniformly distributed.

2. In contrast to the distribution of cobalt, molybdenum sulfide is strongly enriched on the surface of the crystallites formed by nickel deposits with cobalt sulfide. X-ray elemental analysis showed that the average concentration of molybdenum on the surface is about 4-5 times as much as that in the center. The degree of segregation decreases for crystallites smaller than about 15 nanometers. The molybdenum associated with nickel deposits as a segregated surface layer accounts for about 25% of the total molybdenum on the catalyst surface. The rest of the molybdenum sulfide is not directly associated with nickel deposits.

3. The surface enrichment of molybdenum sulfide on the nickel deposits was also confirmed by direct observation on high resolution transmission electron microscopy. For many of the nickel deposits crystallites, we could observed one or two layers of molybdenum sulfide on the surface. Although they were not typical, nickel sulfide crystallites with up to 5 layers of MoS_2 were also observed. In addition, MoS_2 crystal with size up to 30 nanometers was observed as a separate entity on the catalyst surface.

Chapter 7

Mobility of Catalytic Metal Sulfides on Catalyst Surface

The temptation to form premature theories upon insufficient data is the bane of our profession.

——Sherlock Holmes, *The Valley of Fear*
Sir Arthur Conan Doyle

7.1 Chapter Summary

Effects of nickel deposition on the mobilities of molybdenum sulfide and cobalt sulfide are studied. By using hypothetical phase diagrams, it is shown that there is a threshold nickel deposit loading on the catalyst, above which the mobilities of the catalytic metal sulfides would be enhanced. The effect is also directly shown by comparing the surface structures of a bare sulfided catalyst, a heat aged catalyst, and a nickel aged

catalyst. It is shown that the presence of nickel deposits causes more sintering than without it.

7.2 Introduction

There is virtually no reports on the effect of metal deposits on the mobility of the original catalytic metals on hydrodemetallation catalysts, though in the author's view, it is a very important aspect for the understanding of deactivation of hydrodemetallation catalysts. So far in the thesis, we have solely focused our attention on the interaction of deposits with the catalytic metals on the catalysts by looking at mainly the influences of the catalytic components on the deposits. Here in this chapter, we attempt to understand the effect of the deposits on the mobility of the catalytic components on the catalysts. While the consideration here is specifically related to the $CoMo/\gamma Al_2O_3$ catalyst system with nickel deposits, the issues addressed are applicable to any other systems involving the interaction of more than one surface components on a substrate.

7.3 Deactivation of Catalysts by Sintering

In a broad perspective, deactivation by solid state reactions, *e.g.* sintering or phase transformations, is necessarily an ubiquitous phenomena. Indeed, nearly all catalysts are metastable in the conditions of catalytic reactions, considering that they all possess a high surface area, and hence a high surface energy[24].

On the catalyst surface, all the metal sulfides are distributed in very small microcrystallites. Generally, microcrystallites behave in very different fashions from large samples. One of the particular important features is that the melting point of microcrystallite is well below the melting point of a large sample.

As we have discussed in chapter five, The mobility of microcrystallites can be characterized by two characteristic temperatures. The temperature at which lattices begin to be appreciably mobile is called Tammann temperature; and that at which surface atoms become significantly mobile, the Hüttig temperature[99].

Tammann temperature is a very good indication for the mobility of a surface species on a substrate. Baker[4] showed that for both metals and metal oxides, their mobility temperatures on graphite substrates showed a very good agreement with their Tammann temperatures. The mobility temperatures were defined as a temperature in the vicinity of which a rapid change in the rate of movement of ions or atoms occurs.

We have speculated and and then experimentally showed that nickel deposits on the catalyst surface is mobile under the hydrodemetallation experimental conditions. For molybdenum sulfide and cobalt sulfide, we do not expect an appreciable thermal sintering by themselves, because they both have Tammann temperatures higher than the hydrodemetallation temperatures. However, it only applies to one component surface phase.

When there exist more than one components on a substrate, there would be an interaction between the components. Some pertinent work was conducted by Pichaud and Drechsler[77][78] and Bettler et al.[7]. They used field electron microscope method to measure the influence of an absorbed layer on the surface self-diffusion of a metal, with or without a second element. It is suggested that impurities not only strongly affected the shape of metal particles on substrate, but also the surface mobility as is apparent from Figure 7-1. As indicated, silica may block the migration of tungsten, whereas a monolayer of nickel atoms strongly increase the surface mobility of tungsten. It was suggested that the low melting point of tungsten-nickel alloy caused the increasing mobility of molybdenum. It was also showed that carbon had the similar effect on the mobility of tungsten as silica did[7].

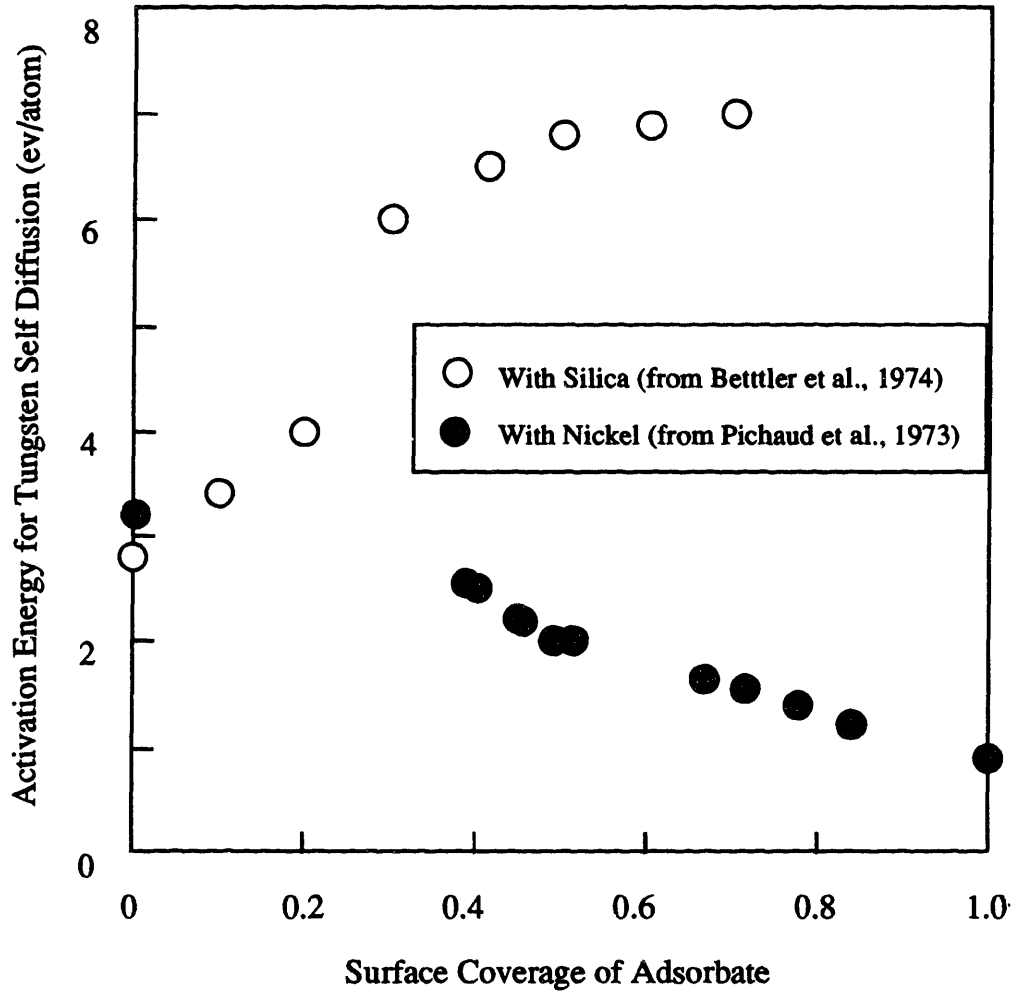

Figure 7-1: Effect of Absorbate Coverage on the Activation Energy of Tungsten Surface Self-Diffusion

7.4 Mobility in Two Component Systems

Rarely, we can find a complete ideal solution between two solid compounds. The solubility between two end components would be dependent on the many factors. The sizes and valences of the involved atoms are among the most important conditions for the atomic compatibility. Before we get into the complexity of the hydrodemetallation catalyst surface with metal deposits, let us first considered some simple cases.

For a system composed of two components, combinations of one or more of the following three cases would be representative of most general systems:

- Case 1: Two compounds are completely soluble in each other;
- Case 2: Two component are partially soluble in each other;
- Case 3: Two compounds are completely insoluble in each other.

The three different cases are schematically shown in Figure 7-2, Figure 7-3 and Figure 7-4. In all the three cases, let suppose that component A has a higher melting temperature than that of the component B, and we will discuss how the lower-melting-point component A will affect the higher-melting-point component A. At temperatures higher than the melting point of component A or lower than component B, the system would be either completely mobile or completely immobile, regardless of the compositions. For temperatures between the two melting points, which are the ones we are interested in, we could generally have three different regions. In region I where the concentration of component B is low, component A would be in complete solid phase as a solid solution formed with component B. In region III, on the other hand, the solution formed by component A and B would be completely in liquid phase, and component A is expected to mobile although the temperature is still lower than its melting point. In region II, component A would be partially mobile, and the mobility would be dependent on the amount of B in the system. In case 3, the region I is

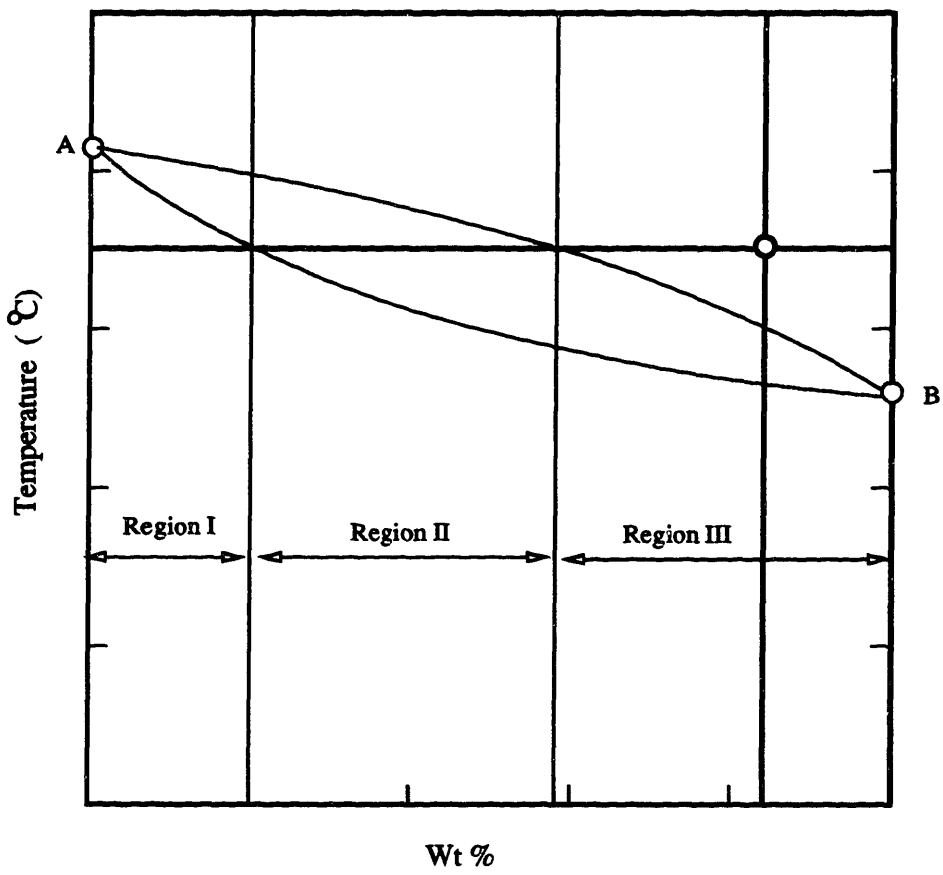

Figure 7-2: Mobility Regions on Hypothetical Phase Diagram: I. Complete Soluble System

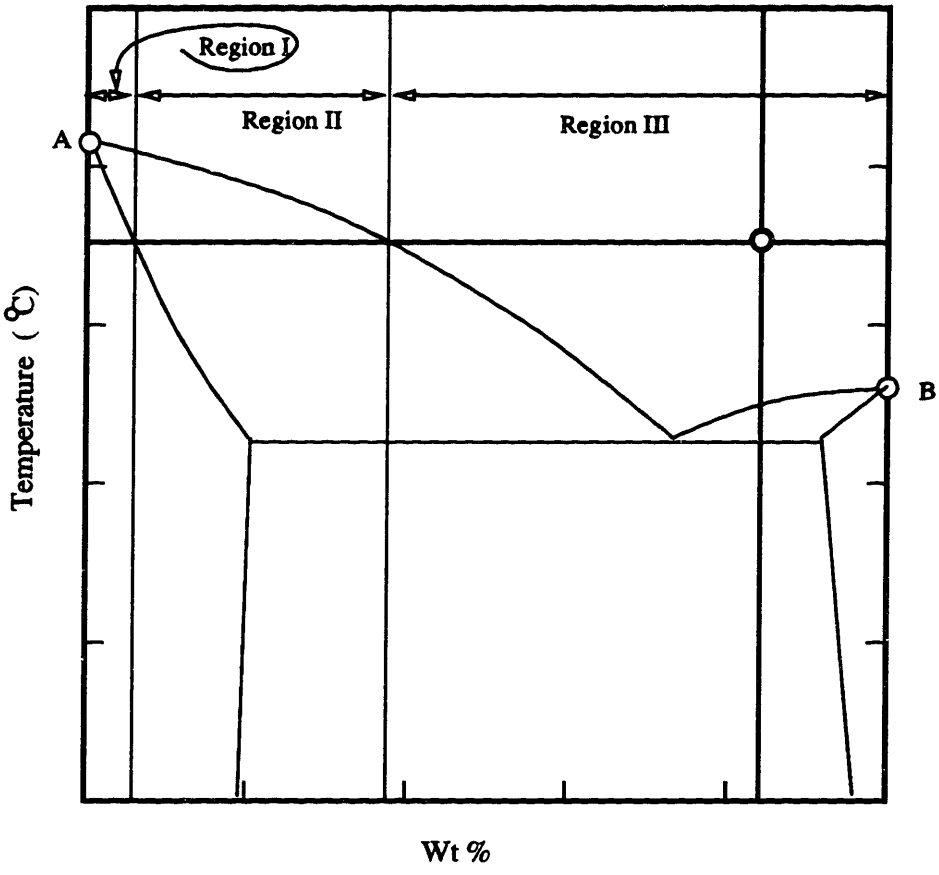

Figure 7-3: Mobility Regions on Hypothetical Phase Diagram: II. Partially Soluble System

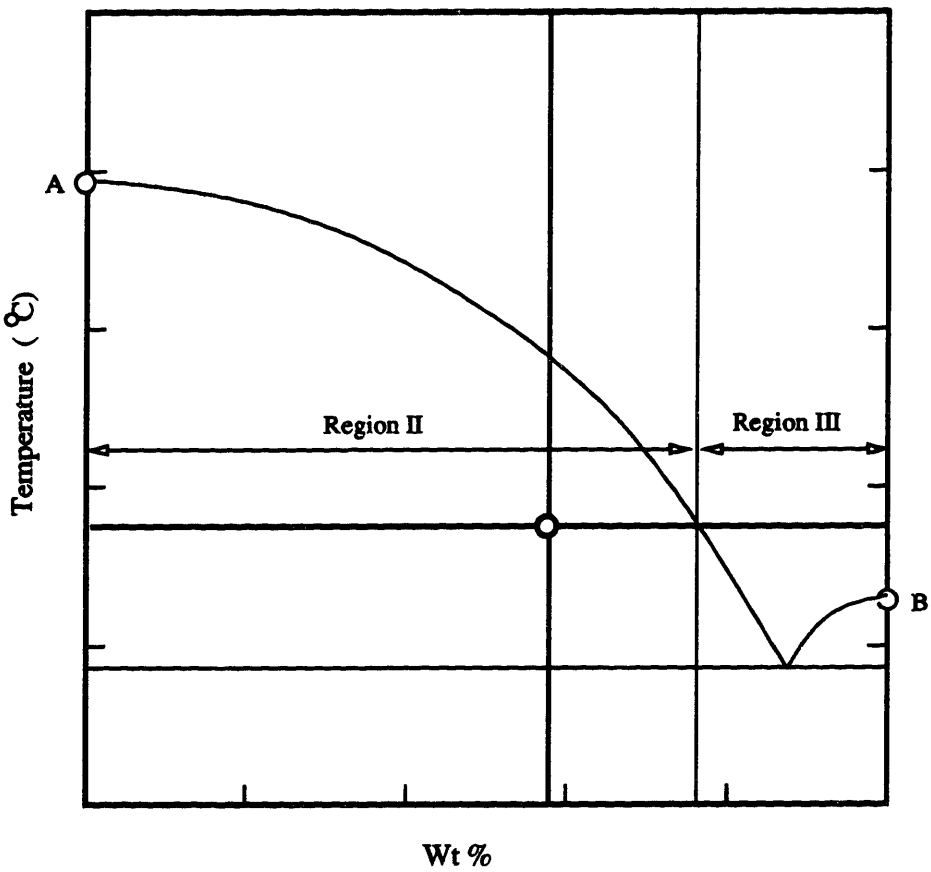

Figure 7-4: Mobility Regions on Hypothetical Phase Diagram: III. Complete Insoluble System

squeezed to the y axis, and only region II and region III exist. Clearly, this is nothing more than basic phase equilibrium. Unfortunately, real systems are never so simple.

First of all, the bulk phase diagrams usually do not apply for catalyst surface where most of the metals are very well dispersed into nano size crystallites. As we have discussed in chapter 4, the mobility of the crystallites can be characterized by their Tammann temperatures, instead of melting points. Now, let us combine the concept of Tammann temperature with the three hypothetical phase diagrams. We would have three very similar phase diagrams, except that the points A and B in the phase diagrams now represents the Tammann temperatures, rather than melting points. If we go back to reconsider the three regions on the phase diagrams, we would have the following conclusions. In region I, component A would still be immobile. In region III, however, component A would be mobile at a temperature lower than its Tammann temperature. Again, region II is a transitional region.

The formation of intermediate compounds is a concern for applying the phase diagrams to systems. In principle, any complex phase diagrams can be decomposed into small units, and analyzed accordingly. For the present system, we can only have a qualitative analysis due to the lacking of information for constructing complete phase diagrams.

7.5 Hydrodemetallation Catalyst Surface

At the surface of an aged hydrodemetallation catalyst, we have at least the following three metal sulfides: Ni_7S_6, Co_9S_8 and MoS_2, excluding any possible species formed with the substrate. According to the discussion in last section, we would need the information of Tammann temperatures of the metal sulfides and the corresponding phase diagrams to discuss the mobilities of the metal sulfides.

The characteristic temperatures of the three metal sulfides are tabulated in Ta-

ble 5.1. It should be pointed out that either Ni_7S_6 or Co_9S_8 is stable under the listed melting point temperatures. The listed temperatures simply indicate the temperatures under which the sulfides becomes liquid. The temperatures are obtained from the respective phase diagrams in reference[61].

In Chapter 2, we have summarized a few phase diagrams associated with the hydrodemetallation catalyst surfaces. Noticeably, the three component phase diagram of Mo-Ni-S system is missing, though we do have a phase diagram for Ni-Co-S system at 1273K.

As we have discussed in chapter six, extensive solid solution between Ni_7S_6 and Co_9S_8 is expected, while little solid solution is expected between Ni_7S_6 and MoS_2. For the sake of simplicity in discussion, let's assume that Ni_7S_6 and Co_9S_8 form ideal solution, while Ni_7S_6 and MoS_2 are completely insoluble in each other, as being schematically shown in Figure 7-5 and Figure 7-6.

For the $Co-Mo/\gamma Al_2O_3$ catalyst with nickel deposits, we very roughly estimated that Co_9S_8 would become partially mobile when the $Ni_7S_6/(Co_9S_8+Ni_7S_6)$ is around 0.1, which corresponds to a nickel loading of about 0.5%. When the nickel loading reaches about 5% to 10%, the Co_9S_8 would be completely mobile. Of course, the data are so roughly obtained that they have only a qualitative meaning. The phase diagram between Ni_7S_6 and MoS_2 is not available, we could not point out even a rough number of the loading of nickel needed for the Mo to become mobile. If we assume that these two sulfide are completely insoluble, which is probably the case judging from their structure, we could see from Figure 7-4 that the system would have a very wide region II. Unless the temperature is very close to the Tammann temperature of MoS_2, the system would be separated into two phases: one with almost completely MoS_2, and the other with mostly Ni_7S_6 plus small amount of MoS_2. Qualitatively, that is exactly what we observed on the aged catalyst surface.

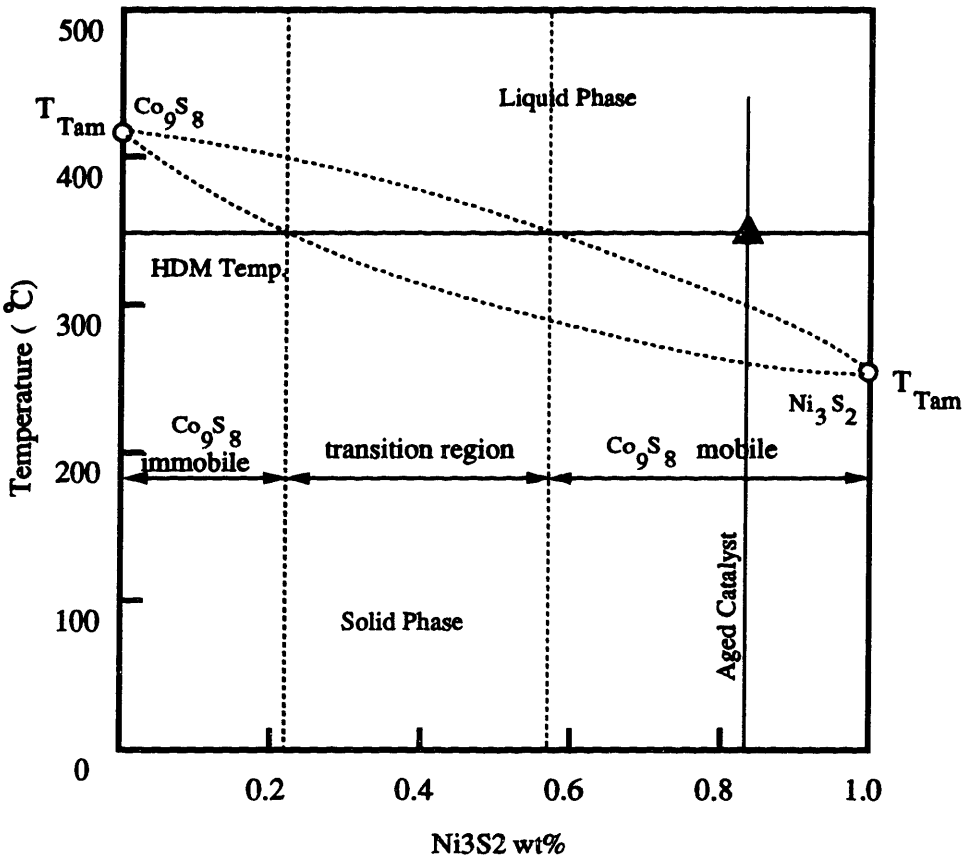

Figure 7-5: Mobility of Co_9S_8 with Ni_7S_6 Deposits

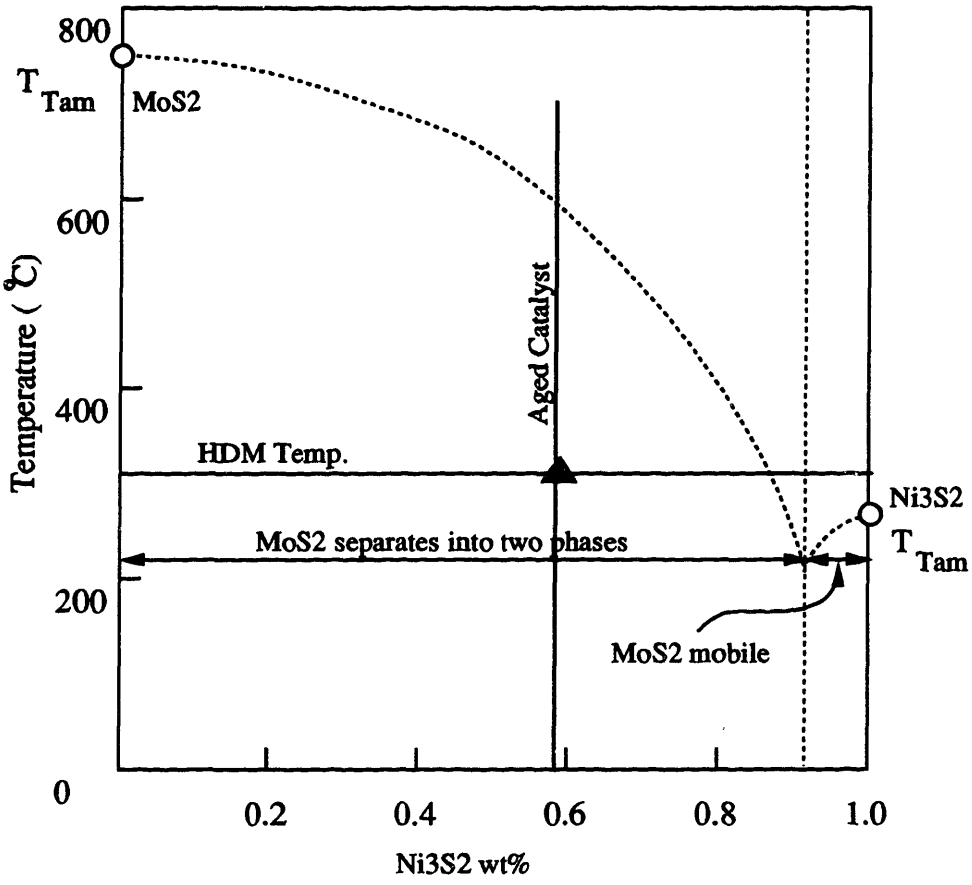

Figure 7-6: Mobility of MoS_2 with Ni_7S_6 Deposits

7.6 Electron Microscopic Results

We have discussed, resorting to the hypothetical phase diagrams, the possible behavior of cobalt and molybdenum sulfides with the presence of nickel sulfides. In the following, we will try to show the effect of nickel deposits on the mobility of catalytic metal sulfides with experiments. The basic idea is to compare the difference between a bare sulfided catalyst, a heat aged catalyst, and a catalyst subjected to hydrodemetallation. The electron microscopic work were conducted on the same machines we have mentioned before.

7.6.1 Sulfided Bare Catalyst

As we have discussed in chapter one and shown in chapter four, the catalytic components: cobalt and molybdenum, sulfides are both very well dispersed on the substrate. Figure 4-3 showed a high resolution micrograph of a sulfided HDS16A catalyst sample. We could clearly see that lattice fringe of MoS_2 ($d_{002} = 0.615nm$) randomly oriented on the catalyst. The sizes of the molybdenum sulfide slabs are usually about a few nanometers in length. The average numbers of the S-Mo-S layers are about four. We tried in vain to locate separate crystals of Co_9S_8. As we have discussed in Chapter four, the difficulty of observing Co_9S_8 may be associate with the low intensity of the main reflections of Co_9S_8 crystals. Comparatively, the existence of a strong (002) reflection for MoS_2 made it relatively easier to be observed and to be distinguished from other crystals. Thus, the absence of electron microscopic evidence does not rule out the existence of tiny Co_9S_8 crystals.

7.6.2 Heat Aged Catalyst

Figure 7-7 shows a high resolution micrograph of a sulfided HDS16A catalyst subjected to *heat aging* for about 200 hours at 648K. The relatively higher temperature

was intended to compensate the shorter aging time compared with the samples aged with nickel deposits at 623K for about 600 hours. The heat aged catalyst still very much resemble the unaged catalyst. Many randomly oriented MoS_2 fringes are observed. It appears that the numbers of the S-Mo-S layers and the lengths of the slabs are both slightly increased. No quantitative analysis was attempted. One slightly unexpected observation is the Co_9S_8 crystal shown in the lower left corner of the picture. The size of the crystal is about 25 nanometers. It should, however, be emphasized that Co_9S_8 crystals with this size were not readily observed. Although it is not necessarily conclusive from the observation itself, the mobility of cobalt sulfide, judging from their Tammann temperatures, should be much higher th an that molybdenum sulfide.

7.6.3 Nickel Aged Catalyst

In chapter six, we have discussed the general characteristics of the aged catalysts. Here we want to reemphasize two additional points. First of all, cobalt sulfide phase is completely incorporated into the crystallites of nickel sulfide deposits, as have been shown in the mapping pictures. The sizes of the cobalt sulfide can be, therefore, considered the same as those of nickel sulfide deposits (see Figure 7-9). Secondly, there exist two forms of molybdenum sulfide. One part is the molybdenum sulfide associated with nickel deposits as a segregated surface layer. Since it is encompassing the nickel crystallites, the lengths of the molybdenum sulfide layers are significantly longer than the slabs on the original catalyst prior to nickel deposition, though there are usually only one to two layers of molybdenum sulfide on the nickel sulfide surface. The other part of the molybdenum sulfide is separately situated on the substrate. Figure 7-8 shows a typical high resolution image of the sulfided HDS16A subjected to hydrodemetallation. The sizes of this part of molybdenum sulfide are apparently bigger and have more layers than those of the bare sulfide catalyst and the heat-aged

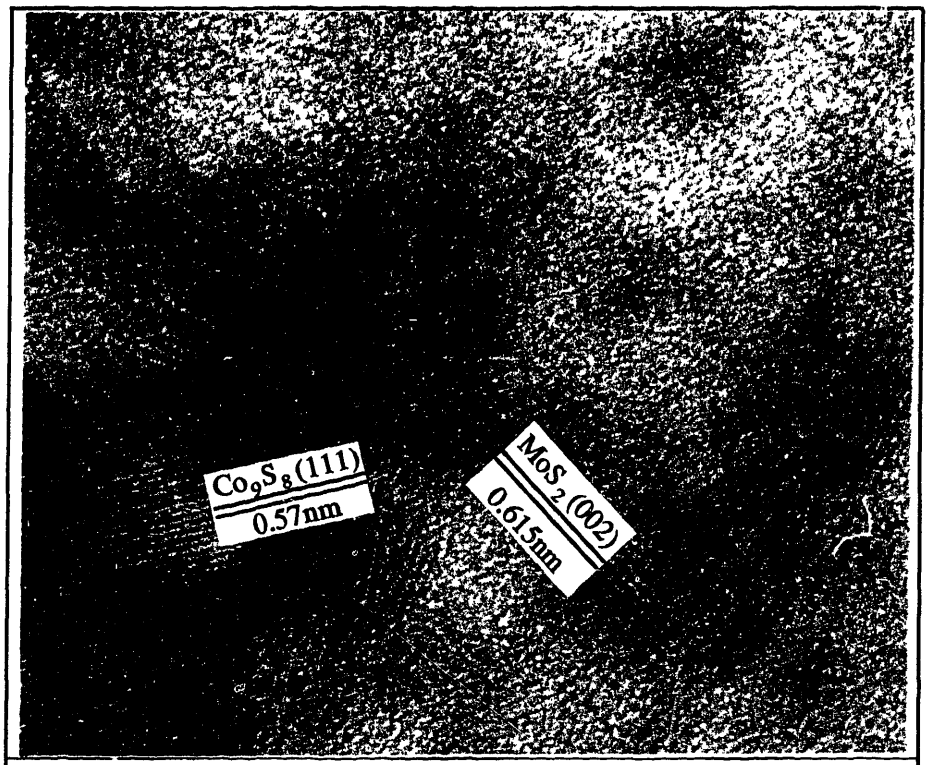

Scale: 5nm

Catalyst: HDS16A	Temperature: 648K
Aging Time: 200hrs.	H_2 Pressure: 4.8 MPa

Figure 7-7: High Resolution Micrograph of Heat Aged Catalyst

catalyst. Molybdenum sulfide crystals with sizes of 30 nanometers were also observed as shown in Figure 6-14. If we assume the original slabs of molybdenum sulfide is about 5 nanometers in length and about 2.5 nanometers in thickness, it takes over four hundreds of them to coalesce to get such a big crystallite. The same, of course, is also true for the large crystallites of cobalt sulfide coexisting with nickel deposits, which could be easily found on the mapping pictures.

7.7 Conclusions

By combining the conception of Tammann temperature and hypothetical phase diagrams, we proposed a criterion for the determination of mobility of the metal sulfides on the surface of hydrodemetallation catalysts. This work was motivated by the desire to understand the effect of nickel deposits on the deactivation of hydrodemetallation catalysts. it is shown that there is a threshold nickel deposit loading on the catalyst, above which the mobilities of the catalytic metal sulfides would be enhanced. The enhancement of mobilities of the catalytic components by nickel deposition is demonstrated by comparing the sintering cobalt and molybdenum with or without nickel deposits on the catalyst surface. The mobilities of the catalytic metals are significantly enhanced as a result of the nickel deposition. While the consideration here is specifically related to the $Co - Mo/\gamma Al_2O_3$ catalyst system with nickel deposits, the issues addressed are applicable to any other systems involving the interaction of more than one surface components on a substrate.

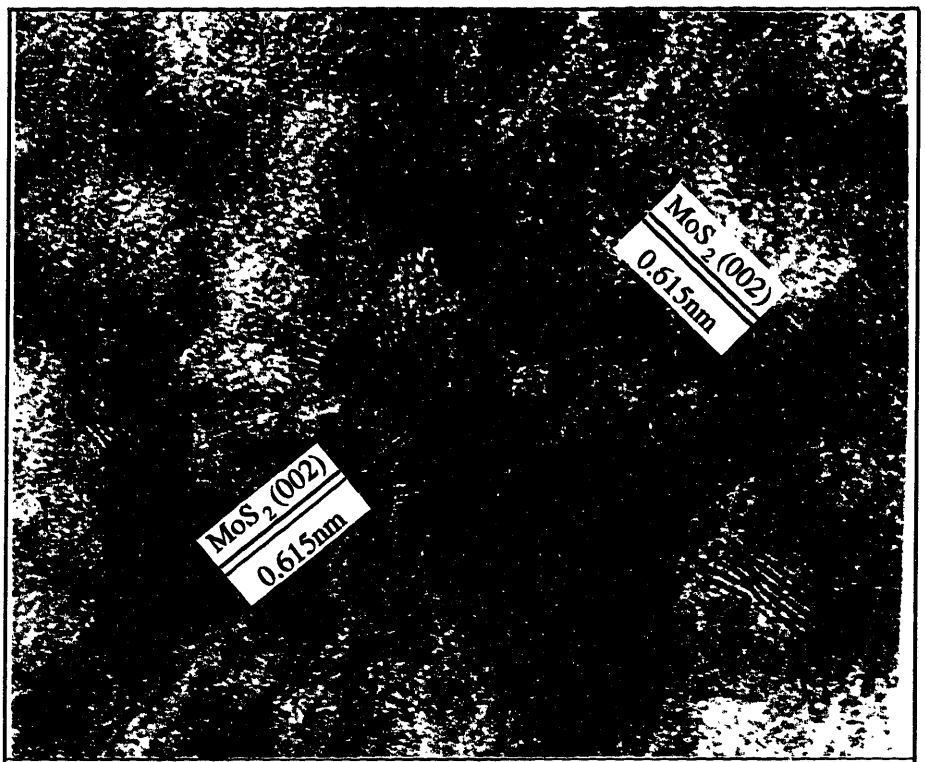

Scale: 5nm

Catalyst: HDS16A	Temperature: 623K
Aging Time: 650hrs.	H_2 Pressure: 4.8 MPa

Figure 7-8: High Resolution MoS_2 Image on Aged Sulfided Catalyst

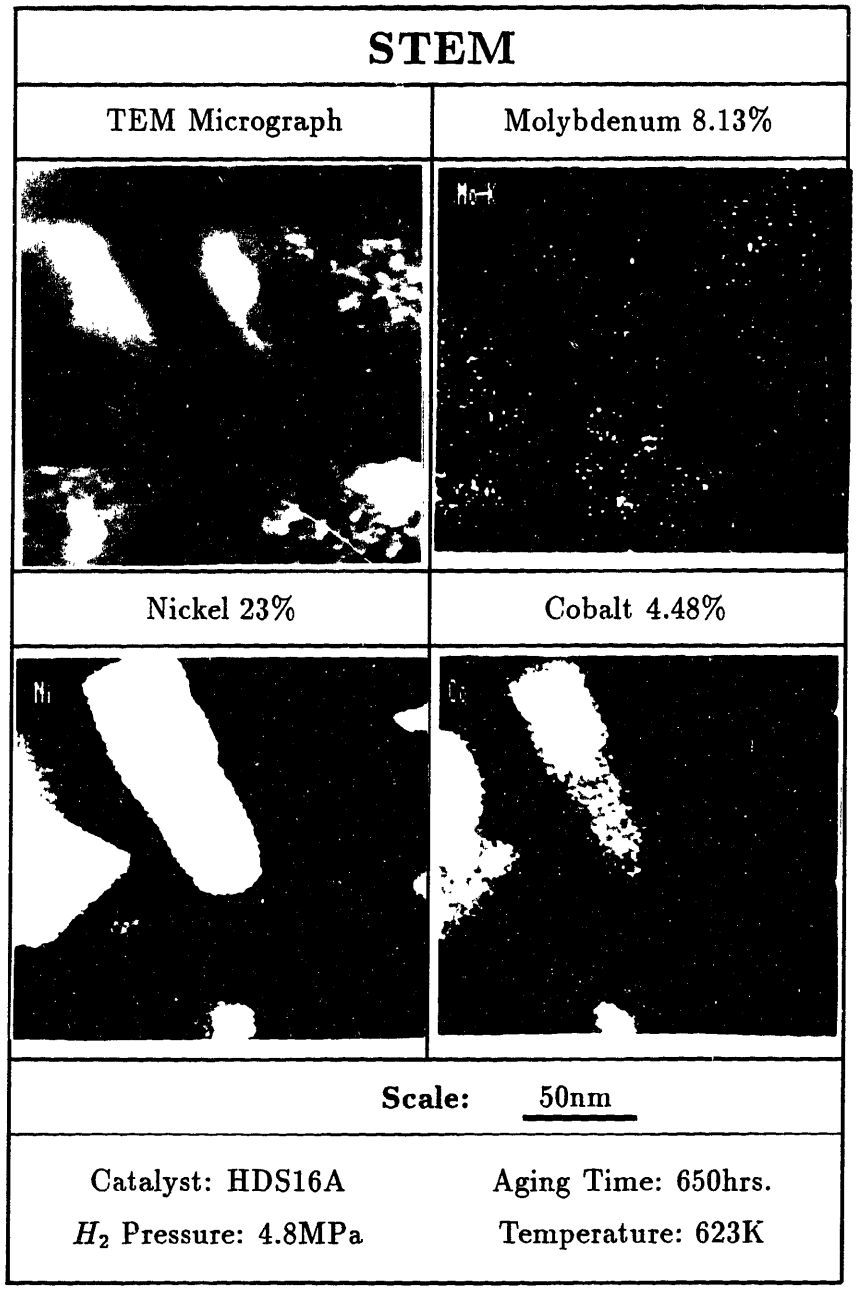

Figure 7-9: Elemental Mapping of Aged HDS16 Catalyst

Chapter 8

Nickel Deposition and Catalyst Deactivation

At least I might go the length of saying that there is some evidence that this may be so.

——Sherlock Holmes, *The Hound of the Baskervilles*
Sir Arthur Conan Doyle

8.1 Chapter Summary

In this chapter, we will summarize results from the previous chapters, and try to come up a complete picture for the deposition process and the development of the deposits on the catalyst surfaces. It is proposed that the nickel deposition pattern is determined by the balance between two mechanisms: deposition and migration. The implications of the deposition phenomena to hydrodemetallation catalyst deactivation

are discussed.

8.2 Development of Nickel Deposits

Based on the development of the nickel deposits on the catalyst, we could divide the deposition process into the following four stages:

- Stage 1: Sulfided $Co - Mo/\gamma - Al_2O_3$ catalyst

  The high resolution images of sulfided catalysts shown in Figure 4-3 indicated that the initial sizes of the molybdenum sulfide slabs are about 5 nanometers. They usually have about four layers. The results are consistent with those reported in literature[13][115].

- Stage 2: Initial deposition sites of nickel on MoS_2

  There is no direct experimental evidence from the present work to show where the nickel initially deposits on. A plausible assumption would be that much of the nickel initially deposit on molybdenum sites, due to the fact that molybdenum sulfide is the active sites for the hydrodemetallation reaction. The initial deposition sites could be important in understanding the deactivation mechanism if the initial stage of catalyst deactivation of is due to chemical poisoning by the nickel deposits, as being suggested[51][113]. Again, we should emphasize that no direct experimental evidence for the initial deposition sites.

- Stage 3: Migration of nickel sulfide towards Co_9S_8

  As we have shown in chapter 5, nickel sulfide is mobile on the catalyst surface under hydrodemetallation conditions, due to its low Tammann temperature. Therefore, nickel deposits are expected to migrate towards cobalt sulfide sites, as a result of the tendency to form solid solution.

- Stage 4: Migration of Co_9S_8 as well as Ni_7S_6

  With the increase of nickel loading on the catalyst, its presence would lower the Tammann temperature of cobalt sulfide to the point eventually that cobalt sulfide becomes mobile. In other word, the system reaches the region II we discussed in Figure 7-5. Meanwhile, much of the molybdenum sulfide would stay on the substrate, and those associated with nickel deposits would be segregated on the surface of the deposits, due to the lower surface energy of molybdenum sulfide. This would be the images we observed on most of the aged catalyst surfaces.

In the above discussion, we arbitrarily divide the deposition into four stages. There are virtually no fundamental differences between stage three and stage four, except for the fact that cobalt sulfide is considered mobile in addition to nickel sulfide. However, stage two represents a completely different mechanism from stages three and four. The balance between the two different mechanisms, *deposition vs. migration*, would determine the final deposition patterns of nickel deposits on the catalyst surface. When deposition is the dominant factor, as in the initial stage of the aging process, much of the nickel deposits would be on molybdenum sulfide sites. When migration dominates the process, as in the case of catalyst with impregnated nickel, the association between nickel and cobalt would be observed.

The balance between the two mechanisms, along with the deposition processes, is schematically shown in Figure 8-1.

8.3 Catalyst Deactivation

Now, let's go back to the starting point of this research, that is the deactivation of hydrodemetallation catalysts. Among many possible causes for the catalyst deactivation, the followings are often cited as the causes:

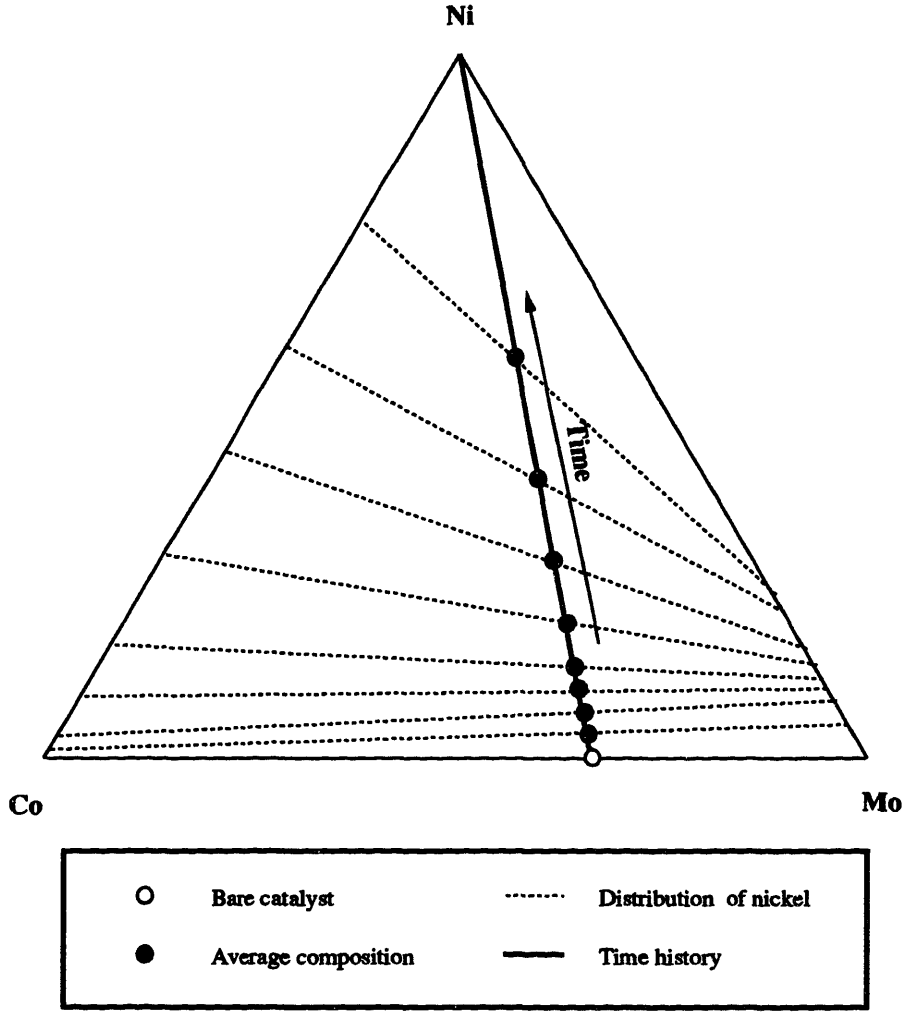

Figure 8-1: Nickel Deposition Mechanism

- Covering-up of active sites[75][76]
- Pore plugging[113]
- Poisoning[10]
- Sintering[9]
- Carbonaceous deposits[83]
- Hindered diffusion[50]

In addition to pore plugging for diffusion control processes, *covering-up of active sites by metal deposits* is the most widely cited causes for the deactivation of hydrodemetallation catalysts. One significant contribution of the present work is that we evidently showed that nickel deposits do *not* cover up the active components molybdenum disulfide. The covering-up of cobalt sulfide sites are irrelevant to the catalyst deactivation. Whatever role cobalt was playing for the original catalyst, nickel is readily available as the substitute. As a matter of fact, the data of Smith & Wei [107] should have disapprove the argument of covering-up of active sites by metal deposits. The catalyst kept virtually the same activity for nickel loading up to about 60%[107], though nickel deposits only possess about one tenth to about one third of the activity of cobalt promoted molybdenum catalyst[16].

Based on the present research, we believe that enhanced sintering due to the deposition of nickel on the catalyst is an important factor for the catalyst deactivation. Naturally, the coalescence of small crystallites into larger ones cause significant reduction of molybdenum sulfide accessible to the reactant. Another factor should be considered is the decreasing of the number of edge sites with the sintering of molybdenum sulfide. It is generally accepted that the edge sites, instead of basal sites, of molybdenum sulfide are the catalytic sites. In addition to the reduction of edge sites

by the coalescence of molybdenum sulfide, the part of molybdenum sulfide segregated on the nickel sulfide surfaces also have less edge sites available than an unaged catalyst. This is due to the fact that the surface layer usually has a much larger patch, though it is a very thin layer. Therefore, the ratio of edge/basal sites are significantly reduced by the enhanced sintering of the catalytic components. This mechanism is probably controlling the second stage of the catalyst deactivation process.

Is the depicted mechanism consistent with the deactivation observation in industry or laboratory data[34][107][113]? It is difficult to conclusively confirm simply because too many factors were involved in the reported activity studies. The mechanism is certainly not contradictory with the reported data.

8.4 Approaches for Improved Catalyst Design

One of the conclusions from the *random sphere model* proposed by Smith & Wei[109] was that segregated large crystallites of nickel deposition lead to less deactivation, in comparison with uniform layers of nickel deposition. Based on the present study, one of the obvious possibility of controlling the the deposition pattern is to control the morphology of cobalt sulfide on the catalyst. Because the strong association between nickel and cobalt sulfide on the catalyst, it might be possible to achieve large segregated crystallites of nickel deposits simply by adding less cobalt to the original catalyst. For hydrodesulfurization reaction, the purported synergic effect between cobalt and molybdenum requires the existence of cobalt. For hydrodemetallation reaction, the addition of cobalt might not be that necessary. First of all, less cobalt might be able to lead to less nucleation sites for nickel deposits. Secondly, whatever role requires cobalt can always be fulfilled by nickel as a substitute. Available literature information does support the above assumption. The data by Hung [38] presented in chapter five showed that the addition of cobalt to a molybdenum catalyst

actually decreases its hydrodemetallation activity. Another set of data, as shown in Figure 8-2 and Figure 8-3, is from Hisamitsu *et al.* [35]. It is clear that although cobalt or nickel has a significant promoter effect for hydrodesulfurization reactions, the promoter effect is much less significant for hydrodemetallation reactions. On the other hand, the addition of cobalt caused a significant acceleration of the deactivation rate. They concluded that the addition of cobalt or nickel was considered to be disadvantageous as far as hydrodemetallation was concerned. The promoter effect of cobalt was also reported to be minimal for hydrodemetallation by Morales *et al.*[67].

Comparing with industrial hydrodemetallation processes, the present study was conducted on a relative short time frame (<700 hours). In spite of the short time, we observed that most of the nickel has undergone through a surface rearrangement process and associated itself with cobalt on the catalyst surface. In industrial catalysts, we can expect that this surface arrangement process occurs even faster, due to the higher operating temperature.

The surface segregation of molybdenum sulfide keeps the catalyst active for further reaction while the enhanced sintering of molybdenum sulfide deactivates the catalysts. Lower temperature would favor the segregation of molybdenum, and slow the sintering process, but activity concerns must be considered.

8.5 Conclusions

Based on the structure of deposits observed on transmission electron microscope and the EDS analysis result from scanning transmission electron microscope, a complete picture of the aged hydrodemetallation catalyst surface and a dynamical deposition mechanism is developed. The implication to the deactivation of hydrodemetallation catalyst is discussed. It is concluded that the deactivation of hydrodemetallation catalyst under diffusion free cases is *not* due to the covering up of active sites by

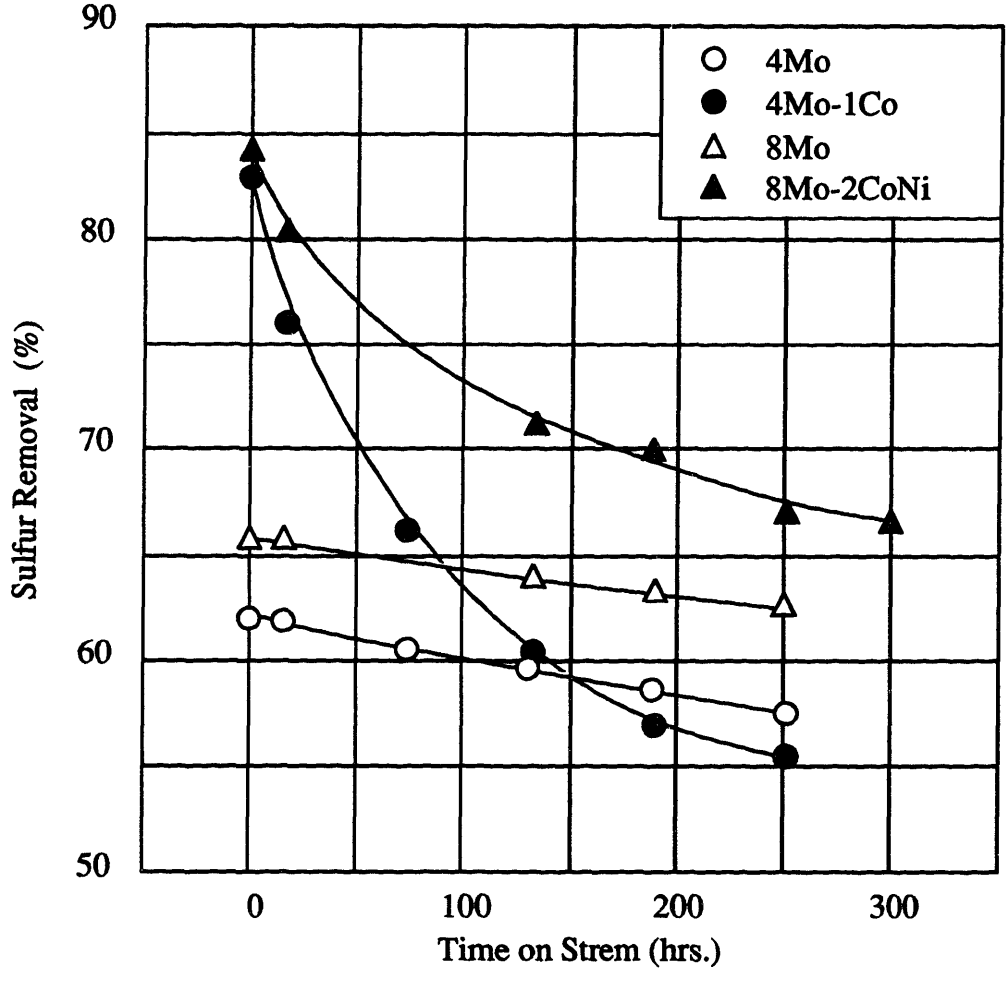

Figure 8-2: Hydrodesulfurization Activity with Different Promoter Contents in Catalysts [35]

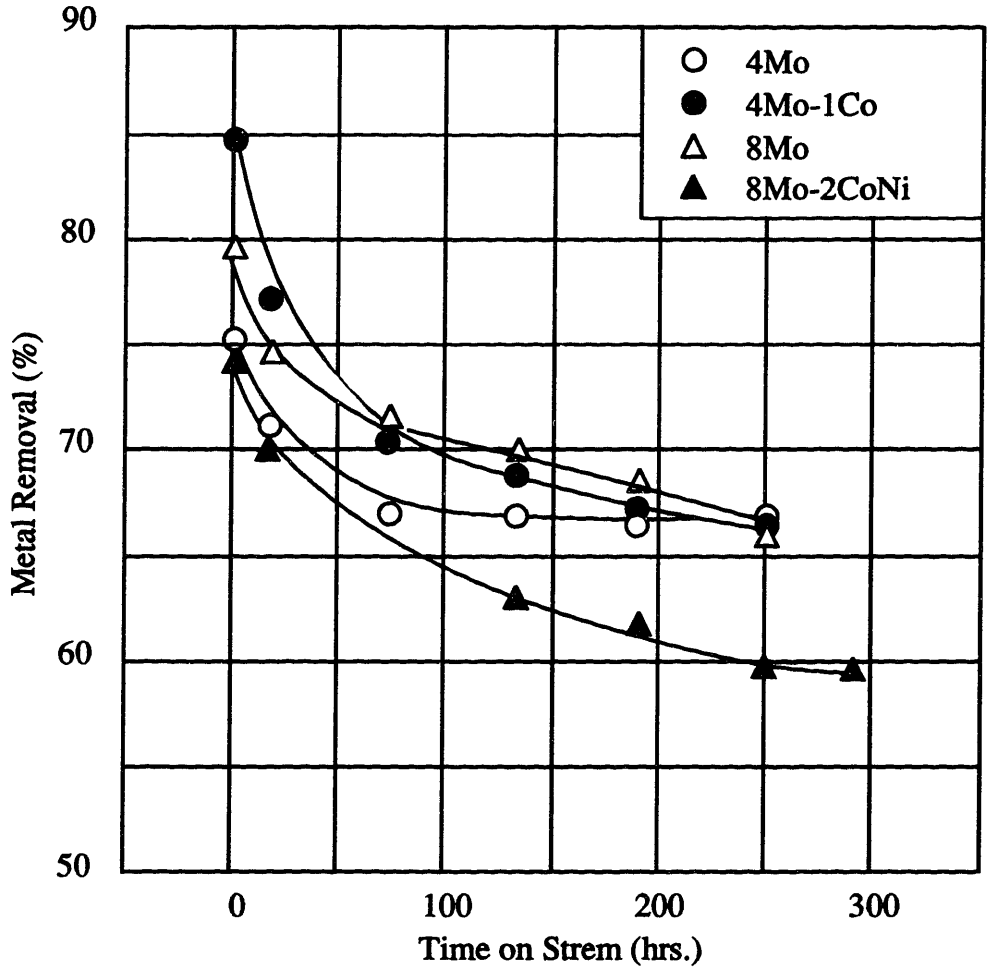

Figure 8-3: Hydrodemetallation Activity with Different Promoter Contents in Catalysts [35]

the nickel deposits. The coelencence of molybdenum is one possible causes of the second stage of the deactivation. Eventually, pore plugging will take over and destroy the catalyst by blocking the further access to the catalyst by the metal-containing molecules.

Chapter 9

Conclusions

Surely our profession, Mr. Mac, would be a drab and sordid one if we did not sometimes set the scene so as to glorify our results.

——Sherlock Holmes, *The Valley of Fear*
Sir Arthur Conan Doyle

We come to the following conclusions from the thesis:

1. **Nickel deposits on hydrodemetallation catalysts in crystallite form. The sizes of these crystallites vary in a wide range. At the metal loading of about 20%, the average sizes are about 10 to 15 nanometers.**

2. **X-ray elemental mapping and XEDS microanalysis on STEM show that nickel deposits are preferentially associated with cobalt for both sulfided and unsulfided systems, but there is no apparent association between nickel and molybdenum on the catalyst surface.**

3. The association of nickel deposits with cobalt, instead of molybdenum is due to subsequent migration after deposition. Since large crystallites of nickel deposition cause less catalyst deactivation in comparison with uniform layers of nickel deposition, it is suggested that control of cobalt morphology may lead to improved catalyst design.

4. Within the crystallites of nickel sulfide deposits, the distribution of nickel and cobalt are relatively uniform, while molybdenum is enriched on the surface of the crystallites as a segregated molybdenum sulfide surface phase. This part of the molybdenum accounts for about 20% to 25% of the total molybdenum on the catalyst. The rest of the molybdenum forms separate entities on the substrate. In addition, the segregation of molybdenum sulfide decreases for crystallites smaller than about 10 to 15 nanometers.

5. Nickel sulfide deposits enhance the sintering of the catalytic metal sulfides by lowering their Tammann temperatures. Electron microscopic study and phase diagram analysis both showed that the sintering of the catalytic metal sulfides, especially cobalt sulfide, increases with the presence of nickel sulfide deposits. It is showed that there exists a threshold nickel loading above which the catalytic metal sulfides become mobile. The threshold value is dependent on the specific systems and the operating temperatures.

6. The enhanced sintering of molybdenum and cobalt sulfides, rather than the covering-up of active sites by deposits as being suggested in many literatures, is considered as the major cause for deactivation by metal deposits for diffusion-free cases. The sintering includes both the increases of crystallite sizes and the decreases of edge sites of

molybdenum sulfide.

Chapter 10

Recommendations

It sounds to me like the beginning of the end.

——Sherlock Holmes, *The Valley of Fear*

Sir Arthur Conan Doyle

As we have stated in the beginning of the thesis, the objective of the work is to understand the interaction of the nickel deposits with the catalytic metal sulfides on the original catalyst. Therefore, the main theme of the thesis has been devoted to understanding rather than solutions. As a matter of fact, it seems we have more questions to answer than before we first started the project. We make the following recommendations for any future studies on the topic.

1. One important question left uncertain by this work is the initial deposition location of nickel on the catalyst. It is an important question because that catalyst deactivation mechanism at the initial stage of hydrotreating is still unknown. If coke deposition is the cause for the initial deactivation, the initial deposition location for nickel deposits would not be an important issue. However, it

would be a very significant issue, if the initial stage of catalyst deactivation is really caused by the poisoning effect of metals on the catalysts by preferentially destroying the synergy effect between molybdenum and cobalt.

2. The function of cobalt on hydrodemetallation catalyst should be further studied. It is clear that molybdenum is more active than cobalt if they are used separately. What the cobalt was put in the catalyst in the beginning. For hydrodesulfurization, the cobalt might have some functions there. For hydrodemetallation, however, the nickel deposition should play any parts that cobalt was playing once the reaction has started. Especially, when one use molybdenum-nickel catalyst for hydrodemetallation, is it really necessary to use nickel at all, or the initial nickel or cobalt is acting as some nucleation sites for deposition. If the latter is true, The conception of improved catalyst in terms of deposition patterns has been substantiated.

3. The entire thesis is devoted to nickel deposition on hydrodemetallation catalyst. The counterpart of the thesis would be vanadium deposition on hydrodemetallation catalysts. It has been reported that vanadium sulfide could form layer structures similar to that of molybdenum sulfide[57]. If this is really the case on catalyst surface, it would be interesting to know how the vanadium would interact with cobalt and molybdenum sulfides on the catalyst surface.

4. Whether or not carboneceous deposits are causing the initial stage of catalyst deactivation, coke is always a deactivation factor. How much of the catalyst deactivation in industrial process can be attributed to coke or metal deposits are yet to be determined. It is important to know how the metal deposits interacts with carboneceous deposits.

5. Finally, the present study was conducted at entirely diffusion-free conditions. It would be useful if the present result can be incorporated into a scheme with the presence of diffusion limitation, as in the real industrial process.

Appendix A

STEM analysis data

It has cost me two years, Watson, but they have not been devoid of excitement.

——Sherlock Holmes, *His Last Bow*
Sir Arthur Conan Doyle

It should be noted that the data listed here did not include all the elements included during the analysis. When the cobalt, molybdenum, and nickel percentages do not add up to 100%, some of the following elements, *e.g.* sulfur, aluminum, iron, phosphorus *etc.* were included in the analysis, though the results are not listed here.

A.1 XEDS Microanalysis: Unsulfided HDS16A

Catalyst: HDS16A	Temperature: 623K
Nickel Loading: 22.6%	H_2S: 0%vol.

	Co%	Mo%	Ni%		Co%	Mo%	Ni%
1	7.16	10.25	82.59	9	7.43	26.88	65.69
2	5.16	2.15	92.69	10	2.32	18.18	79.50
3	5.44	5.64	88.92	11	6.71	2.02	91.27
4	6.99	17.69	75.31	12	12.43	47.44	40.14
5	2.60	7.03	90.37	13	15.61	41.24	43.14
6	3.91	5.41	90.68	14	13.08	35.47	51.46
7	13.61	0.00	86.39	15	8.76	0.00	91.24
8	7.62	14.92	77.46				

Note: This set of data corresponds to Figure 4-11.

A.2 XEDS Microanalysis: Sulfided HDS16A

Catalyst: HDS16A	Temperature: 623K
Nickel Loading: 23.0%	H_2S: 0.3%vol.

	Co%	Mo%	Ni%		Co%	Mo%	Ni%
1	1.100	0.55	76.94	8	4.250	10.68	0.000
2	1.114	0.000	62.770	9	2.860	26.65	16.530
3	0.080	6.620	67.470	10	2.910	2.980	26.450
4	2.110	2.310	70.760	11	3.600	1.910	51.630
5	5.730	26.490	2.930	12	3.790	2.740	67.080
6	2.760	5.300	61.32	13	4.930	4.280	60.430
7	3.79	4.660	55.470	14	3.270	5.110	18.960

Note: This set of data corresponds to Figure 4-8.

A.3 XEDS Microanalysis: HDS16A with Impregnated Nickel

Catalyst: HDS16A	Temperature: 303K
Nickel Loading: 10%wt.	H_2S: 0%vol.

	Co%	Mo%	Ni%		Co%	Mo%	Ni%
1	5.45	9.54	10.01	13	10.25	9.26	13.39
2	7.26	12.73	15.13	14	10.42	9.61	14.18
3	7.75	13.51	15.95	15	11.12	11.27	13.76
4	6.68	14.26	14.29	16	9.76	11.26	14.52
5	7.60	14.86	14.29	17	10.99	12.72	14.98
6	7.48	14.89	15.68	18	11.49	8.06	14.37
7	8.55	14.41	17.11	19	11.80	13.25	15.66
8	9.05	14.73	16.84	20	11.33	11.41	14.47
9	7.84	12.56	15.08	21	13.52	15.99	17.31
10	6.75	12.43	14.50	22	13.17	10.94	15.86
11	11.26	10.90	13.91	23	10.09	11.82	11.71
12	14.33	12.46	17.55				

Note: This set of data corresponds to Figure 5-3.

A.4 XEDS Microanalysis: HDS16A with Impregnated Nickel after Heating

Catalyst: HDS16A	Temperature: 648K
Nickel Loading: 10%wt.	H_2S: 0.3%vol.

	Co%	Mo%	Ni%		Co%	Mo%	Ni%
1	15.980	28.310	17.760	15	18.190	27.330	20.240
2	15.440	23.210	21.700	16	18.990	22.970	22.310
3	11.370	29.500	18.420	17	8.140	37.740	6.030
4	13.590	28.420	19.780	18	21.970	26.920	13.730
5	14.530	26.800	17.440	19	10.030	35.930	11.870
6	16.000	21.010	23.670	20	15.940	30.870	14.030
7	14.070	32.560	21.400	21	11.490	34.510	10.250
8	15.990	29.420	20.960	22	15.650	31.950	12.450
9	17.740	26.130	24.970	23	21.130	19.670	20.900
10	21.660	25.610	22.770	24	13.240	31.550	18.100
11	17.740	24.550	20.680	25	13.550	30.210	15.460
12	14.580	29.270	19.340	26	10.270	35.260	10.440
13	18.050	25.030	21.490	27	15.580	26.990	15.910
14	14.350	34.120	11.980	28	25.770	22.610	14.280

Note: This set of data corresponds to Figure 5-4.

A.5 XEDS Microanalysis: HDS16A (Within One Crystallite)

Catalyst: HDS16A	Temperature: 623K
Nickel Loading: 23.0%	H_2S: 0.3%vol.

	Co%	Mo%	Ni%		Co%	Mo%	Ni%
1	11.420	7.330	68.810	9	15.650	1.470	80.390
2	10.520	10.730	67.540	10	14.580	0.540	80.490
3	9.420	17.540	53.970	11	14.190	2.050	79.050
4	14.620	0.000	82.790	12	13.040	4.220	77.430
5	12.680	1.750	81.160	13	14.970	2.360	80.080
6	11.660	0.000	84.200	14	2.350	13.490	80.680
7	12.130	4.550	75.390	15	16.190	0.000	81.320
8	11.390	15.680	57.190				

Note: This set of data corresponds to Figure 6-3.

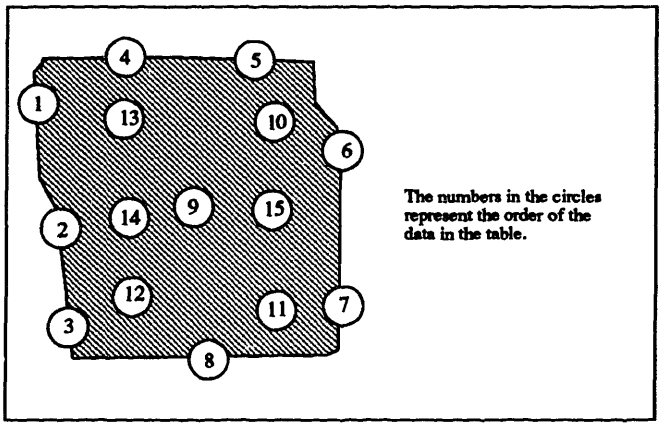

A.6 XEDS Microanalysis: SN6931 (Within One Crystallite)

Catalyst: SN6931	Temperature: 588K
Nickel Loading: 22.1%	H_2S: 0.3%vol.

	Co%	Mo%	Ni%		Co%	Mo%	Ni%
1	3.180	0.250	54.850	5	2.210	0.000	46.240
2	2.830	1.620	40.350	6	2.190	0.420	43.100
3	1.280	1.480	10.080	7	6.000	0.010	49.500
4	2.300	0.280	39.440	8	2.430	0.150	55.520

Note: This set of data corresponds to Figure 6-6.

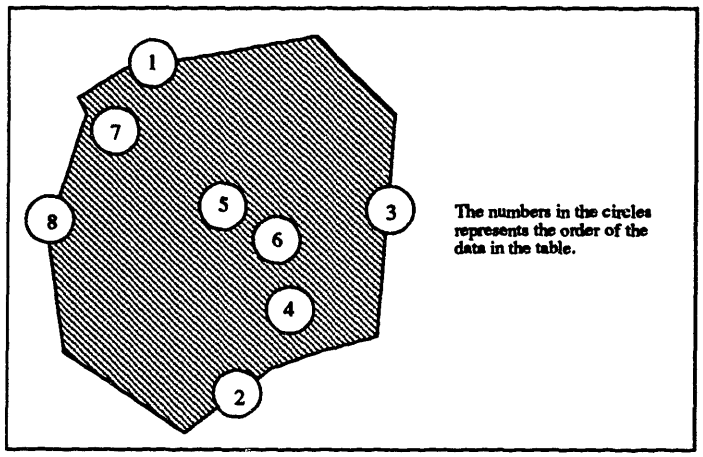

A.7 XEDS Microanalysis: Surface Segregation Data

Catalyst: HDS16A	Temperature: 623K
Nickel Loading: 23.0%	H_2S: 0.3%vol.

	Center			Edge			Particle Size
	Co%	Mo%	Ni%	Co%	Mo%	Ni%	(nm)
1	17.61	0.00	69.96	11.96	3.73	71.86	30
2	14.19	1.34	71.55	13.79	13.21	62.87	35
3	13.80	4.13	68.35	10.29	23.63	54.96	20
4	12.12	4.10	68.47	11.08	9.29	69.01	20
5	17.34	7.60	63.49	14.52	16.79	57.52	15
6	15.57	7.34	66.31	11.81	15.96	60.54	25
7	16.13	4.14	65.09	11.76	10.14	66.97	10
8	7.09	21.53	70.39	7.48	32.31	58.07	7
9	10.69	10.06	78.49	10.93	15.16	73.03	8
10	15.65	1.47	80.39	11.99	8.42	71.34	55
11	2.21	0.00	46.24	3.00	1.96	40.20	32

Note: 1. This set of data corresponds to Figure 6-11.

2. No. 10 corresponds the crystallite in A.5.

3. No. 11 corresponds to the crystallite on SN6931 catalyst in A.6.

Appendix B

Acronyms

It is obviously an attempt to convey secret information.

——Sherlock Holmes, *The Valley of Fear*

Sir Arthur Conan Doyle

AAS	atomic absorption spectrophotometry
AES	Auger electron spectroscopy
AEM	analytical electron microscopy
BET	Brunauer-Emmerr-Teller
EMPA	electron microprobe
EPR	electron paramagnetic resonance
ESR	electron spin resonance
EXAFS	extended X-ray absorption fine structure
HDM	hydrodemetallation
HDN	hydrodenitrogenation
HDO	hydrodeoxygenation
HRTEM	high resolution transmission electron microscopy
MES	Mössbauer spectroscopy
NMR	nuclear magnetic resonance
SEM	scanning electron microscopy
SIMS	Secondary Ion Mass Spectroscopy
STEM	scanning transmission electron microscopy
TEM	transmission electron microscopy
XAFS	X-ray absorption fine structure
XPS	X-ray photoelectron spectroscopy
XRD	X-ray diffraction analyzer

Bibliography

Now, if you please, we will get off on what I hope is the last stage of our journey.

——Sherlock Holmes, *The Problem of Thor Bridge*
Sir Arthur Conan Doyle

[1] R. Agrawal and J. Wei. Hydrodemetallation of Nickel and Vanadium Porphyrins: 1. Intrinsic Kinetics. *Ind. Eng. Chem. Process Des. Dev.*, **23**:505 – 514, 1984.

[2] N. V. Agreev. *Diagrammy Sostoiniia Metallicheskikh Sistem, Vol.XIX.* Viniti, Moscow, 1973.

[3] M. Arai, T. Ishikawa, and T. Nishiyama. Surface Migration of Ni on C, SiO_2, and Al_2O_3. *The Journal of Physical Chemistry*, **86**:577–581, 1982.

[4] R. T. K. Baker. The Relationship between Particle Motion on a Graphite Surface and Tammann Temperature. *Journal of Catalysis*, **78**:473–476, 1982.

[5] C. H. Bartholomew. Carbon Deposition in Steam Reforming and Methanation. *Catal. Rev.-Sci. Eng.*, **24**:67–112, 1982.

[6] J. S. Berkes and R. Roy. Use of Ion Properties for the Prediction of the Phase Relations in a Binary System. *Zeitschrift für Kristallographie*, **131**:60–72, 1970.

[7] P. C. Bettler, B. H. Bennum, and C. M. Case. Effect of Impurities on Surface Self-Diffusion and Surface Structure. *Surface Science*, **44**:360–376, 1974.

[8] J. Biswas, G. M. Bickel, P. G. Gray, D. D. Do, and J. Barbier. The Role of Deposited Poisons and Crystallite Surface Structure in the Activity and Selectivity of Reforming Catalysts. *Catal. Rev. Sci. Eng.*, **30**:161–247, 1988.

[9] J. M. Bogdanor and H. F. Rase. Characteristics of a Commercially Aged $Ni - Mo/Al_2O_3$ Hydrotreating Catalyst: Component Distribution, Coke Characteristics, and Effects of Regeneration. *Ind. Eng. Chem. Prod. Res. Dev.*, **25**:220–230, 1986.

[10] R. Bonné. *Hydrodemetallisation of Ni-TPP and VO-TTP over Sulfided Molybdenum and Vanadium Catalysts.* PhD thesis, University of Amsterdam, 1992.

[11] S. Boškovič and M. Stevanovič. Reaction Sintering of CoO-NiO System. In G. C. Kuczynski, editor, *Sintering and Catalysis*, volume **10**, pages 455–463, 1975.

[12] D. Briggs and M. P. Seah. *Practical Surface Analysis : by Auger and X-ray Photo-electron Spectroscopy.* John Wiley, Chichester, 1983.

[13] R. Candia, B. S. Clausen, J. Bartholdy, N. Y. Topsøe, B. Lengeler, and H. Topsøe. Nature of Active Sites in Sulfided HDS Catalysts. In *8th International Congress on Catalysis*, volume , pages II–375, Verlag Chemie, 1984.

[14] J. R. Chelikowsky. Predications of Surface Segregation in Intermetallic Alloys. *Surface Science*, **139**:L197–L203, 1984.

[15] H. J. Chen and F. E. Massoth. Hydrodemetallation of Vanadium and Nickel Porphyrins over Sulfided $CoMo/Al_2O_3$ Catalysts. *Ind. Eng. Chem. Res.*, **27**:1629–1639, 1988.

[16] R. R. Chianelli. Fundamental Studies of Transition Metal Sulfide Hydrodesulfurization Catalysts. *Catal. Rev. Sci. Eng.*, **26**:361–393, 1984.

[17] M. W. J. Craje, E. Gerkeme, V. H. J. de Beer, and A. M. van der Kraan. Mössbauer Study of the Sulfidation of Hydrodesulfurization Catalysts: So-Called $Co - Mo - S$ Phase observed in Carbon-Supported Co and $Co - Mo$ Sulfided Catalysts. In M. L. Occelli and R. G. Anthony, editors, *Hydrotreating Catalysts: Preparation, Characterization and Performance*, volume **50**, page 165, 1989.

[18] J. Cruz, M. Avalos-Borja, M. H. Farias, and S. Fuentes. Hydrodesulfurization Catalysts Prepared by Two Methods Analyzed by Transmission Electron Microscopy. *Journal of Catalysis*, **137**:232–242, 1992.

[19] F. Dautzenberg and J. C. de Deken. Modes of Operation in Hydrodemetallization. In R. H. Filby and J. F. Branthaver, editors, *Metal Complexes in Fossil Fuels*, volume ACS Symp. Ser. **344**, pages 233–256, 1987.

[20] F. Delannay. High Resolution Microscopy of Hydrodesulfurization Catalysts: A Review. *Applied Catalysis*, **16**:135–152, 1985.

[21] F. Delannay, P. Gajardo, P. Grange, and B. Delmon. Genesis, Nature and Dispersion of Active Phase in Sulphided $CoMo/\gamma - Al_2O_3$ Hydrodesulphurization Catalysts. *J. of Chemical Society, Faraday Transanction I*, **76**(5):988–997, 1980.

[22] B. Delmon. *Proceedings of the Third International Conference on Chemistry and Uses of Molybdenum ed. by H. F. Barry and P. C. H. Mitchell.* Climax Molybdenum Co., Ann Arbor, 1979.

[23] B. Delmon. Advances in Hydropurification Catalysts and Catalysis. In D. L. Trimm et al, editor, *Catalysts in Petroleum Refining*, volume **53**, pages 1–40, Amsterdam, 1990. Elsevier.

[24] B. Delmon and P. Grange. Solid State Chemical Phenomena in Aging and Deactivation of Catalysts. In B. Delmon and G. F. Froment, editors, *Catalyst Deactivation*, volume **6**, pages 507–544, Amsterdam, 1980. Elsevier.

[25] T. H. Fleisch, B. L. Meyers, J. B. Hall, and G. L. Ott. Multitechnique Analysis of a Deactivated Resid Demetallation Catalyst. *Journal of Catalysis*, **86**:147–157, 1984.

[26] P.C. Flynn and S. E. Wanke. A Model of Supported Metal Catalyst Sintering: I. Development of Model. *Journal of Catalysis*, **34**:390–399, 1974.

[27] P.C. Flynn and S. E. Wanke. A Model of Supported Metal Catalyst Sintering: II. Application of Model. *Journal of Catalysis*, **34**:400–410, 1974.

[28] W. Furdanowicz. *Effects of Diffraction on Microanalysis of Embedded Precipitates.* PhD thesis, Massachusetts Institute of Technology, 1991.

[29] E. Gail. Modeling of Hydrodemetallation. Technical report, Massachusetts Institute of Technology, Department of Chemical Engineering, 1990.

[30] A. J. Garratt-Reed. Applications of High-Resolution X-ray Mapping. In J. R. Micheal and Peter Ingram, editors, *Microbeam Analysis*, pages 272–274, 1990.

[31] J. W. Gibbs. *The Scientific Papers of J. Willard Gibbs*, volume **I**. Dover, New York, 1961.

[32] J. Haber. Crystallography of Catalyst Types. In J. R. Anderson and M. Boudart, editors, *Catalysis: Science and Technology*, volume **2**, pages 14–95, 1981.

[33] C. R. Helms. Segregation Effects in Small Particles Used In Catalysis. In W. C. Johnson and J. M. Blakely, editors, *Interfacial Segregation*, pages 175–190, 1977.

[34] A. M. Henke. Gulf's Residual HDS Process. *Oil and Gas Journal*, 68(14):97, 1970.

[35] T. Hisamitsu, K. Komori, and H. Ozaki. The Role of Cobalt and Nickel Added to Molybdenum-Alumina in Hydrotreating Catalysts. In B. Delmon and G. F. Froment, editors, *Catalyst Deactivation 1987*, volume , page 259, 1987.

[36] R. Hughes. *Deactivation of Catalysts.* Academic Press, New York, 1984.

[37] J. E. Huheey. *Inorganic Chemistry.* Harper and Row, Publisher, New York, 1983.

[38] C. W. Hung. *The Kinetics of Hydrodemetallation of Metalloporphyrins.* PhD thesis, Massachusetts Institute of Technology, 1979.

[39] C. W. Hung and J. Wei. The Kinetics of Porphyrin Hydrodemetallation: 1. Nickel Compounds. *Ind. Eng. Chem. Process Des. Dev.*, **19**:250–257, 1980.

[40] K. T. Jacob. Isothermal Section of the Ni-Co-S Phase Diagram at 1273K. *Metallurgical Transactions B*, **11B**:640–643, 1980.

[41] W. C. Johnson and J. M. Blakely. *Interfacial Segregation.* American Society of Metals, Metals Park, Ohio, 1977.

[42] B. R. Jones. *Electron Microscopy.* Library Research Associates, Monroe, New York, 1983.

[43] S. J. Khang and J. F. Mosby. Catalyst Deactivation due to Deposition of Reaction Products in Macropores during Hydroprocessing of Petroleum Residuals. *Ind. Eng. Chem. Process Des. Dev.*, **25**:437, 1986.

[44] W. D. Kingery, H. K. Kent, and D. R. Uhlmann. *Introduction to Ceramics.* Wiley, New York, 1976.

[45] I. Kostov and J. Minčeva-Stefanova. *Sulphide Minerals: Crystal Chemistry, Parageneses and Systematics.* E. Schweizerbart'sche Verlagsbuchhandlung, Stuttgart, 1982.

[46] H. K. Kuo, P. Ganesan, and R. J. de Angelis. The Sintering of Silica-Supported Nickel Catalyst. *Journal of Catalysis*, **64**:303, 1980.

[47] H. Kwart, G. C. Schuit, and B. C. Gates. Hydrodesulfurization of Thiophenic Compounds: The Reaction Mechanism. *Journal of Catalysis*, **61**:128, 1980.

[48] M. Kwauk. Legacy and Growth - Chemical Engineering in China. *Chemical Engineering Science*, **44**:2421–2434, 1989.

[49] J. Laine, J. Brito, J. Gallardo, and F. Severino. The Role of Nickel in the Initial Transformations of Hydrodesulfurization Catalysts. *Journal of Catalysis*, **91**:64, 1985.

[50] M. J. Ledoux, O. Michaux, and S. Hantzer. Hydrodesulfurization(HDS) Poisoning by Vanadium Compounds: EPR and Metal Solid NMR Analysis. *Journal of Catalysis*, **106**:525–537, 1987.

[51] M. J. Ledoux, O. Michaux, and S. Hantzer. Poisoning of Hydrodesulfurization Catalysts by Vanadium. In B. Delmon and G.F. Froment, editors, *Catalyst Deactivation 1987*, volume **34**, pages 269–277, 1987.

[52] W. Y. Liang. Electron Properties of Transition Metal Dichalcogenides and Their Intercalation Complexes. In M. S. Dresselhaus, editor, *Intercalation in Layered Materials*, volume **148**, pages 31–73, 1986.

[53] K. W. Limbach. *Hydrodemetallation Catalyst Design Considerations.* PhD thesis, Massachusetts Institute of Technology, 1989.

[54] K. W. Limbach, J. M. Nitsche, and J. Wei. Partitioning of Nonspherical Molecules between Bulk Solution and Porous Media. *AIChE Journal*, **35**(1):42 – 52, 1989.

[55] K. W. Limbach and J. Wei. Restricted Diffusion through Granular Materials. *AIChE Journal*, **36**(2):242–248, 1990.

[56] J. M. J. G. Lipsch and G. C. A. Schuit. The $CoO - MoO_3/Al_2O_3$ Catalyst: III. Catalytic Properties. *Journal of Catalysis*, **15**:179, 1969.

[57] M. Loos, I. Ascone, P. Friant, J. Goulon, N. Senglet, J. M. Barbe, R. Guilard, and D. Faure. Modelisation of the Interactions of Vanadyl Porphyrins with Hydroprocessing Catalysts. *Physica B*, **158**:191–194, 1989.

[58] M. Loos, I. Ascone, C. Goulon-Ginet, J. Goulon, C. Guillard, M. Lacroix, M. Breysse, D. Faure, and T. Descourieres. X.A.F.S. Study of Model Vanadium Sulfide Phases Suspected to Form on HDM Catalyst Surfaces. *Physica B*, **158**:145–148, 1989.

[59] D. Lundqvist. X-ray Studies on the Ternary System of Fe-Ni-S. *Arkiv Kemi, Mineral. Geol.*, **24A**(22):12, 1947.

[60] O. Macé and J. Wei. Diffusion in Random Particles Models for HDM Catalysts. *Ind. Eng. Chem. Res.*, **30**:909–918, 1990.

[61] T. B. Massalski. *Binary Alloy Phase Diagrams, Second Edition.* ASM International, 1990.

[62] F. E. Massoth. Characterization of Molybdena Catalysts. In *Advances in Catalysis*, volume **27**, pages 265–310. Academic Press, 1978.

[63] J. B. McKinley. Hydrodesulfurization of Liquid Petroleum Fractions. In P. H. Emmett, editor, *Catalysis*, volume **5**, page 405, 1957.

[64] R. R. Melkote and K. F. Jensen. Models for Catalytic Pore Plugging: Application to Hydrodemetallation. *Chemical Engineering Science*, **44**(3):649–663, 1989.

[65] Kh. M. Minachev and E. S. Shpiro. *Catalyst Surface: Physical Methods of Studying.* CRC Press, Boca Raton, 1990.

[66] R. J. Moore and J. White. Equilibrium Relationships in the system $NiO - CoO - O_2$. *Journal of Material Sciences*, **9**:1393–1400, 1974.

[67] A. Morales, N. P. Martinez, J. Laine, and J. Grimblot. Correlation between HDS or HDV Activity with Spectroscopic Characterization of Molybdenum-Alumina and Cobalt-Molybdenum-Alumina Catalysts Modified by Extraction. *Applied Catalysis*, **6**:329–340, 1983.

[68] R. E. Newnham. Phase Diagrams and Crystal Chemistry. In Allen M. Alper, editor, *Phase Diagrams: Materials Science and Technology*, volume **5**, pages 1–74, New York, 1978. Academic Press.

[69] E. Newson. Catalyst Deactivation Due to Pore Plugging by Reaction Products. *Ind. Eng. Chem. Process Des. Dev.*, **14**(1):27, 1975.

[70] H. Nitta, T. Takatsuka, S. Kodama, and T. Yokoyama. Deactivation Model for Residual Hydrodesulfurization Catalysts. *86th Annual AIChE Meeting, Houston*, **34E**, 1979.

[71] N. Nourbakhsh, B. J. Smith, I. A. Webster, J. Wei, and T. T. Tsotris. Metal Deposition in Porous Anodic Alumina Films Under Hydrotreating Conditions. *Journal of Catalysis*, **127**:178, 1991.

[72] J. Nowotny and L. C. Dufour. *Surface and Near Surface Chemistry of Oxide Materials.* Elsevier, Amsterdam, 1988.

[73] E. S. Parkin, J. S. Paraskos, and J. A. Fryer. . *Natioinal AIChE Meeting, 74th, New Orlreans*, 1979.

[74] J. M. Pazos, J. C. Gonzalez, and A. J. Salazar-Guillen. Effect of Catalyst Properties and Operating Conditions on Hydroprocessing High Metals Feeds. *Ind. Eng. Chem. Process Des. Dev.*, **22**:653, 1983.

[75] C. J. Pereira. Metal Deposition in Hydrotreating Catalyst. 1. A Regular Perturbation Solution Approach. *Ind. Eng. Chem. Res.*, **29**:512–519, 1990.

[76] C. J. Pereira, J. W. Beeckman W. C. Cheng, and W. Suarez. Metal Deposition in Hydrotreating Catalyst. 2. Comparison with Experiment. *Ind. Eng. Chem. Res.*, **29**:520–521, 1990.

[77] M. Pichaud and M. Drechsler. A field Emission Measurement of the Influence of Adsoption on Surface Self-Diffusion. *Surface Science*, **32**:341–348, 1972.

[78] M. Pichaud and M. Drechsler. Surface Self-Diffusion of Tungsten under the Influence of Adsorbed Nickel. *Surface Science*, **36**:813–816, 1973.

[79] T. S. Prasada Rao and P. G. Menon. Physicochemcial Studies on Silica-Supported Multicomponent Molybdate Catalyst before and after Use in Ammoxidation of Propylene. *Journal of Catalysis*, **51**:64–71, 1978.

[80] K. C. Pratt, J. V. Sanders, and V. Christov. Morphology and Activity of MoS_2 on Various Supports: Genesis of the Active Phase. *Journal of Catalysis*, **124**:416–432, 1990.

[81] R. Prins. On the Structure and Role of Promoters and Modifiers in Hydrotreating Catalysts. In M. Graziani and C. N. R. Rao, editors, *Advances in Catalyst Design*, volume , page 42, 1990.

[82] R. Prins, V. H. J. de Beer, and G. A. Somorjai. Structure and Function of the Catalyst and Promoter in $Co-Mo$ Hydrodesulfurization Catalysts. *Catal. Rev. Sci. Eng.*, **31**:1–41, 1989.

[83] J. D. Pults and S. P. Ho. Characterization of Hydrotreating Catalysts for Heavy Oils Upgrading. *AIChE 1990 National Meeting, Chicago*, 1990.

[84] B. Pulvermacher and E. Ruchenstein. Identification of the Rate Determining Step in Aging of Supported Metals. *Journal of Catalysis*, **35**:115–139, 1974.

[85] R. J. Quann, R. A. Ware, C. W. Hung, and J. Wei. Catalytic Hydrodemetallation of Petroleum. *Advances in Chemical Engineering*, **14**:94–259, 1988.

[86] K. Rajagopalan and D. Luss. Influence of Catalyst Pore Size on Demetallation Rate. *Ind. Eng. Chem. Process Des. Dev.*, **18**:459, 1979.

[87] J. Ramirez and R. Cuevas. Effect of Fluorine on Hydrogenation of Cyclohexene on Sulfided $Ni(orCo) - Mo/Al_2O_3$ Catalysts. *Applied Catalysis*, **57**:223–240, 1990.

[88] L. A. Rankel and L. D. Rollmann. Catalytic Activity of Metals in Petroleum and Their Removal. *Fuel*, **62**:44–46, 1983.

[89] L. Reimer. *Transmission Electron Microscopy: Physics of Image Formation and Microanalysis.* Springer-Verlag, Berlin, 1989.

[90] S. B. Rice and M. J. Treacy. The Art of the Impossible: An overview of Catalyst Specimen Preparation Techniques for TEM Studies. *Mat. Res. Soc. Symp. Proc.*, **115**:15–27, 1988.

[91] J. T. Richardson. *Principles of Catalyst Development.* Plenum Press, New York, 1989.

[92] J. T. Richardson and G. Crump. Crystallite Size Distribution of Sintered Nickel Catalysts. *Journal of Catalysis*, **57**:417–425, 1979.

[93] T. Rosenqvist. . *J. Iron Steel Inst. (London)*, **176**:37, 1954.

[94] E. Ruckenstein and B. Pulvermacher. Kinetics of Crystallite Sintering During Heat Treatment of Supported Metal Catalysts. *AIChE Journal*, **19**:356–364, 1973.

[95] J. C. Russ. *Fundamentals of Energy Dispersive X-Ray Analysis.* Butterworths, London, 1984.

[96] R. C. Ryan, R. A. Kemp, J.A. Smegal, D. R. Denley, and G. E. Spinnler. Stacking of Molybdenum Disulfide Layers in Hydrotreating Catalysts. In M.L. Occelli and R.G. Anthony, editors, *Hydrotreating Catalysts*, pages 21–40, 1989.

[97] W. M. H. Sachtler. Surface Composition of Binary Alloys. In R. Prins and G. C. A. Schuit, editors, *Chemistry and Chemical Engineering of Catalytic Processes*, pages 317–336, Alphen aan den Rijn, The Netherlands, 1980. Sijthoff and Noordhoff.

[98] J. V. Sanders. The Electron Microscopy of Catalysts. In J. R. Anderson and M. Boudart, editors, *Catalysis: Science and Technology*, volume **7**, pages 51–158, 1985.

[99] C. N. Satterfield. *Heterogeneous Catalysis in Practice.* McGraw Hill, New York, 1991.

[100] W. R. Scheidt. Porphyrin stereochemistry. In D. Dolphin, editor, *The Porphyrins*, volume **3**, New York, 1978. Academic Press.

[101] M. P. Seah. Quantitative Prediction of Surface Segregation. *Journal of Catalysis*, **57**:450–457, 1979.

[102] S. T. Sie. Catalyst Deactivation by Poisoning and Pore Plugging in Petroleum Processing. In B. Delmon and G. F. Froment, editors, *Catalyst Deactivation*, volume **6**, pages 545–570, Amsterdam, 1980. Elservier.

[103] B. G. Silbernagel. Metal Chemistry on Hydrotreating Catalysts: NMR and EPR Surveys of Vanadium on Spent Catalyst Materials. *Journal of Catalysis*, **56**:315–320, 1979.

[104] B. G. Silbernagel and K. L. Riley. Heavy Feed hydroprocessing Deactivation: The Chemistry and Impact of Vanadium Deposits. In B. Delmon and G. F. Froment, editors, *Catalyst Deactivation*, volume **6**, page 313, 1980.

[105] M. J. Sinnott. *The Solid State for Engineers.* John Wileys and Sons, Inc., New York, 1958.

[106] B. J. Smith. *Deactivation in Catalytic Hydrodemetallation.* PhD thesis, Massachusetts Institute of Technology, 1989.

[107] B. J. Smith and J. Wei. Deactivation in Catalytic Hydrodemetallation I. Model Compound Kinetic Studies. *Journal of Catalysis*, **132**:1–20, 1991.

[108] B. J. Smith and J. Wei. Deactivation in Catalytic Hydrodemetallation II. Catalyst Characterization. *Journal of Catalysis*, **132**:21–40, 1991.

[109] B. J. Smith and J. Wei. Deactivation in Catalytic Hydrodemetallation III. Random-Spheres Catalyst Model. *Journal of Catalysis*, **132**:41–57, 1991.

[110] M. Speight. *The Desulfurization of Heavy Oils and Residue.* Marcel Dekker, New York, 1981.

[111] S. A. Stevenson, J. A. Dumesic, R. T. K. Baker, and E. Ruckenstein. *Metal-Support Interactions in Catalysis, Sintering and Dispersion.* VanNostrand Reinhold Company Inc., New York, 1987.

[112] C. Takeuchi, S. Asaoka, S. Nakata, and Y. Shiroto. Characteristics of Residue Hydrodemetallation Catalysts. *Div. of Petro. Chem., ACS Symposium Series*, **30**:96, 1985.

[113] P. W. Tamm, H. F. Harnsberger, and A. G. Bridge. Effects of Feed Metals on Catalyst Aging in Hydroprocessing Residuum. *Ind. Eng. Chem. Process Des. Dev.*, **20**:262, 1981.

[114] H. Topsφe, B. S. Clausen, N. Y. Topsφe, and E. Peterson. Recent Basic Research in Hydrodesulfurization Catalysis. *Ind. Eng. Chem. Fund.*, **25**:25, 1986.

[115] H. Topsφe, B. S. Clausen, N. Y. Topsφe, and P. Zeuthen. Progress in the Design of Hydrotreating Catalysts Based on Fundamental Molecular Insight.

In D. L. Trimm et al, editor, *Catalysts in Petroleum Refining*, volume **53**, pages 77–102, 1989.

[116] H. Toulhoat, J. C. Plumail, G. Martino, and Y. Jacquin. Modeling HDM Catalysts Deactivation by Metal Sulfides Deposits: An Original Approach Supported by HREM Investigations and Pilot Tests Results. *ACS Div. Petrol. Chem., Symposium on Advances in Resid Upgrading, Denver*, 1987.

[117] D. L. Trimm. Deactivaiton, Regeneration and Disposal of Hydroprocessing Catalysts. *Catalysts in Petroleum Refining 1989 ed. by D. L. Trimm et al.*, **53**:41–60, 1990.

[118] J. van Doorn, J. L. Bosch, R. J. Bakkum, and J. A. Moulijn. Temperature Programmed Oxidation as an Analysis Technique for Deactivated Hydrotreating Catalysts. In B. Delmon and G.F. Froment, editors, *Catalyst Deactivation 1987*, volume **34**, pages 391–402, 1987.

[119] R. J. H. Voorhoeve. Electron Spin Resonance Study of Active Centers in Nickel-Tungsten Sulfide Hydrogenation Catalysts. *Journal of Catalysis*, **23**:243, 1971.

[120] R. J. H. Voorhoeve and J. C. M. Stuiver. Kinetics of Hydrogenation on Supported and Bulk Nickel-Tungsten Sulfide Catalysts. *Journal of Catalysis*, **23**:228, 1971.

[121] R. A. Ware. *Reactivity of Nickel Porphyrins in Catalytic Hydrodemetallation.* PhD thesis, Massachusetts Institute of Technology, 1983.

[122] R. A. Ware and J. Wei. Catalytic Hydrodemetallation of Nickel Porphyrins. I. Porphyrin Structure and Reactivity. *Journal of Catalysis*, **93**:100 – 121, 1985.

[123] R. A. Ware and J. Wei. Catalytic Hydrodemetallation of Nickel Porphyrins. II. Effect of Pyridine and of Sulfiding. *Journal of Catalysis*, **93**:122 – 134, 1985.

[124] I. A. Webster. *Catalytic Hydrodemetallation of Nickel Porphyrins: Reactivity and Catalyst Surface Studies.* PhD thesis, Massachusetts Institute of Technology, 1984.

[125] J. Wei. Toward the Design of Hydrodemetallation Catalysts. In L.L. Hegedus, editor, *Catalyst Design: Progress and Perspectives*, pages 245–272, New York, 1987. Wiley.

[126] J. Wei. Catalytic Hydrodemetallation and the Pattern of Metal Deposition. *Research Proposal*, , 1989.

[127] J. Wei and X. Zhao. Metal Deposition and Deactivation of Hydrodemetallation Catalysts. *Chem. Engng. Sci.*, **47**:2721–2726, 1992.

[128] J. Weitkamp, W. Gerhardt, and D. Scholl. Hydrodemetallation of Nickel Porphyrins over Sulfided and Reduced $CoO - MoO_3/\gamma - Al_2O_3$. *8th International Congress on Catalysis, Verlog Chemie*, :II–269, 1984.

[129] P. Wynblatt and R. C. Ku. Surface Energy and Solute Strain Energy Effects in Surface Segregation. *Surface Science*, **65**:511–531, 1977.

[130] T. F. Yen. *The Role of Trace Metals in Petroleum.* Ann Arbar Science Pub., Ann Arbar, 1975.

[131] D. Yitzhaki and C. Aharoni. Kinetics and Mechanism of Catalytic Hydrodesulfurization of Gas Oil: Adsorption and Hydrogenation of Sulfur Compounds. *Journal of Catalysis*, **107**:255, 1987.

Biographical Note

The candidate, Xinjin Zhao, was born on August 17, 1961 in *Taiyuan, China.* His childhood years were spend growing up at Jinle, a small town in Shanxi Province at northern China.

Xinjin received his Bachelor of Science in chemical engineering at *Taiyuan University of Technology*, at *Taiyuan, China* in July 1982. He was very active in various school activities. Among other accomplishment and honors, he received three consecutive First-Standing Scholarships for the four years he stayed, and ranked number one in the chemical engineering class.

Before attending graduate school in 1983, he worked in *Xinzhou Prefectural Bureau of Standards* at *Shanxi, China* for a year, where he gained part of his real-world experience. During the course of graduate study at the *Institute of Coal Chemistry, Academia Sinica* at *Taiyuan, China*, he conducted research on gas-solid turbulent fluidization for his master's thesis. He later worked in the same Institute for over two more years upon receipt of his Master of Science in chemical engineering at April 1986. During his stay at the *Institute of Coal Chemistry*, he met Luhong Bo, who later became his beloved wife.

He came to *Massachusetts Institute of Technology* at *Cambridge, Massachusetts* in September 1988. After spending the summer of 1989 at *Chevron Research Company* in *Richmond, California*, he received his Master of Science in Chemical Engineering Practice, which he has been always proud of. He then began his doctoral research work on catalytic hydrodemetallation under the supervision of Professor James Wei. He received Arthur D. Little Fellowship and Practice School Fellowships from General Electric and Chevron Corporation while at *Massachusetts Institute of Technology.*